Development of a nature-based Geo-engineering solution to reduce soil permeability in-situ

Zhou, Jianchao

DOI
10.4233/uuid:4122ce24-5973-4afc-a084-1520dc8c5738

Publication date
2020

Document Version
Final published version

Citation (APA)
Zhou, J. (2020). *Development of a nature-based Geo-engineering solution to reduce soil permeability in-situ.* [Dissertation (TU Delft), Delft University of Technology]. https://doi.org/10.4233/uuid:4122ce24-5973-4afc-a084-1520dc8c5738

DEVELOPMENT OF A NATURE-BASED GEO-ENGINEERING SOLUTION TO REDUCE SOIL PERMEABILITY IN-SITU

DEVELOPMENT OF A NATURE-BASED GEO-ENGINEERING SOLUTION TO REDUCE SOIL PERMEABILITY IN-SITU

Proefschrift

ter verkrijging van de graad van doctor
aan de Technische Universiteit Delft,
op gezag van de Rector Magnificus Prof. dr. ir. T.H.J.J. van der Hagen,
voorzitter van het College voor Promoties,
in het openbaar te verdedigen op woensdag, 24 juni, 2020 om 15:00 uur

door

Jianchao ZHOU

Master of Science,
Technische Universiteit Delft, Delft, Nederland,
geboren te Anhui, China.

Dit proefschrift is goedgekeurd door de promotoren.

Samenstelling promotiecommissie:

Rector Magnificus,	voorzitter
Prof. dr. T.J. Heimovaara,	Technische Universiteit Delft, promotor
Dr. B. Jansen,	Universiteit Van Amsterdam, copromotor
Onafhankelijke leden:	
Prof. dr. M. Kok,	Technische Universiteit Delft
Prof. dr. R. Sethi,	Polytechnic University of Torino
Dr. T. A. Bogaard,	Technische Universiteit Delft
Prof. dr. R.N.J. Comans,	Wageningen University & Research
Prof. dr. K. G. Gavin,	Technische Universiteit Delft

Keywords: building with nature, in-situ permeability reduction, metal-organic matter complexation, flow barrier, reactive transport modelling, metal-organic matter flocs

Printed by: ProefschriftMaken, Utrecht

Front & Back: ProefschriftMaken

ISBN 978-94-6366-288-8

An electronic version of this dissertation is available at
http://repository.tudelft.nl/.

Dedicated to my grandmother

CONTENTS

Summary xi

Samenvatting xiii

1 Introduction 1
- 1.1 Dike stability in the Netherlands . . . 2
- 1.2 A nature-inspired geo-engineering solution . . . 3
- 1.3 Co-makership model for carrying out the research project . . . 4
- 1.4 Structure of this thesis . . . 5
- References . . . 7

2 A numerical toolbox to investigate the feasibility of using aluminium-organic matter complexes to reduce soil permeability in-situ 11
- 2.1 Introduction . . . 13
- 2.2 Theoretical background . . . 14
  - 2.2.1 The chemical characteristics of OM . . . 14
  - 2.2.2 Hydrolysis of monomeric Al^{3+} . . . 15
  - 2.2.3 Complexation between OM and Al . . . 16
  - 2.2.4 Precipitation/flocculation of Al-OM complexes . . . 16
  - 2.2.5 Physico-chemical behaviour of Al-OM flocs . . . 17
  - 2.2.6 Flow and transport . . . 18
  - 2.2.7 Reduction in permeability . . . 19
- 2.3 Material and methods . . . 19
  - 2.3.1 Two approaches of applying Al-OM flocs . . . 19
  - 2.3.2 Aims and site conditions of the two field experiments . . . 20
  - 2.3.3 Modelling and scenario analysis . . . 21
- 2.4 Results and discussion . . . 23
  - 2.4.1 1^{st} field experiment: using mixing and reaction of two components . . . 23
  - 2.4.2 2^{nd} field experiment: direct injection of Al-OM flocs . . . 28
- 2.5 Conclusions . . . 30
- References . . . 33

3 Applying aluminium-organic matter precipitates to reduce soil permeability in-situ: a field and modelling study 37
- 3.1 Introduction . . . 39
- 3.2 Materials and methods . . . 40
  - 3.2.1 Workflow and site information . . . 40
  - 3.2.2 Chemicals and preparation of solutions . . . 41
  - 3.2.3 Modelling . . . 41
  - 3.2.4 Design of the field experiment and baseline scenario analysis . . . 43

3.2.5 Well installation . . . 45
3.2.6 Field implementation and monitoring . . . 45
3.2.7 Pumping tests after the injection and well hydraulics . . . 46
3.3 Results and discussion . . . 46
3.3.1 Design of the field experiment and adaptations to the injection strategy . . . 46
3.3.2 Permeability reduction induced by Al-OM injection and precipitation . . . 50
3.3.3 Quantification of the permeability reduction . . . 52
3.3.4 Verification of the spatial distribution of Al-OM precipitates and uncertainties in the quantification . . . 53
3.4 Implications for future applications of Al-OM precipitates as a nature-based engineering technique . . . 54
References . . . 56

4 Direct injection of Al-OM flocs to reduce soil permeability and create a vertical flow barrier in-situ 61
4.1 Introduction . . . 63
4.2 Materials and methods . . . 66
4.2.1 Site description . . . 66
4.2.2 Design of the field experiment and implementation . . . 66
4.2.3 Monitoring and data analysis . . . 68
4.2.4 Site-specific flow model . . . 69
4.3 Results . . . 69
4.3.1 Effect of the direct floc injection on the hydraulic gradient . . . 69
4.3.2 Hydraulic characterisation by pumping and infiltration tests . . . 70
4.3.3 Transport of the injection fluid . . . 71
4.4 Discussion . . . 73
4.4.1 Permeability of the flow barrier in zone A . . . 73
4.4.2 Verification of the quantification and the impact of dredging . . . 75
4.4.3 Localised reduction in permeability in zone B . . . 77
4.4.4 Challenges in process control and implementation . . . 77
4.5 Conclusions . . . 78
References . . . 80

5 A mechanistic understanding of the flocculation of organic matter induced by aluminium ions 83
5.1 Introduction . . . 85
5.2 Material and methods . . . 86
5.2.1 Batch experiment . . . 86
5.2.2 Modelling approach . . . 86
5.2.3 The implementation . . . 92
5.3 Results and discussion . . . 92
5.3.1 Conceptual model of OM flocculation . . . 92
5.3.2 Al^{3+} as the coagulant . . . 95
5.3.3 Flocculation of OM using Al^{3+} . . . 97

5.4 Conclusions and implications . . . 101
References . . . 102

6 Conclusions and outlook **107**
6.1 Process understanding of Al-OM complexation and flocculation . . . 108
6.2 Applying the Podzolization-inspired concept in the context of engineering . 109
6.2.1 Define the objectives of the field experiment . . . 109
6.2.2 Design the field experiment . . . 109
6.2.3 Evaluate the field experiment . . . 110
6.3 Future outlook . . . 111
References . . . 114
References . . . 115

Acknowledgements **125**

Appendix A **129**

Appendix B **137**

Appendix C **143**

Curriculum Vitæ **147**

List of Publications **149**

SUMMARY

Stability of dikes is a national security issue for densely populated low-lying countries situated in delta areas, like the Netherlands. One of the dominant dike failure mechanisms in the Netherlands is piping, where high seepage flow rates transport sand particles and subsequently form a 'pipe' under a dike structure. As such, one manner to reinforce dike lies in the modification of the seepage flow field. Though many of conventional approaches have demonstrated varied degree of success in creating flow barrier, which is a subsurface structure that can alter the seepage flow field, they are commonly costly in terms of energy and labour. Facing the ever-growing awareness of climate change as well as the large economic scale of the dike stability issue in the Netherlands, the development of alternative techniques is thus desired. The focus of this research project is to develop a cost-effective, robust and environmentally compatible technology for in-situ permeability reduction of sub-surface systems. We took inspiration from nature, where a natural soil stratification process (namely Podzolization) shows the viability of organo-metallic complexes precipitation in reducing soil permeability in-situ. The aim of the research presented in this thesis is to quantitatively study the feasibility of using Podzolization-derived approaches to install flow barrier in dikes.

Chapter 2 of this thesis presents two approaches for applying organo-metallic complexes to reduce soil permeability in-situ, which are derived from the detailed analysis of Podzolization and the flocculation process between metal salt with organic matter. The first approach bases on the in-situ mixing and reaction between two components (i.e., aluminium (Al) and organic matter (OM) solutions), while the second approach makes use of the direct injection of Al-OM flocs. To understand the feasibility of using these approaches to install flow barrier on site, a 3D process-oriented model was developed. An important aspect of this model development is to incorporate engineering conditions on site into the simulation of processes. A series of scenario analyses were therefore performed with the model in order to facilitate the design and evaluation of the full-scale experiments where the two delivery approaches were applied to install a flow barrier in two dikes.

In Chapter 3, the results of a field experiment, where two component in-situ mixing and reaction approach was applied to create a cylindrical flow barrier in a sand layer at depth, were presented. The primary objectives of this field experiment were 1) to test whether the concept of in-situ Al-OM precipitation is a suitable engineering tool and 2) to quantify the extent of permeability reduction that can be achieved under field conditions. According to the simulation results using the 3D process-oriented model, the cylindrical flow barrier can be constructed by separate injection of Al and OM solutions using a combined injection/extraction strategy. During the field installation, it was found that the local soil layering differed considerably from information used in the initial scenario analysis. As a result, significant modifications to the design were made on site and further scenario analyses with the model were conducted to adapt the original

design and to understand the consequences of these modifications. The results show that a cylindrical flow barrier was created, where the permeability of the treated sand was reduced to 2 % of its original value. This demonstrates that applying Al-OM precipitates is a suitable engineering tool to reduce soil permeability in-situ.

Chapter 4 reports on the other field experiment, where a continuous 70 m long and 7 m high vertical flow barrier in a dike body surrounding a water reservoir was created by direct Al-OM floc injection. This alternative approach is proposed to improve the applicability of using Al-OM precipitates to reduce soil permeability for larger-scale applications. The ease of implementation as well as the low cost for field installation are considered as favourable. The scale of this field experiment was much larger with the aim to demonstrate the impact of a flow barrier on the hydraulic head profile in the dike. The field site was divided into two zones (A and B), where two different Al-OM floc concentrations were applied. The results show that a continuous flow barrier is created in zone A. This demonstrates the viability of the direct Al-OM floc injection approach. However, the uncertainties in the actual spatial distribution of the flow barrier makes the quantification of its permeability difficult. In zone B, where a higher floc concentration was applied, field monitoring results reveal that significant local reduction in permeability was achieved. This indicates that the spatial distribution of the Al-OM flocs in-situ is controlled by the input concentration.

Chapter 5 we explore the interaction between OM and Al and the subsequent flocculation process which is one of the fundamental aspects of the technique. A conceptual model is constructed to explain the flocculation mechanism after which a semi-mechanistic model is developed to obtain a quantitative insight regarding the flocculation between Al and OM. Scenario analyses were performed using the model to provide detailed insight into the OM flocculation induced by Al^{3+} ions, in which the role of the type of OM and pH on the OM flocculation with Al^{3+} ions was examined. The results reveal that the competition between cations for binding with OM together with the background pH is crucial in the flocculation of OM. A low pH-level (<4) enhances the protonation of functional groups on OM, as such limits the site-specific binding of Al^{3+} ions to OM molecules. At pH-levels above 6, the availability of ionic Al^{3+} is capped by the precipitation of aluminium hydroxides and consequently deteriorates the effectiveness of Al^{3+} as the coagulant. The optimal pH for Al^{3+} ions to coagulate OM is found between 5 and 6, in which range the Al^{3+} ions out competes H^{+} for binding with OM molecules and thus can lower the surface change on OM adequately to induce flocculation.

This PhD-thesis represents a major step forward towards the application of Al-OM precipitates as a nature-based engineering tool to reduce soil permeability in-situ. Further research effort is required to have a better control of the processes which occur in consortia, and to test this concept under different site conditions and using different implementation strategies.

SAMENVATTING

Het waarborgen van de stabiliteit van dijken is een nationaal veiligheidsvraagstuk voor dichtbevolkte laaggelegen landen in deltagebieden zoals Nederland. Piping is één van de dominante dijkbreukmechanismen in Nederland, waarbij hoge kwelstroomdebieten zanddeeltjes transporteren en vervolgens een 'pijp' vormen onder de dijk. Aanpassing van het kwelstroomveld is daarmee een manier om de dijk te versterken. Er zijn veel succesvolle conventionele benaderingen om een ondergrondse stroombarriére te maken die het kwelstroomveld kunnen veranderen, echter, deze zijn gewoonlijk kostbaar in termen van materialen, energie en arbeid. Gezien de almaar groeiende noodzaak tot het reduceren van CO_2-emissies om klimaatverandering tegen te gaan en de grote economische schaal van het probleem van de dijkstabiliteit in Nederland, is ontwikkeling van alternatieve technieken gewenst. De focus van dit onderzoeksproject is het ontwikkelen van een kosteneffectieve, robuuste en milieuvriendelijke technologie voor in-situ permeabiliteitsreductie van ondergrondse systemen. We hebben ons laten inspireren door de natuur, waar een natuurlijk proces van bodemstratificatie (namelijk podzolisatie) de haalbaarheid aantoont van het benutten van neergeslagen organometallische complexen om de bodempermeabiliteit in situ te verminderen. Het doel van het in dit proefschrift gepresenteerde onderzoek is om, kwantitatief, de haalbaarheid te onderzoeken van het gebruik van van podzolisatie afgeleide benaderingen om een ondergrondse stroombarrière in dijken te realiseren.

Hoofdstuk 2 van dit proefschrift presenteert twee benaderingen voor het toepassen van organometallische complexen om de permeabiliteit van de bodem in situ te verminderen. Deze benaderingen zijn afgeleid van een gedetailleerde analyse van podzolisatie en de daarbij horende flocculatieproces tussen een metaalzout en opgelost organisch materiaal. De eerste benadering is gebaseerd op het in situ mengen en reageren van twee componenten (d.w.z. aluminium (Al) en opgeloste organische stof (OM)) waarbij in-situ vlok vorming optreedt. De tweede benadering maakt gebruik van de directe injectie van reeds gevormde Al-OM-vlokken. Om de haalbaarheid te onderzoeken van het gebruik van deze benaderingen om een ondergrondse stroombarrière ter plaatse te realiseren, is een 3D-procesgericht model ontwikkeld. Een belangrijk aspect van deze modelontwikkeling is het meenemen van de technische randvoorwaarden ter plaatse in de simulatie. Met het model is een reeks scenarioanalyses uitgevoerd om het ontwerp en de evaluatie van de grootschalige experimenten te ondersteunen.

In hoofdstuk 3 worden de resultaten gepresenteerd van een veldexperiment, waarbij we twee componenten in-situ hebben laten mengen en reageren zodat er een cilindrische stromingsbarrière in een zandlaag op diepte is gecreëerd. De doelstellingen van dit veldexperiment waren 1) om te testen of het concept van in-situ Al-OM-precipitatie een geschikt technisch methode is en 2) om de mate van permeabiliteitsvermindering te kwantificeren die onder veldomstandigheden kan worden bereikt. De 3D-simulatieresultaten laten zien dat de cilindrische stroombarrière kan worden geconstrueerd door afzonder-

lijke injectie van Al- en OM-oplossingen. Hiervoor is wel een combinatie van injectie en extractie noodzakelijk. Tijdens installatie van de benodigde infrastructuur in het veld bleek dat de lokale bodemopbouw aanzienlijk verschilde van de informatie die werd gebruikt in de initiële scenarioanalyse. Hierdoor was het nodig om ter plaatse belangrijke wijzigingen in het ontwerp aan te brengen. Additionele scenarioanalyses met het model zijn uitgevoerd om de oorspronkelijke injectie-/extractiestrategie aan te passen en de gevolgen van deze aanpassingen te begrijpen. Interpretatie van de monitoring resultaten laat zien dat er inderdaad een cilindrische stroombarrière is gemaakt in de zandlaag. In deze barrière is de doorlaatbaarheid van het zand teruggebracht tot 2% van de oorspronkelijke waarde. Dit toont aan dat het toepassen van Al-OM-precipitaten een geschikt technisch hulpmiddel is om de permeabiliteit van de bodem in situ te verminderen.

Hoofdstuk 4 beschrijft de tweede veldexperiment, waar een 70 m lange en 7 m hoge verticale stroombarrière is gerealiseerd in een dijklichaam rond een waterreservoir door directe Al-OM vlokinjectie. Deze alternatieve benadering is een doorontwikkeling op wat is beschreven in hoofdstuk 3 en is een verbetering van de toepasbaarheid van het gebruik van Al-OM-precipitaten. Zowel het implementatiegemak als de lagere kosten voor veldinstallatie worden als gunstig beschouwd. De schaal van dit veldexperiment was veel groter in vergelijking met de eerste veldproef omdat er een duidelijke impact van de stromingsbarrière op het hydraulische profiel in de dijk moet worden aangetoond. De veldsite was verdeeld in twee zones (A en B), waar twee verschillende Al-OM-vlokconcentraties zijn toegepast. De resultaten tonen aan dat er een continue stroombarrière wordt gecreëerd in zone A. Dit toont de levensvatbaarheid van de directe Al-OM floc-injectiebenadering aan. De onzekerheden in de daadwerkelijke ruimtelijke verdeling van de stroombarrière maken de kwantificering van de permeabiliteit echter moeilijk. In zone B, waar een hogere vlokconcentratie werd toegepast, laten monitoringresultaten zien dat een significante lokale vermindering van de permeabiliteit werd bereikt. Dit geeft aan dat de ruimtelijke verdeling van de Al-OM-vlokken in situ wordt geregeld door de invoerconcentratie.

In hoofdstuk 5 verkennen we de interactie tussen opgelost organische stof (DOM, 'dissolved organic matter') en Al en het daaropvolgende flocculatieproces dat een van de fundamentele aspecten van de techniek is. Een conceptueel model wordt geconstrueerd om het flocculatiemechanisme te verklaren, waarna een semi-mechanistisch model wordt ontwikkeld om een kwantitatief inzicht te krijgen in de flocculatie tussen Al en DOM. Scenario-analyses werden uitgevoerd met behulp van het model om gedetailleerd inzicht te geven in de DOM-flocculatie veroorzaakt door Al^{3+} ionen, waarin de rol van het type DOM en pH op de DOM-flocculatie met Al^{3+} ionen werd onderzocht. De resultaten laten zien dat de concurrentie tussen kationen voor binding met DOM samen met de achtergrond-pH cruciaal is in de uitvlokking van DOM. Een laag pH-niveau (<4) verbetert de protonering van functionele groepen op het DOM, aangezien dit de plaatsspecifieke binding van Al^{3+} ionen aan DOM-moleculen beperkt. Bij pH-waarden boven 6 wordt de beschikbaarheid van ionisch Al^{3+} beperkt door de precipitatie van aluminiumhydroxiden en verslechtert daardoor de effectiviteit van Al^{3+} als coagulant. De optimale pH voor Al^{3+} ionen om DOM te coaguleren, wordt gevonden tussen 5 en 6. In dit bereik concurreren de Al^{3+} ionen met H^{+} voor binding met DOM-moleculen en de lading aan het oppervlakte van de DOM voldoende kunnen verlagen om flocculatie te

veroorzaken.

Dit proefschrift is een grote stap voorwaarts in de richting van de toepassing van Al-OM-neerslagen als een op de natuur gebaseerd technisch hulpmiddel om de doorlaatbaarheid van de bodem in situ te verminderen. Naast het ontwikkelen van de technologie is verder onderzoek nodig om het maatschappelijk draagvlak te onderzoeken en hoe dergelijke op natuur geïnspireerde methoden in de context van praktijk (met alle complexiteit van dien) kunnen worden ontwikkeld.

1

INTRODUCTION

1

1.1. DIKE STABILITY IN THE NETHERLANDS

Stability of dikes is a national security issue for densely populated low-lying countries situated in delta areas, like the Netherlands. The Netherlands faces a serious threat of flooding because large parts of the Netherlands lie below the mean sea level and the country is faced with potentially high water levels in the main rivers flowing through the county (the rivers Rhine and Meuse). Currently, the Netherlands primarily relies on an extensive flood defence network, which consists of a total length of 3000 kilometres of dams and dikes [1]. The ongoing climate change undeniably increases the occurrence of weather extremes [2]. As a consequence, the sea level continues to rise and river discharges fluctuate with a larger magnitude [3]. The reinforcement of dike structures is a pressing issue in the Netherlands.

One of the imperatives for dike reinforcement is the prevention of the dike failure. One of the dominant dike failure mechanisms in the Netherlands is piping [4, 5], which is caused by high seepage flow rates that transport sand particles and subsequently form a 'pipe' under a dike structure. The progression of the pipe eventually destabilises the entire dike slope if no dike reinforcement measures are taken on time. Typical reinforcement measures either tackle this stability concern using the concept of providing extra confinement to the underlain sand layers (i.e., using berms) or by modifying the seepage flow field [6]. The latter concept has become increasingly attractive because the additional berms require a large amount of surface space that is often not economic or feasible in the Dutch context, where many residents are located in the close vicinity of dikes. Modification of the seepage flow field is commonly achieved by the installation of a flow barrier in the dike body. A number of different approaches are available for the creation of the flow barrier. Conventional approaches use the direct installation of a cut-off sheet pile wall, a diaphragm wall or a sheet pile screen into the dike body [6], while in deep-soil mixing, an example of an alternative approach, the soil is mechanically mixed with hydraulic binder material in-situ to create a flow barrier [7].

The development of alternative techniques is nevertheless desired. Facing the ever-growing awareness of climate change as well as the large economic scale of the dike stability issue in the Netherlands, the requirements for reinforcement techniques have evolved over time. As stated in the Delta Programme [3], new strategies for flood management should address the interplay between water, environment and economy in the context of society. From an economic and environmental perspective, the costs for energy and labour of conventional reinforcement techniques [6, 8] are too high to make them profitable in case of the extensive dike network in the Netherlands. Instead of changing the seepage flow to the level that is necessary for the dike safety, these methods often create a completely impermeable wall in the subsurface and thus reduce the seepage flow to almost stagnant flow conditions. Weber *et al.* [9] concluded that such heavily modified water systems damage the local eco-system severely. An ideal alternative technique should therefore be capable to manage the flow field to meet the engineering requirements, while staying economically effective and environmentally friendly.

1.2. A NATURE-INSPIRED GEO-ENGINEERING SOLUTION

This PhD-thesis is part of the research program Water2014 with project title as SOil Sealing by Enhanced Aluminium and DOM Leaching (SoSEAL), which is financed by the Netherlands Organisation for Scientific Research (NWO). The SoSEAL research project aims to develop the foundations for a cost-effective, robust and environmentally compatible technology for in-situ permeability reduction of sub-surface systems. Controlled reduction in soil permeability is appealing as it allows the construction of a flow barrier that meets the required characteristics (i.e., geometry and permeability) for the particular site. In this way the adverse effects of existing engineering practices on the local environment can be minimised.

The inspiration for developing this new technique comes from the understanding of natural Podzol soils. During Podzolization, the complexation of organic matter (OM) with polyvalent metals, such as iron (Fe) and aluminium (Al) that are naturally present in the soil, leads to the formation of soluble organo-metallic complexes [10, 11]. As a result of their mobility, the soluble organo-metallic complexes infiltrate into high permeability soil layers [11, 12], where the local environmental conditions, i.e., a higher pH level and the abundance of metal cations, become favourable for inducing the precipitation of the organo-metallic complexes [13–15]. The precipitation and accumulation of these organo-metallic precipitates results in a distinct soil layer: the spodic B-horizon. In this spodic B-horizon, the soil permeability is reduced significantly [11, 16]. In addition, due to the persevering effect brought by the metal-OM complexation [17, 18], degradation of precipitated organic matter is little [19] and thus keeping the permeability low. The development of a spodic B-horizon in Podzols inspired us to develop a nature-based geo-engineering solution to reduce soil permeability in-situ using organo-metallic complexes. However, concentrations and species distribution of solutes that naturally infiltrate in soils are often insufficient for reducing permeability for engineering purposes. Therefore, the treatment will be to introduce such solutes in the form of natural OM and Al.

One of the key challenges is to understand the precipitation reaction of OM and Al quantitatively. The metal-OM interaction has been studied relatively extensively in the research communities of soil science and wastewater treatment [20–22]. However, to our understanding, the precipitation aspect of the metal-OM interaction is yet to be developed. A quantitative mechanistic model for describing this precipitation process is particularly crucial for this research project for the desired reduction in soil permeability relies on the quantity of organo-metallic precipitates. In addition, such a mechanistic model could also reflect the impact of environmental conditions, i.e., pH level and metal cation concentrations, on the amount of organo-metallic precipitates. This is because earlier researches [13–15] revealed that the precipitation of organo-metallic precipitates is a function of these environmental conditions. The development of fundamental understanding at the molecular scale is therefore necessary.

The focus of this research project is to innovate a geo-engineering solution based on the studies of Podzolization. Therefore, it is crucial to project the concept in the context of engineering. Full-scale field experiments are a great way to develop the understanding regarding the viability of using Al-OM precipitates to reduce soil permeability in-situ. The design and implementation of full-scale field experiments is challenging

and requires a process understanding that addresses 1) the essence derived from Podzolization, which is the interaction between Al and OM, the subsequent precipitation of Al-OM complexes and the corresponding reduction in soil permeability; and 2) the impact of the achieved reduction in permeability on the engineering perspective of the site, where the engineering conditions are often site specific. In order to translate the concept into a viable geo-engineering solution, multi-physics quantitative modelling was applied. Instead of diving in to the full details of all processes, this model incorporates the essence of the concept while maintaining a high level of flexibility in order to adapt to the engineering conditions on site.

1.3. CO-MAKERSHIP MODEL FOR CARRYING OUT THE RESEARCH PROJECT

In order to implement the full-scale field experiments, this research project embraced the model of 'co-makership', where various partners, i.e., universities, contractors, consultancies and authorities, were engaged. This is particularly necessary because many aspects of the full-scale field experiments are beyond the capacity of universities. In the first place, the sites, i.e., dikes, for executing the experiment had to be made available for applying Al-OM complexes to reduce soil permeability. Also, the stability of dike is a national security issue for the Netherlands. The regulatory requirements are understandably strict [6] and need to be followed. Furthermore, as some have argued that technological innovation is rooted more in technology than in the advancement of science [23], the importance of engineering capacity as well as management expertise available at the industrial partners should not be underestimated. By adapting the 'co-makership' model, we relied on the close collaborations among these partners and thus carried out the innovation in a non-linear way. Also, each of these partners profits collaboratively (illustrated in Table 1.1).

Field-scale field experiments or pilot projects are not only the vehicle for the 'co-makership' concept, where pilot projects can create a safe environment that encourages the partners to take more responsibility proactively and thus strengthen the mutual trust among all partners involved [24], but also essential for demonstrating the viability of the technique in reducing soil permeability in-situ. From the perspective of the intended technique, the requirements on soil permeability reduction are highly specific with respect to each engineering site. Therefore, it is vital to carry out the research in the context of application. In other words, three questions need to be addressed for specific engineering challenges: 1) why reduce soil permeability in-situ can be the solution; 2) how can soil permeability be reduced and 3) what activities are required to implement the approach on site. This all leads to the main focus of this thesis: performing full-scale field experiments to investigate the feasibility of creating vertical flow barriers in dikes using organo-metallic complexes.

The monitoring of the field implementation is important to demonstrate the success of the project, which is crucial for maintaining the result-driven partnership. What is more important is that being able to understand what has occurred during the implementation provides valuable insights for process control. An effective monitoring strategy should enable the quantitative detection of the changes in the system, which in this

case the reduction in permeability leads to changes in the local hydraulic field, i.e., a change in the groundwater table. Though many monitoring methods are available for detecting the change in groundwater table, for instance the installation of monitoring wells [25], the challenge lies in the locality of the change in the hydraulic field. As stated in the literature [26, 27], the de-watering effect of a finite flow barrier is strongest at close vicinity. Furthermore, due to the occurrence of preferential flow, a discontinuity in the constructed flow barrier may offset its de-watering effect entirely [28], implying that the passive monitoring of change in groundwater table may not be able to reflect the impact of the reduction in permeability. Therefore, we explicitly emphasised devising the monitoring strategy for both of the field experiments. Results obtained from scenario analyses performed with multi-physics quantitative models were used to determine the locations of monitoring wells where the expected changes in groundwater table are most pronounced. Further scenario analyses were performed to design pumping or infiltration tests in the monitoring wells in order to provide an additional set of data for quantifying the reduction in soil permeability. In the evaluation of the field experiments, data acquired on-site were interpreted collectively with the modelling results which led to a better insight into the in-situ processes and options for controlling these processes.

1.4. STRUCTURE OF THIS THESIS

The main objective of this thesis is to innovate a nature-based technique for reducing soil permeability in-situ. In order to facilitate the development of the nature-based technique, four research question were formulated: 1) what are the mechanisms that dominate the precipitation reaction between Al and OM and how can the amount of precipitates be quantified? 2) how should the concept derived from Podzolization and subsequent research be translated into an approach that can be used to engineer a flow barrier in dikes? 3) what approaches should be used to quantify the reduction of the soil permeability in order to evaluate the success of implementation in the field experiments? and 4) how can the efficiency of the technique be improved? These four research questions are addressed in this thesis.

This thesis is structured as follows. In Chapter 2, we give a literature review and propose two approaches for applying organo-metallic complexes to reduce soil permeability in-situ. The first is an in-situ approach based on a two component mixing and reaction process and the second uses direct injection of Al-OM flocs. A 3D reactive transport model was developed to study the feasibility of using these two approaches to create flow barriers in dikes at two different sites. In Chapters 3 and 4 we report the implementation and evaluation of two full-scale field experiments where these two approaches were applied, in which the approach applied in the second field experiment was proposed to improve the cost-effectiveness of the technique. In Chapter 5 we explore the interaction between OM and Al and the subsequent flocculation process which is one of the fundamental aspects of the technique. A conceptual model is constructed to explain the flocculation mechanism after which a semi-mechanistic model is developed to obtain a quantitative insight in to the flocculation between Al and OM. In Chapter 6 we summarise the effectiveness of the 'co-makership' model in innovating this nature-based geo-engineering technique, after which we identify some remaining knowledge gaps for further research and development.

1

Table 1.1: Definition of actors in the 'co-makership' model

Actor	Contributions	Collective benefits
Universities	• Research effort for understanding fundamentals of processes • Developing the concepts of the technique	• Scientific and applied knowledge • A new technique to diversify the engineering tool kits • Access to potential markets • A model to carry out innovation • Network opportunities
Contractors	• Technical innovation of delivery hardware • Engineering capacity	
Consultancies	• Management expertise • Engineering experience	
Government	• Research funding • Regulatory guidelines	
Problem owners	• Real sites for study the viability of the technique • Additional funding for applying the technique	

REFERENCES

[1] K. W. Pilarczyk, *Flood protection and management in the Netherlands,* in *Extreme Hydrological Events: New Concepts for Security* (Springer Netherlands, Dordrecht, 2007) pp. 385–407.

[2] D. Coumou and S. Rahmstorf, *A decade of weather extremes,* Nature Climate Change **2**, 491 (2012).

[3] Delta Commissioner, *Ministry of transport public works and water management, Ministry of agriculture nature and food quality, ministry of housing spatial planning and the environment, Dutch national government*, Tech. Rep. (2010).

[4] S. van Baars and I. M. van Kempen, *The causes and mechanisms of historical dike failures in the Netherlands,* E-WAter **2009**, 1 (2009).

[5] R. M. J. Schielen and L. F. M. Van Den Aarsen, *A strategy for Dutch rivers to handle climate change and new Safety Standards,* in *6th International Conference on Flood Management* (2014) pp. 1–9.

[6] J. M. van Loon-Steensma, H. A. Schelfhout, and P. Vellinga, *Green adaptation by innovative dike concepts along the Dutch Wadden Sea coast,* Environmental Science and Policy **44**, 108 (2014).

[7] A. Porbaha, S. Shibuya, and T. Kishida, *State of the art in deep mixing technology. Part III: Geomaterial characterization,* Ground Improvement **4**, 91 (2000).

[8] P. Suer, N. Hallberg, C. Carlsson, D. Bendz, and G. Holm, *Biogrouting compared to jet grouting: Environmental (LCA) and economical assessment,* Journal of Environmental Science and Health - Part A Toxic/Hazardous Substances and Environmental Engineering **44**, 346 (2009).

[9] A. Weber, X. F. Garcia, and C. Wolter, *Habitat rehabilitation in urban waterways: the ecological potential of bank protection structures for benthic invertebrates,* Urban Ecosystems **20**, 759 (2017).

[10] H. A. Anderson, M. L. Berrow, V. C. Farmer, A. Hepburn, J. D. Russell, and A. D. Walker, *A reassessment of podzol formation processes,* Journal of Soil Science **33**, 125 (1982).

[11] U. Lundström, N. van Breemen, and D. Bain, *The podzolization process. A review,* Geoderma **94**, 91 (2000).

[12] P. van Hees, U. Lundström, and R. Giesler, *Low molecular weight organic acids and their Al-complexes in soil solution—composition, distribution and seasonal variation in three podzolized soils,* Geoderma **94**, 173 (2000).

[13] U. S. Lundström, N. van Breemen, D. C. Bain, P. A. van Hees, R. Giesler, J. P. Gustafsson, H. Ilvesniemi, E. Karltun, P. A. Melkerud, M. Olsson, G. Riise, O. Wahlberg, A. Bergelin, K. Bishop, R. Finlay, A. G. Jongmans, T. Magnusson, H. Mannerkoski,

A. Nordgren, L. Nyberg, M. Starr, and L. Tau Strand, *Advances in understanding the podzolization process resulting from a multidisciplinary study of three coniferous forest soils in the Nordic Countries,* Geoderma **94**, 335 (2000).

[14] K. G. Nierop, B. Jansen, and J. M. Verstraten, *Dissolved organic matter, aluminium and iron interactions: Precipitation induced by metal/carbon ratio, pH and competition,* Science of the Total Environment **300**, 201 (2002).

[15] B. Jansen, K. G. J. Nierop, and J. M. Verstraten, *Influence of pH and metal/carbon ratios on soluble organic complexation of Fe(II), Fe(III) and Al(III) in soil solutions determined by diffusive gradients in thin films,* Analytica Chimica Acta **454**, 259 (2002).

[16] V. C. Farmer and D. G. Lumsdon, *Interactions of fulvic acid with aluminium and a proto-imogolite sol: The contribution of E-horizon eluates to podzolization,* European Journal of Soil Science **52**, 177 (2001).

[17] D. Sauer, H. Sponagel, M. Sommer, L. Giani, R. Jahn, and K. Stahr, *Podzol: Soil of the year 2007. A review on its genesis, occurrence, and functions,* Journal of Plant Nutrition and Soil Science **170**, 581 (2007).

[18] R. Mikutta and K. Kaiser, *Organic matter bound to mineral surfaces: Resistance to chemical and biological oxidation,* Soil Biology and Biochemistry **43**, 1738 (2011).

[19] T. Scheel, B. Jansen, A. J. van Wijk, J. M. Verstraten, and K. Kalbitz, *Stabilization of dissolved organic matter by aluminium: a toxic effect or stabilization through precipitation?* European Journal of Soil Science **59**, 1122 (2008).

[20] E. Tipping, C. Rey-Castro, S. E. Bryan, and J. Hamilton-Taylor, *Al (III) and Fe (III) binding by humic substances in freshwaters, and implications for trace metal speciation,* Geochimica et Cosmochimica Acta **66**, 3211 (2002).

[21] L. Weng, E. P. M. J. Fest, J. Fillius, E. J. M. Temminghoff, and W. H. Van Riemsdijk, *Transport of Humic and Fulvic acids in relation to metal mobility in a copper-contaminated acid sandy soil,* Environmental Science & Technology **36**, 1699 (2002).

[22] J. Duan and J. Gregory, *Coagulation by hydrolysing metal salts,* Advances in Colloid and Interface Science **100-102**, 475 (2003).

[23] N. Rodet-Kroichvili, K. Cabaret, and F. Picard, *New Insights into Innovation: The Business Model Approach and Chesbrough's Seminal Contribution to Open Innovation,* Journal of Innovation Economics **15**, 79 (2014).

[24] J. van Popering-Verkerk and A. van Buuren, *Developing collaborative capacity in pilot projects: Lessons from three Dutch flood risk management experiments,* Journal of Cleaner Production **169**, 225 (2017).

[25] M. O. Cuthbert, L. A. McMillan, S. Handley-Sidhu, M. S. Riley, D. J. Tobler, and V. R. Phoenix, *A field and modeling study of fractured rock permeability reduction using microbially induced calcite precipitation,* Environmental Science & Technology **47**, 13637 (2013).

[26] P. F. Hudak, *Locating groundwater monitoring wells near cutoff walls*, Advances in Environmental Research **5**, 23 (2001).

[27] E. I. Anderson and E. Mesa, *The effects of vertical barrier walls on the hydraulic control of contaminated groundwater*, Advances in Water Resources **29**, 89 (2006).

[28] Y. Yihdego, *Evaluation of Flow Reduction due to Hydraulic Barrier Engineering Structure: Case of Urban Area Flood, Contamination and Pollution Risk Assessment*, Geotechnical and Geological Engineering **34**, 1643 (2016).

2

A NUMERICAL TOOLBOX TO INVESTIGATE THE FEASIBILITY OF USING ALUMINIUM-ORGANIC MATTER COMPLEXES TO REDUCE SOIL PERMEABILITY IN-SITU

Developing a nature-based geo-engineering technique to reduce soil permeability can provide a solution to a wide range of engineering challenges. Inspired by a natural soil formation process, Podzolization, we aim to reduce soil permeability in-situ by applying the precipitates of aluminum (Al) and organic matter (OM). Two different delivery approaches were proposed to introduce the Al-OM flocs into the soils, where one approach makes use of the two component (i.e., Al and OM solutions) mixing and reaction and the other approach adapts the direct-push injection of Al-OM flocs. Given the aim is to develop a practical technique, it is therefore essential to test the concept in the context of engineering, for instance, with full-scale field experiments.

A 3D process-oriented model was developed in COMSOL Multiphysics (v5.3) in order to facilitate the design and evaluation of the full-scale experiments where the two delivery approaches were applied to install a flow barrier in two dikes. This model was developed with the idea to incorporate the essence of the proposed approaches while maintaining a high level of flexibility in order to adapt to the engineering conditions on site. Scenario analyses were performed with the model to 1) specify the requirements of the flow barrier in regard to the aims of respective field experiment; 2) design the injection strategy using corresponding delivery approach to create the flow barrier on sites and 3) assess the quantifiability of permeability reduction using exiting monitoring technique.

Regarding the quantifiability of permeability reduction, the simulations show that a cylindrical flow barrier is necessary for the first field experiment, which was aimed to test the feasibility of using Al-OM precipitates to reduce soil permeability in-situ and thus is small in size. The simulation results indicate that the two component mixing and reaction is feasible to create the cylindrical barrier with a unique injection well setting and a specific injection strategy. Further scenario analyses were applied to determined the optimal design parameters, such as injection rate and extraction rate. The aim of the other field experiment was to demonstrate the impact of the installed flow barrier on the local hydraulic field, and this barrier was intended to be installed with the direct injection of Al-OM flocs. The injection strategy to install a 70 m long vertical flow barrier with a height of 7 m in the dike body using the direct-push system was designed based on the simulation results. These results were later applied to guide the implementation of the field experiments and to facilitate the interpretation of field-acquired data in order to understand to what extent the permeability has been reduced on site.

2.1. INTRODUCTION

One way of innovating environmentally friendly engineering solutions is to seek inspiration from naturally occurring processes. One example is microbially induced calcite precipitation (MICP), which relies on in-situ calcite precipitation to reduce soil permeability and strengthen the soil [1–3]. We took inspiration from a natural soil formation process, namely Podzolization, to develop a bio-based geo-engineering solution to reduce soil permeability in-situ. During Podzolization, a nearly impermeable spodic B-horizon is formed by the precipitation and accumulation of organo-metallic precipitates [4–6]. The formation of organo-metallic precipitates is commonly understood as the consequence of the complexation of organic matter (OM) with polyvalent ions of metals, such as iron (Fe) and aluminum (Al) [4, 5].

In addition to being environmentally friendly, the particular appeal of using organo-metallic complexes to reduce the permeability of soil lies in its promising effectiveness and potentially broad applicability. Organo-metallic precipitates occur as floc-like structures with sizes that can be as large as 1 cm [7]. Given their large size, these flocs can reduce the permeability of a porous medium by covering the pore throat [8, 9] instead of filling the pores as it is the case for calcite mineral [1]. This implies that less mass of metal-OM flocs is needed to lower the permeability of soil to the targeted level in comparison to the usage of mineral precipitates.

Based on the unique chemical/physico-chemical characteristics of the metal-OM complexation, we propose two approaches to apply metal-OM flocs to reduce soil permeability in-situ: 1) the in-situ mixing and reaction of two components (i.e., Al and OM solution); and 2) the shear-dependent direct metal-OM flocs injection. The precipitation of metal-OM flocs can be induced by separate injection of required components (i.e., metal and OM solutions) and their subsequent mixing and reaction in-situ. On the other hand, it is well known that the floc size of metal-OM flocs is shear-dependent [10–12], meaning that a high shear condition leads to the breakage of the floc structure and thus results in colloids that are small enough to be transported through a porous medium for a certain distance [1, 13, 14]. More importantly, these small flocs will re-grow in size as soon as low shear conditions prevail [11, 12], and the re-grown flocs can subsequently reduce the soil permeability. Due to the fact that the shear is linearly correlated to the Darcy flow velocity [15], the floc transportation can therefore be manipulated by controlling the flow field. In this study, the Al is chosen as metal cation source, meaning that metal-OM flocs are in the form of Al-OM flocs.

The crucial step towards realising an innovative concept into a compelling technique lies the examination of the application under field conditions. Though the viability of using these two approaches to reduce soil permeability had been proven by a number of laboratory experiments performed in this research project, the intrinsic limitations of these lab-based experiments are obvious: they are small in scales and are under well-controlled conditions. For instance, the flow condition in the column experiment setting is strictly linear while the injection practice on-site often leads to a radial flow field, where the flow rates decrease along with increasing radial distance [15]. This implies that the knowledge derived from laboratory experiments is not directly applicable to field applications. Testing the nature-based geo-engineering technique under real field conditions is the only way to understand its viability and thus provides insights for the

further development. Prior to the implementation of a field experiment, a proper design is necessary, given the high-cost and high-complexity nature of such experiment.

The aim of this study is to develop a numerical toolbox that incorporates the essence of the proposed approaches while maintaining a high level of flexibility in order to adapt to the engineering conditions on site. The development of the 3D reactive transport model was based on a review of the fundamental processes behind the two proposed approaches. Given the fact that a fully mechanistic understanding of the metal-OM interaction as well as the metal-OM flocs behaviour has yet to develop, these processes were approximated empirically in the model development based on earlier experimental observations. A series of scenario analyses were performed with the model to determine the design parameters for two field experiments, which are using the mixing and reaction of two components to install a flow barrier in a confined aquifer; and applying direct injection of Al-OM flocs to install a flow barrier in an unconfined aquifer respectively. The objectives of the scenario analysis are 1) capturing the essential site conditions of each field site; 2) simulating deterministic aspects of processes that control the Al-OM flocs production, mobility and precipitation; 3) designing the injection/extraction strategy for introducing Al-OM flocs in to the soils in order to achieve the required permeability reduction; 4) assessing the cost effectiveness of the approaches in regard to the material usage and implementational time; 5) assessing the quantifiability of permeability reduction given available measurement techniques; and 6) providing a framework for qualitatively and quantitatively interpreting the field-acquired data.

2.2. THEORETICAL BACKGROUND

2.2.1. THE CHEMICAL CHARACTERISTICS OF OM

Organic matter, especially natural organic matter, is known to be a mixture of various organic compounds that consist of plant residuals and highly oxidised carbon in carboxylic acids [16]. As a result, a high level of intrinsic complexity has been observed when describing the chemical characteristics of OM. According to Lehmann and Kleber [17], a fundamentally robust characterisation of OM should address the contribution of all individually distinct compounds, meaning that a continuum model is preferred. However, the development of such continuum models relies on extensive dataset at a very detailed level, which are often not available or feasible [18]. Alternatively, the conventional humification theory focuses on the overall characteristics of a bunch of unidentifiable organic compounds [18, 19]. These unknown/unidentifiable organic compounds are called humic substances [18, 19], and are subdivided into HA (humic acid), FA (fulvic acid) and Humin based on an operational proxy, i.e., the solubility of OM in alkaline extracts [20].

The complexation between metal ions with OM is often interpreted in the context of metal-ligand interaction [18, 19]. The ion-binding characteristics of OM are accordingly defined by its functional groups. Carboxylic and phenolic groups, among a large variety of functional groups that are identified on OM, are often considered as the dominating binding sites [18, 19]. According to Rittle *et al.* [21], the carboxylic group accounts for 78%-90% of the total acidity of FA, while HA contains less (69-82%) (i.e., based on standardised samples from the International Humic Substances Society, IHSS), and the remaining acidity is mostly attributed to the phenolic group. The protonation/deprotonation

reaction of carboxylic and phenolic groups is an important process to define their reactivity and is shown in Equation 2.1 [22, 23]. Carboxylic group is known to be a stronger acid than phenolic group. Consequently, the deprotonation of the phenolic group takes place when the pH is higher than 9.5, while the carboxylic group deprotonates at pH-values higher than 4.4 [23]. As expressed in Equation 2.1, the deprotonation of functional groups leads to a negative charge on the surface of OM molecules.

$$\begin{cases} \mathrm{RCOOH} \longleftrightarrow \mathrm{RCOO^- + H^+} & \text{Carboxylic} \\ \mathrm{ROH} \longleftrightarrow \mathrm{RO^- + H^+} & \text{Phenolic} \end{cases} \tag{2.1}$$

Given the abundance and high acidity of carboxylic group (i.e., dissociates completely under neutral pHs), carboxylic group is the major contributor of the net negative surface charge on OM molecules. On the other hand, Chappaz and Curtis [24] concluded that phenolic group is the most important binding sites for the interaction with metal ions. In fact, the binding affinities of various metal ions such Al^{3+}, Fe^{3+} and Cu^{2+} to the phenolic group are much higher than that to the carboxylic group [25, 26].

2.2.2. HYDROLYSIS OF MONOMERIC AL^{3+}

The hydrolysis of metal cations in water is a well-known process. The successive hydrolysis reaction of monomeric Al^{3+} is summarised in Table 5.1, in which the precipitation reaction of aluminium hydroxides is also included for it affects the availability of ionic Al^{3+} in liquid phase significantly. It should be noted that reactions listed in Table 5.1 is an oversimplification, where other hydrolysis products of Al such as dimeric, trimeric and polynuclear product are known to exist. However, these products are often ignored because they may not noticeably affect the speciation process [27].

In addition to the determination of the set of reactions, the concentration of hydrolysed species depends heavily on the equilibrium constants (K) of respective reactions. The equilibrium constants (K) in Table 5.1 are taken from the minteq.v4 database. For the solid Al-phase product we selected the solubility constant of amorphous aluminium hydroxides mineral. According to Duan and Gregory [27], the amorphous precipitates that form initially are highly relevant in the context of metal-OM interaction. As reflected by the inclusion of the proton concentration in all equilibrium reaction equations in Table 5.1, the hydrolysis of Al is strongly influenced by the background pH. With equilibrium constants available, the concentrations of the various hydrolysed species as a function of pH can be simulated. We use the ORCHESTRA simulator [28] to calculate the concentrations of each hydrolysed Al species in the liquid solution as well as the amount of precipitated amorphous aluminium hydroxides as a function of pH (shown in Figure 2.1).

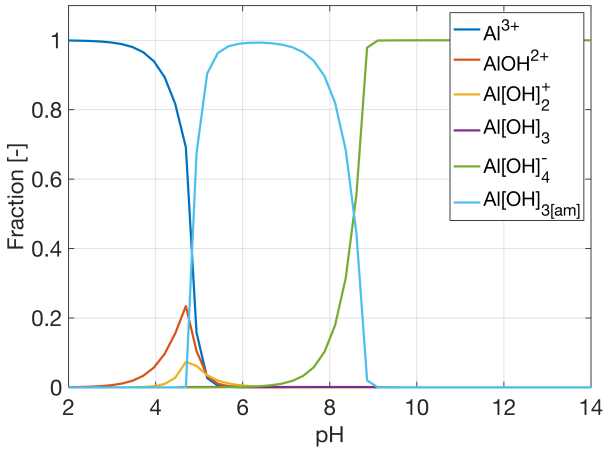

Figure 2.1: Mole fractions of dissolved hydrolysis products in equilibrium with amorphous hydroxides.

Table 2.1: Hydrolysis of Al^{3+} ions in an aqueous system

Liquid phase		
$Al^{3+} + H_2O \longleftrightarrow Al(OH)^{2+} + H^+$	$\log_{10} K_1 = -4.99$	(1)
$Al^{3+} + 2H_2O \longleftrightarrow Al(OH)_2^+ + 2H^+$	$\log_{10} K_2 = -10.09$	(2)
$Al^{3+} + 3H_2O \longleftrightarrow Al(OH)_{3(aq)} + 3H^+$	$\log_{10} K_3 = -16.79$	(3)
$Al^{3+} + 4H_2O \longleftrightarrow Al(OH)_4^- + 4H^+$	$\log_{10} K_4 = -22.60$	(4)
Solid phase		
$Al^{3+} + 3H_2O \longleftrightarrow Al(OH)_{3[am]} + 3H^+$	$\log_{10} K_{sp} = -10.80$	(5)

2.2.3. COMPLEXATION BETWEEN OM AND AL

The complexation between metal ions and OM is often understood to be a combined process of metal-ligand binding and electrostatic interaction [18, 29]. The deprotonation of carboxylic and phenolic sites, the dominating functional groups on OM, creates free pairs of electrons and thus leads to coordination with cations in order to achieve a completed electronic outer shell [19, 30]. This process is called site-specific ion-binding [30]. In addition to the site-specific ion-binding, the deprotonation of functional groups on OM also create a net negative charge on OM molecules (Equation 2.1). As a consequence, electrostatic interaction takes place between OM molecules (negatively charged) and metal cations (positively charged) in solution.

2.2.4. PRECIPITATION/FLOCCULATION OF AL-OM COMPLEXES

The metal-OM precipitates contribute to the reduction of soil permeability. Nierop *et al.* [31] and Jansen *et al.* [32] performed a serious of experiments to understand the precipitation behaviour of Al-OM complexes at different pH-levels. Their results show that

the occurrence of the precipitation/flocculation of Al-OM complexes primarily correlates with the relative availability of Al: precipitation occurs as soon as the molar metal to carbon ratio (M/C ratio) is above 0.03 [31, 33].

Weng *et al.* [34] took a step further where they approached the relative abundance of metal cation from the perspective of calculated electrostatic potential. They found that the increasing metal cation concentration leads to a decrease of the Donnan potential on OM molecules, and when the Donnan potential is sufficiently lowered (< -0.08 V), the precipitation/flocculation takes place [34]. In fact, this view of interpreting the precipitation/flocculation aligns well with DLVO theory that prevails in the field of water treatment. DLVO theory has been often cited to explain the flocculation of OM using metal salts [27, 35, 36]. According to DLVO theory, the addition of positively charged metal cations neutralises the negative charge of OM particles and as a consequence, precipitation/flocculation occurs.

In addition, another mechanism that leads to the flocculation of OM using Al salt has been reported in the literature [27, 37, 38], namely sweep flocculation. Sweep flocculation involves little ion-OM interaction, instead it is attributed to formation of amorphous aluminium hydroxides, which are very small in size and thus have a very large surface area. For this reason, amorphous aluminium hydroxides co-precipitate with OM molecules when they are formed in large quantity [10].

2.2.5. PHYSICO-CHEMICAL BEHAVIOUR OF AL-OM FLOCS

The Al-OM flocs are cloud-like aggregates, which are formed by the constant collision between particles [7, 39]. Depending on the characteristics of OM and environmental conditions, the flocs found in an aquatic system can range from a few µm [23] up to 1000 µm [7]. The size of these flocs is important for it directly determines the settling velocity and thus transportation distances [40]. For instance, flocs with a size in the low range can be transported through a porous medium for a certain distance [1, 14], while larger flocs are subject to filtration and thus leads to their deposition [9].

In natural systems or during practical applications, flocs are nearly always under the influence of background fluid motion [27], which has a profound impact on the size of flocs. The size of flocs is capped by the applied shear because existing floc aggregates can not withstand large shear forces and thus break into smaller particles [10, 41]. In addition, the collision efficiency inevitably decreases as the floc size gets bigger [42]. Due to this dynamic balance between floc growth and breakage, a steady particle size distribution is often observed and this distribution primarily depends on the applied shear force [7, 27, 39, 43, 44]. The floc size as a function of shear is expressed mathematically as Equation 2.2 [7].

$$\log d = \log C - \gamma \log G \tag{2.2}$$

where d is the floc diameter $[L]$; C is the floc strength constant $[-]$; γ is the stable floc size exponent and G is the average velocity gradient $[1/T]$, which is equivalent of shear.

Though high shear conditions lead to the breakage of large-sized flocs almost instantaneously, this breakage is reversible, meaning that small flocs will regrow in size when the imposed shear conditions become low again [11, 12, 41, 45]. The extent of the recovery of size and regrow kinetics depend on many factors, including the type coagulant

(i.e., polymer or monomer) [45], the dosage of coagulant [12], the flocculation mechanisms (i.e., charge neutralisation and sweep flocculation) [10] and the shear history [41].

2.2.6. FLOW AND TRANSPORT

The flow of groundwater through soils is often described with Darcy's law, which shows that the flow velocity is collectively controlled by hydraulic gradient and the hydraulic conductivity of the porous medium (shown in Equation 4.4) [46].

$$\mathbf{u} = \frac{\mathbf{K} k_r(S_e)}{\mu}(\nabla p + \rho g \nabla z) \tag{2.3}$$

By conserving the mass balance, the governing equation for flow of a fluid through porous media is formulated mathematically as Equation 2.4 [47].

$$\frac{\partial}{\partial t}(\varepsilon_p \rho) + \nabla \cdot (\rho \mathbf{u}) = Q_m \tag{2.4}$$

where t is time $[T]$; ε_p is the porosity $[L^3/L^3]$;$\mathbf{u}$ is the Darcy velocity $[L/T]$; S_w is the saturation degree $[L^3/L^3]$; k_r is the relative permeability $[-]$, which is a function of effective saturation degree S_e, $[L^3/L^3]$; Q_m is the volumetric source/sink term $[L^3/L^3T]$; μ is dynamic viscosity of the fluid $[M/LT]$; ρ is the fluid density $[M/L^3]$; g is the gravity acceleration constant $[L/T^2]$; $\mathbf{K}$ is the hydraulic conductivity tensor $[L/T]$. p indicates the pressure head $[L]$; and z is the vertical direction assumed positive upwards $[L]$.

The movement of solutes/particles is another important transport phenomenon. For completely dissolved compounds, transport is based on advection and hydrodynamic dispersion [47]. The governing equation of advection and dispersion under fully saturated situation is given below in Equation 2.5.

$$\frac{\partial c_i}{\partial t} - \nabla \cdot \mathbf{D}_i \nabla c_i + \nabla \cdot \mathbf{u} c_i = R_i + S_i \tag{2.5}$$

As stated above, the Al-OM complexes are not necessarily fully dissolved. In term of the transport of Al-OM flocs, modification to the advection-dispersion equation is required to represent the interaction with the solid matrix, such as the deposition of flocs by the filtration mechanism [9, 48] (Equation 2.6) .

$$\begin{cases} \frac{\partial}{\partial t}(\varepsilon_p c_i) + \frac{\partial(\rho_b s)}{\partial t} = \nabla \cdot \mathbf{D}_i \varepsilon_p \nabla c_i - \nabla \cdot \mathbf{u} \varepsilon_p c_i + R_i + S_i \\ \frac{\partial(\rho_b s)}{\partial t} = f(c_i, s) \end{cases} \tag{2.6}$$

where c_i is the concentration of solute i $[M/L^3]$; $\mathbf{D}_i$ is the dispersion tensor $[L^2/T]$; R_i is the reaction term of solute i $[M/L^3T]$ and S_i is the volumetric source/sink term of solute i $[M/L^3T]$; s is the mass of deposited particles per unit mass of the porous medium $[M/M]$; ρ_b is the buck density of deposited particles $[M/L^3]$ and f is the user-specific function denoting the deposition particles as a function of flocs concentration in both liquid and solid phase.

2.2.7. REDUCTION IN PERMEABILITY

The precipitation reaction or deposition process in a porous medium results in a reduction in permeability [8, 49–52]. Some researchers interpret this reduction in permeability as the direct consequence of a reduction of porosity, which is caused by the precipitates in the pore spaces [49, 50, 52]. In line with this view, the empirical Kozeny Carman equation (Equation 2.7 [53].), which correlates the change in permeability to the change in porosity, is adapted to describe the reduction in permeability achieved by precipitation [52, 53].

$$K(s) = \left(\frac{\varepsilon_p(s)}{\varepsilon_{p_o}}\right)^3 K_o \tag{2.7}$$

where $K(s)$ express the hydraulic conductivity as a function of the mass of precipitates $[L/T]$; $\varepsilon_p(s)$ is reduced porosity which is a function of the mass of precipitates $[L^3/L^3]$, and ε_{p_o} and K_o are the initial porosity and hydraulic conductivity respectively.

However, this pore-filling based estimation might be problematic when it comes to address the particle-deposition caused permeability reduction, especially for large-sized particles that are larger than the pore space. Fundamentally, the permeability of a porous medium is a combined result of the size and quantity of pore space and how these pore spares are connected [54]. Large-sized particles therefore are subject to mechanical filtration, which refers to the complete retention of particles at the pore throat, and thus can lead to a much more enhanced reduction in permeability [8, 9, 51]. The mathematical formulation of the filtration-caused permeability is, to our knowledge, has yet to be further developed.

2.3. MATERIAL AND METHODS

2.3.1. TWO APPROACHES OF APPLYING AL-OM FLOCS

Two approaches for reducing soil permeability using Al-OM complexes were proposed. The first approach took direct inspiration from Podzolization, where the interaction between OM and metal cation leads to the precipitation of metal-OM complexes in-situ. The formation of Al-OM precipitates was induced by separate injection of Al and OM solutions into the subsurface, and the mixing of the components was stimulated by dispersion.

The second approach was developed after a first pilot experiment using the first approach had been evaluated, where the improvement of efficiency (i.e., implementation duration and material usage) was identified as the key focus for further development. This new approach inherited the essence of the concept, which is to reduce soil permeability with Al-OM complexes, while adapted an alternative delivery method to introduce the Al-OM complexes to the targeted zone. The alternative delivery method depended on the ex-situ production Al-OM flocs and made use of the shear-dependent size of Al-OM flocs to inject the flocs into the subsurface. Due to the fact that this approach only involved one component, no mixing and reaction were therefore needed in-situ. A schematic illustration of the two approaches is given in Figure 2.2.

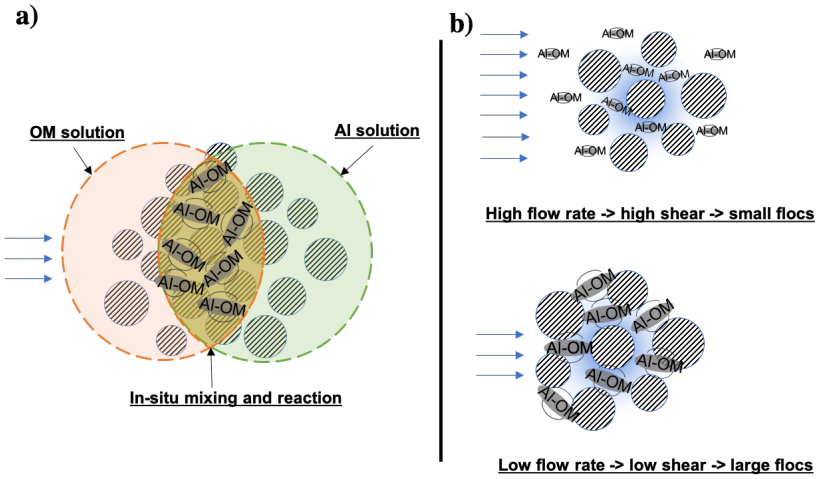

Figure 2.2: Schematic illustration of these two approaches, where a) denotes the in-situ mixing and reaction of two components and b) shows the shear-dependent direct Al-OM flocs injection.

2.3.2. AIMS AND SITE CONDITIONS OF THE TWO FIELD EXPERIMENTS

The two approaches were applied to install flow barriers under distinctly different site conditions. The two-component mixing and reaction approach was applied at a dike along the river Lek, the Netherlands. The aim of this first field experiment was to test the feasibility of reducing soil permeability in-situ using Al-OM complexes. The size of this pilot site covers a surface area of 100 m^2 and is small in comparison to the total length of the dike stretch (approximately 900 m). The flow barrier was planned to be installed in the confined Holocene sand aquifer located between 6 and 8 m below ground surface (bgs), which has a hydraulic conductivity of around 10^{-4} m/s. Further details on the site conditions are available in Chapter 3.

A second field experiment was intended with different aim, which was to demonstrate the impact of a flow barrier on the hydraulic head profile in the dike, and was carried out using the shear-dependent direct flocs injection approach. The field site covers a surface area of 1260 m^2, and it is part of an 8 km long dike that surrounds the water reservoir de Gijster in the Biesbosch. At this particular site, the groundwater table at the toe of the dike is above the surface and results in wet soil conditions, which then requires considerable maintenance effort. The installation of a flow barrier in the dike was designed to lower the groundwater table at the toe of the dike. The dike body consists of medium to coarse sand in the dike structure and is underlain by a fine to medium sand that reaches to a depth of approximately -3.5 m NAP (Dutch reference system). Below this we find a low permeability peat layer with varying thickness (up to 1.5 m). Hydraulically this is a unconfined aquifer that consisted of multiple layers. The hydraulic conductivity of the unconfined aquifer is approximately 10^{-4} m/s. Chapter 4 elaborates in details about this field experiment.

2.3.3. MODELLING AND SCENARIO ANALYSIS

The aim of the model development is to provide a design tool to investigate the feasibility of installing a flow barrier using the different approaches in-situ. We chose to focus on the detailed description of deterministic processes, such as flow of groundwater and reactive solute/particle transport. In addition, we correlated the mass of precipitated Al-OM flocs to soil permeability reduction in the system based on our laboratory observations because little quantitative understanding of the permeability reduction effect of Al-OM flocs can be found in the literature. The interaction between Al and OM solutions as well as the breakage and regrowth behaviour of Al-OM flocs were approximated using empirical correlations as well. A 3D reactive transport model was implemented in COMSOL Multiphysics (v5.3), coupling Darcy's law (Equation 4.4 and 2.4), solute/particle transport (Equation 2.5 or 2.6) and other user-defined processes.

FIRST APPROACH: MIXING AND REACTION OF TWO COMPONENTS

The mixing and reaction of the two injected solutions results in the formation of Al-OM precipitates and thus reduces the soil permeability. Earlier laboratory experiments were carried out to understand the reactivity of Al and OM source that were used in this research project (details are available in Chapter 3, and will not be repeated here). The results of these experiments reveal that insoluble Al-OM complexes precipitate instantaneously when the M/C ratio is above 0.06. Therefore, the interaction between Al and OM is implemented as a two-component reaction in the model (Equation 2.8), where the first order precipitation rate (Equation 2.9) is assumed.

$$a\mathrm{Al}_{(aq)} + b\mathrm{OM}_{(aq)} \rightarrow c\text{Al-OM}_{(s)} \tag{2.8}$$

$$R_p = \begin{cases} k_p c_{\mathrm{OM}} & \mathbf{c}_{\mathrm{Al}}/\mathbf{c}_{\mathrm{OM}} \geqq 0.06 \\ 0 & \mathbf{c}_{\mathrm{Al}}/\mathbf{c}_{\mathrm{OM}} < 0.06 \end{cases} \tag{2.9}$$

where a, b and c are stoichiometric coefficients, in this study we assumed $b = c = 1$ and $a = 0.06$; R_p is the precipitation rate $[M/TL^3]$; k_p is the rate constant for precipitation $[1/T]$; c_{Al} and c_{OM} are the concentration of Al and OM respectively. The challenge in this modelling development is to correlate the mass of Al-OM precipitates to the permeability reduction. This was done empirically using an embedded ramp function in COMSOL Multiphysics, where a threshold precipitate mass level is specified, above which a maximum permeability reduction of 4 orders of magnitude occurs. This magnitude of permeability reduction was derived from a laboratory experiment (data not shown). The fast reaction kinetics are approximated by adjusting the rate parameters in Equation 2.9, and the occurrence of the precipitation reaction is determined by the M/C ratio.

SECOND APPROACH: SHEAR-DEPENDENT DIRECT FLOCS INJECTION

This approach relies on the shear-dependency of Al-OM flocs size to manipulate the transportation status of injected Al-OM flocs. This shear-dependent transport status is implemented by specifying Equation 2.10 in the governing equation for particle transport (Equation 2.6).

$$\frac{\partial(\rho_b s)}{\partial t} = f(c_{\text{flocs}}, u) = \begin{cases} k_f c_{\text{flocs}} & u \leqq u_{Lim} \\ 0 & u > u_{Lim} \end{cases} \tag{2.10}$$

where k_p is the rate constant for the filtration of Al-OM flocs [$1/T$], and its value is derived from our lab observation, in which the re-growth of Al-OM flocs completes in minutes. We assumed the immediate filtration of large-sized Al-OM flocs, meaning that k_p is equivalent to the re-growth rate.

Because the shear is linearly correlated to the Darcy flow velocity [15], we therefore directly linked the deposition/precipitation of Al-OM flocs with the Darcy velocity (**u**). We assumed the presence of a critical flow velocity (u_{Lim}) that distinctly defines the deposition/precipitation of Al-OM flocs: a higher flow velocity than u_{Lim} results in completely mobile flocs and vice versa. The determination of the critical flow velocity (u_{Lim}) is based on Equation 2.2, which shows that the logarithm of floc size is linear to the logarithm of flow rate. We further assumed that flocs that grew 10 times in size are sufficiently big to be filtered in the porous medium, which corresponds to a flow rate that is an order of magnitude lower than the highest flow rate (i.e., injection rate). The critical flow velocity (u_{Lim}) is thus 1/10 of the injection rate. In regard to the reduction in permeability, the same empirical method described above was applied, however the maximal reduction in permeability was adapted to 50 times, which is derived from detailed evaluation of the first pilot (Chapter 3).

SCENARIO ANALYSIS

The stimulated domain for each field experiment was constructed in accordance to respective field site. The confined aquifer (i.e., the site where the mixing and reaction approach was applied) was approximated as cube-shaped and covers an area of 50 m (length) by 50 m (width). For the other field site, an entire dike section with a lateral length of 30 m was simulated. The respective soil layering together with corresponding transport properties are based on information derived from either drillings carried out in the field or earlier site investigations in the close vicinity, and the simulated profile can be found in Chapter 3 and 4 respectively. The local hydraulic field on site was approximated by imposing realistic hydraulic boundary on the domain boundaries. Initial concentrations for Al and OM or Al-OM flocs are set to zero as their background concentrations are orders of magnitude lower than that of the injected solutions.

The first set of scenario analyses was dedicated to design the structure of the flow barrier. Given the fact that the purpose of pilot experiment is to understand to what extent the the nature-based technique can reduce the soil permeability and how the achieved reduction in permeability is distributed, the design of the flow barrier had to take the measurability aspect into account. This is particularly relevant to the first pilot experiment, which has a small size. As stated in the literature, the impact of the intended flow barrier on the local hydraulic depends on the scale of the flow barrier and is rather regional [55, 56]. In this scenario analysis, the location and geometry of the flow barrier were manually defined in the domain in order to assess its impact on the hydraulic field. Being able to quantitively assessing the permeability reduction is vital to obtain insight for the process control.

The other series of scenario analyses were performed to identify the injection strategy that can achieve the designed flow barrier in-situ. Both of these two approaches rely on the injection to deliver Al-OM flocs to the subsurface. Injection and extraction wells are specified in the domain at their corresponding locations with realistic length and diameter. The scenario analysis was carried out by varying the boundary conditions that are related to the injection activities. The design of the field experiment was based on adjusting parameters related to the location of the injection/extraction wells, the injection/extraction rate and duration of injection/extraction.

2.4. RESULTS AND DISCUSSION

2.4.1. 1ST FIELD EXPERIMENT: USING MIXING AND REACTION OF TWO COMPONENTS

DESIGN OF THE STRUCTURE OF FLOW BARRIER

In this field experiment, the installation of the flow barrier was planned for a relatively small segment of the dike structure. In order to overcome the intrinsic limitation of measurability caused by the small scale, the structure of flow barrier was designed with emphasis on improving the strength of field-detectable signal, which in this case is the hydraulic head measured at pre-selected locations (i.e., monitoring wells). Two types of flow barriers, line-shaped and cylindrical structure, were simulated with a scenario analysis to understand its respective impact on the hydraulic field. Results of the analysis reveal that the cylindrical geometry (inner diameter of 5 m) is most favourable for differentiating the hydraulic signals and thus for detecting the reduction in permeability. As demonstrated in Figure 2.3, though either a linear or cylindrical flow barrier can effectively diverge the groundwater flow, the appeal of a cylindrical structure lies in the distinctively different hydraulic heads that can be measured in and out the barrier. As such, the cylindrical geometry was chosen for this pilot experiment.

The feasibility of creating a cylindrical flow barrier using the two component mixing and reaction approach had to be examined. This was done with the other scenario analysis where the coupled processes (i.e., water flow, solute transport, precipitation, and the permeability reduction induced by the precipitates) were simulated. The results of this scenario analysis showed that a cylindrical flow barrier is achievable with a unique well arrangement: 20 injection wells distributed in two circles with a radius of 2.5 m for the Al injection wells (Al1-10) and 3 m for the OM injection wells (C1-10) (illustrated in Figure 2.4 b). An extraction well was placed in the centre of the two injection circles, because a continuous extraction at this location can enhance the mixing between Al and OM and confine the injected solutions within the test site. The simultaneous injection of Al and OM solutions via separated wells creates a mixing band that is located in between the injection wells, at these locations the precipitation of Al-OM complexes eventually results in the formation of the flow barrier. As shown in the simulation results, a 'flower-like' cylindrical flow barrier was created at the end of the injection practice (Figure 2.4 a). As for the measurability concern, the simulations confirmed that distinctive hydraulic signals can be found at locations inside and outside the flow barrier: the hydraulic head contrast can reach up to 18 cm according to this scenarios analysis. This magnitude of difference is practically meaningful given that the natural variation in hydraulic head

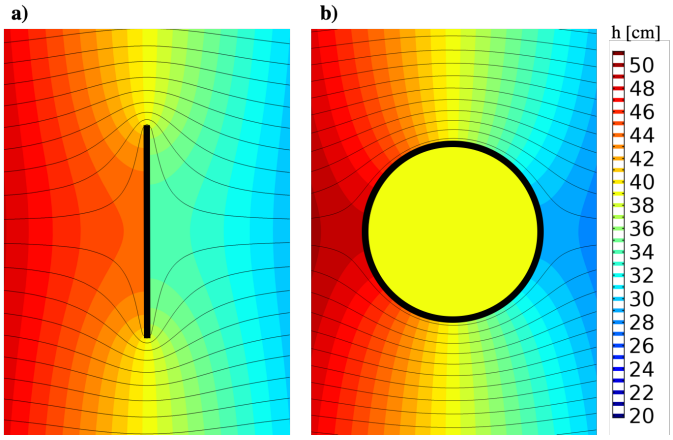

Figure 2.3: The effect of the geometry of the flow barrier on local hydraulic field, where a) represents the line-shaped flow barrier and b) is the cylindrical flow barrier. The colour map denotes the hydraulic head under stationary status, the thin-dark lines are the streamline. The locations of the flow barrier are shown as thick-dark lines.

caused by tide is around 20 cm in this field site. However, it should be noted that this scenario adapted ideal conditions, where no constrains on material usage as well as implementation duration were imposed.

DETERMINATION OF THE DESIGN PARAMETERS

Additional scenario analyses were performed to identify the realistic design parameters, which had to be feasible with the engineering capacity. The determination of injection/extraction rate and duration is of highest importance for they directly decide the total mass of injected material as well as the implementation duration. For costs concern, the preferred design was to achieve the flow barrier with minimal material consumption and implementation time.

The effect of the injection rate was studied with a scenario analysis where the injection rate (per well) varied from 0.5 to 1 and 2 m^3/d. The simulation results are shown in Figure 2.5. A higher injection rate corresponds to a larger amount of precipitates and a wider flow barrier after a 3 days of injection (Figure 2.5 a, b and c). This is the direct consequence of hydrodynamic dispersion of injected solutions, where higher injection rates lead to larger dispersion. This means that high injection rates lead to wider mixing zones, and the mixing also occurs at higher concentrations. Higher injection rates also contribute to offset the effect of the background groundwater flow, which shifts the location of the flow barrier towards its downstream direction (as shown in Figure 2.5 a). When the injection rates are sufficiently high (such as 2 m^3/d, Figure 2.5 c), the mobilising effect of the background flow becomes less pronounced. Consequently, the geometry of the flow barrier resembles that of the ideal case better (Figure 2.4 a).

However, the comparison made above (Figure 2.5 a, b and c) is based on different injected mass. Though a high injection rate appears to be more advantageous with respect to creating a wider flow barrier, it is less cost-effective than using a lower injection

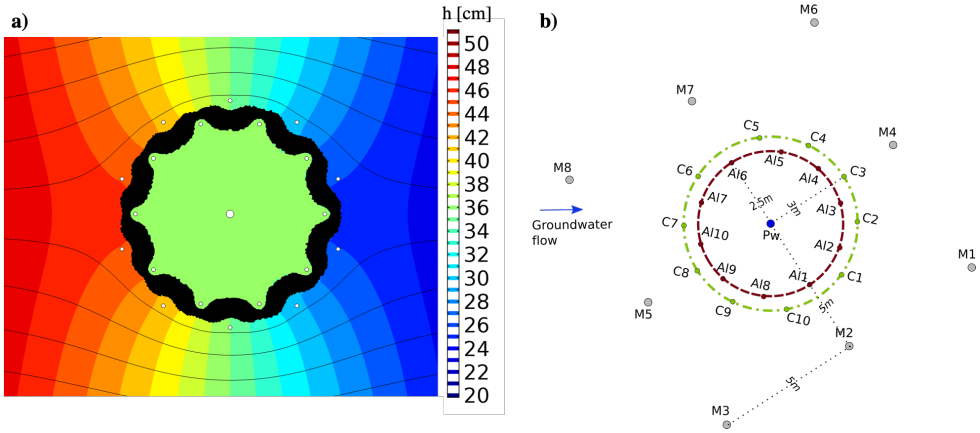

Figure 2.4: Simulated distribution of the flow barrier and its impact on local hydraulic field (a) and b) illustrates well arrangement, where M1-8 indicate the location of proposed monitoring wells.

rate. When examining the distribution of the flow barrier under same injected mass (Figure 2.5 a, d and e), the low injection rate is more effective. Again, this can be explained with hydrodynamic dispersion, where the enhanced spreading caused by high injection rates implies that 1) the mixing of two components took place over a larger area. Given that the total injected mass was constrained, the concentrations at the mixing zone were reduced and thus limited amount of precipitates precipitated; 2) larger fraction of injected material spread outside the mixing zone, which was later either extracted via the extraction well or mobilised by the background flow. Among the tested injection rates, the injection rate of 0.5 m^3/d per well is considered as most cost-effective.

In addition to cost-effectiveness, a low injection rate is vital for preserving the functionality of injection wells over time. One example can be found in Figure 2.5 c), where the entire injection circles (20 wells in total) were situated in the flow barrier. These injection wells therefore can no longer be used as pumping/infiltration wells for pumping tests in order to characterise the change of permeability at the site because they were clogged. This implies that lower injection rates (i.e., 0.5 m^3/d per well) are also favourable for improving the measurability of the achieved reduction in permeability. Therefore, the injection rate of 0.5 m^3/d per well was chosen for this field experiment.

The other design parameter, the extraction rate, had to be specified too, and this was done with a scenario analysis that varied the extraction rate from 10 to 15 and 20 m^3/d. The results reveal the combined effect of the extraction and the background flow field on the geometry of the flow barrier (Figure 2.6 a, b and c). Due to the central location of the extraction well, the flow field induced by the extraction further enhances the effect of the background flow in its upstream direction while counteracts the background flow for the downstream part. Consequently, an increase in the extraction rate results in reduced mixing of injected solutions in the upstream part, while at the same time leads to a more profound confining effect on compounds injected at wells located in the downstream. According to the simulations (Figure 2.6 a, b and c), a high extraction rate enhances the precipitation at the downstream part, but this is achieved at the cost of the

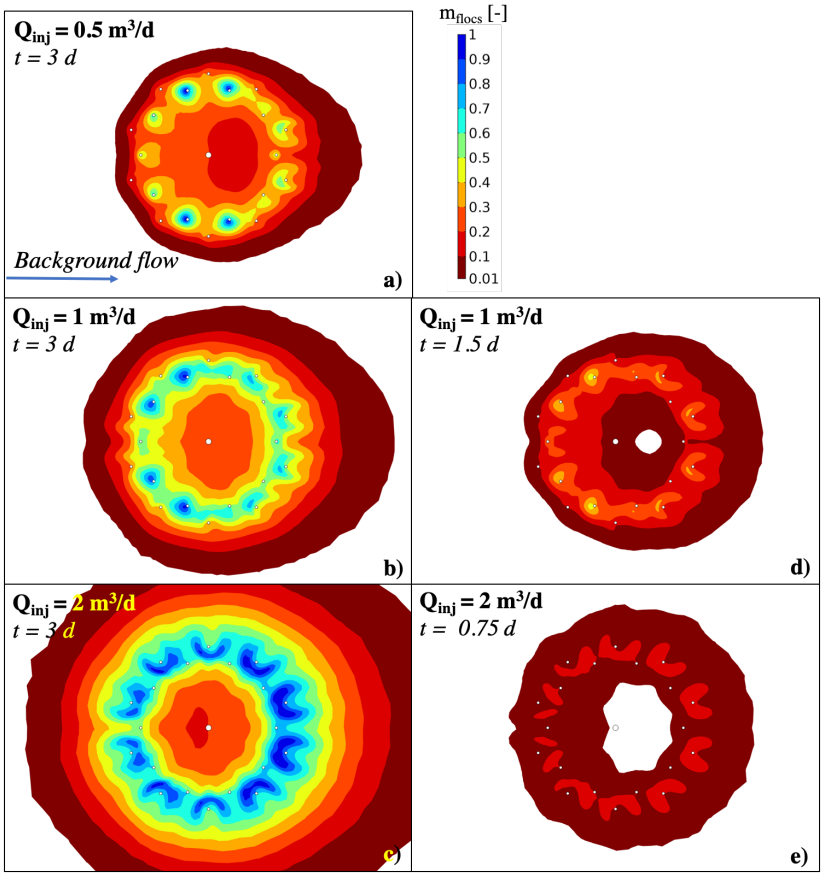

Figure 2.5: Effects of the injection rate on the simulated spatial distribution of the Al-OM precipitates in the horizontal cross section in the middle of the confined aquifer, where a), b) and c) are results using injection rate of 0.5, 1 and 2 m^3/d for 3 days respectively; d) and e) show the resulted distribution of the Al-OM precipitates with the same mass as in a). The colour bars represent the mass of precipitates (normalised to the concentration of injection solution).

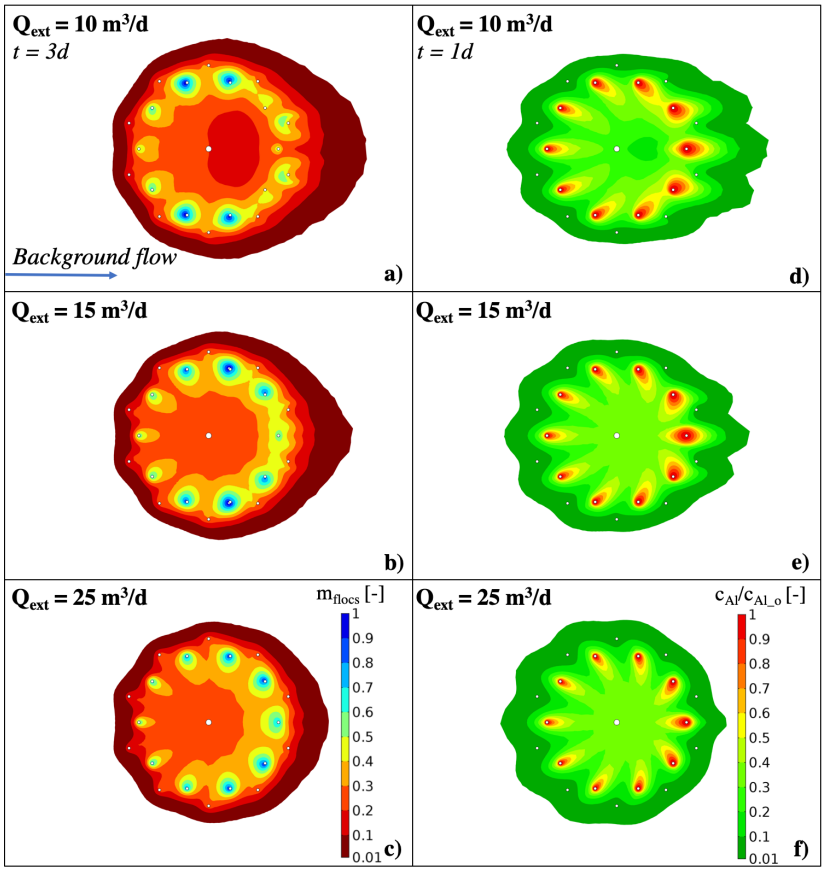

Figure 2.6: Effects of the extraction rate on the simulated spatial distribution of the Al-OM precipitates in the horizontal cross section in the middle of the confined aquifer, where a), b) and c) are results using an extraction rate of 10, 15 and 25 m^3/d for 3 days respectively; d), e) and f) show the spreading of injected Al solution during the injection (at day 1). The colour bars in f) represent the normalised Al concentration.

continuity of the flow barrier in the upstream direction. Given the fact that the integrity of the flow barrier is essential for the detection and quantification of achieved reduction in permeability, a more homogenous distribution of precipitation zone is thus preferred. In regard to the spreading of the injected Al solution, simulation results suggest that all tested extraction rates (i.e, 10, 15 and 25 m^3/d) are sufficient to confine the injected solutions in the domain (Figure 2.6 d, e and f). Therefore, the extraction rate was chosen to be 10 m^3/d.

EXECUTION OF THE FIELD EXPERIMENT

The scenario analyses above constitute the baseline injection strategy for creating a cylindrical flow barrier on site, and the execution of this field experiment began with the installation of wells. Adaptations to the baseline injection strategy were made due to new information discovered on site during the well installation activities. The new injection

strategy was again proposed using the scenario analysis. Results from this simulation result provide insight regarding the spatial distribution of the flow barrier in 3D domain. Hypothetical pumping tests were thus performed using the model to predict the results of the field pumping tests with and without the installation of the flow barrier. Bringing this knowledge into the interpretation of data came from field pumping tests allowed us to quantify the actual permeability of the flow barrier. All of these results and discussions are presented in Chapter 3 in details and are thus not repeated here.

2.4.2. 2ND FIELD EXPERIMENT: DIRECT INJECTION OF AL-OM FLOCS

DETERMINATION OF THE STRUCTURE FOR THE FLOW BARRIER

Because of the aim of the second field experiment was to demonstrate the impact of a flow barrier on the hydraulic head profile in the dike (Section 2.3.2), the scale of the second pilot site is considerably larger and the requirement on the structure of the flow barrier was thus different. The primary concern in designing the geometry of the flow barrier was to achieve a sufficiently lowered groundwater table at the toe of the dike (Section 2.3.2). A large-scale flow barrier has the potential to modify the local hydraulic characteristics to a much larger extent [56], implying that the detection of the reduction in permeability should be less concerned. The geometry of the flow barrier was determined to be linear: a 70 m long vertical flow barrier with a height of 7 m in the dike body.

VERIFICATION OF THE FEASIBILITY

The feasibility of creating a flow barrier using direct injection of Al-OM flocs was studied with a scenario analysis using the 3D model, where the particle transport, deposition and the reduction in permeability were simulated. This direct injection of Al-OM flocs relies heavily on the flow field (i.e., equivalent to shear field) to manipulate the transport and deposition of injected Al-OM flocs. It is therefore vital to have the realistic injection rate incorporated in the design phase. For this field experiment, the injection machine (MDE Drive, Heijmans bv, The Netherlands) can inject at a flow rate higher than 60 m^3/d. By assuming a homogeneously distributed flow over an 1 m long filter screen with a diameter of 0.15 m (i.e., smaller diameter is not compatible with the large 3D domain), the Darcy velocity profile in the 3D domain can be obtained (shown in Figure 2.7 a). The highest Darcy velocity is found at the injection inlet at a rate of approximately 130 m/d. As a result of the radial flow system, the Darcy velocity decays significantly with an increasing radial distance from the injection inlet. At the radial distance of 0.5 m, the local flow rate (10 m/d) is an order of magnitude lower than the injection rate (130 m/d), thus meets the criteria of the critical flow rate (detailed in Section 2.3.3). This implies that at radial distances larger than 0.5 m, the immobilisation of Al-OM flocs by trapping at the pore throats occurs.

The implementation time is another crucial factor to be considered in the design phase. This direct flocs injection was developed with the aim to improve the efficiency of the implementation. Using the low shear conditions at larger radial distances, which are larger than 0.5 m in this case, to precipitate injected Al-OM flocs requires a long duration of injection in order to have sufficient mass of Al-OM flocs transported to these locations. This is especially true for a radial flow system where the flow rate decreases significantly with an increasing radial distance. Alternatively, the low shear conditions

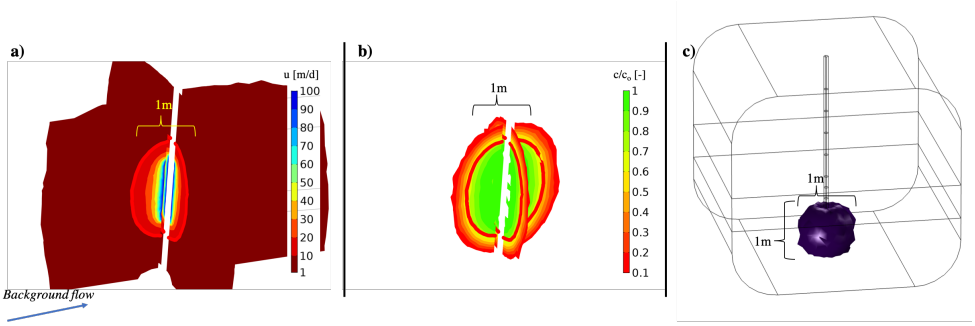

Figure 2.7: Illustration of the direct Al-OM flocs injection approach, where a) shows the Darcy velocity profile in the 3D domain, b) gives the spatial distribution of mobile Al-OM flocs after 20 mins of injection and c) denotes the location of precipitated Al-OM flocs after the termination of injection. The red coloured thick lines represent the contour of critical velocity (10 m/d). The colour bars in a) and b) represent the Darcy flow velocity and the normalised concentration of mobile Al-OM flocs.

caused by the stopping of the injection can be applied to induce the precipitation of Al-OM flocs. As revealed by the simulation results (Figure 2.7 b), a relatively short injection duration is needed to have meaningful amount of Al-OM flocs introduced into the area where the flow rate is high (i.e., shown as red sphere in Figure 2.7 b), and as soon as the injection stopped, these mobile Al-OM flocs precipitate and form an oval-shaped zone with reduced permeability (Figure 2.7 c). As such, the optimal radius of influence (ROI) was determined to be 0.5 m.

DESIGN OF THE INJECTION STRATEGY

The required flow barrier has a height of 7 m and a length of 70 m, and needs to be implemented with the direct-push system. The injection strategy was to divide the construction of the barrier into a series of mutually connected columns, where each of them has a height of 7 m. The feasibility study (results shown in Figure 2.7 c) revealed that the injection creates an 1 m wide oval-shaped zone with deposited flocs, implying that a 7 m high and 1 m wide column with reduced permeability can be achievable by dividing its construction into multiple vertical intervals.

A new scenario analysis was performed to understand the effect of the injection strategy, especially on the integrity of the created column. In this scenario, 7 injection intervals was simulated, where the first injection took place at the deepest location and was immediately followed by the second injection that is 1 m above and so on. As shown in Figure 2.8 a), the injection in 3D domain leads to an oval-shaped contour of flow rate. Consequently the immediate start of the follow-up injection maintains the high shear conditions at the overlapping section located in between two sequential injection intervals. The presence of the overlapping section favours a more continuous distribution of injected Al-OM flocs. As revealed by the simulation results (shown in Figure 2.8 c), the high shear conditions in the overlapping section prevent the precipitation of earlier injected Al-OM flocs, and these mobile Al-OM flocs become thoroughly mixed with Al-OM flocs came from the ongoing injection. As a consequence, a continuous column with reduced permeability can be installed with this injection strategy (illustrated in Figure 2.8

d).

The continuity of the flow barrier in the lateral direction is equally important an thus needs to be considered. As indicated by the simulations (Figure 2.8), the newer injection can prevent the regrowth and deposition of Al-OM flocs that were injected earlier especially when the distance between these two injections is small. This implies that there is a risk that the installation of the follow-up column might damage the integrity of the installed column for the deposition of injected mobile Al-OM flocs can be still ongoing. To minimise this risk, a back and forth injection pattern was designed. In this specific injection pattern, no neighbouring injections were implemented in sequential time (illustrated in Figure 2.9). As such, this provides longer time for earlier injected Al-OM flocs to precipitate. The other advantage of this injection patter is that it optimises the distribution Al-OM flocs into areas where the local soil permeability remains high. As shown in Figure 2.9 a), the come-back injection can effectively introduce Al-OM flocs to the unaffected or less affected area, and close off the remaining gap (Figure 2.9 b). As a consequence, the simulations suggest that a continuous flow barrier, in both lateral and vertical direction was created with the proposed injection strategy. This injection pattern was thus applied on site.

2.5. CONCLUSIONS

In order to understand the viability of using Al-OM flocs to reduce soil permeability in-situ, we developed a numerical toolbox to design two field applications that apply two different approaches to introduce Al-OM flocs. A 3D process-based model was implemented in COMSOL Multiphysics (v5.3), and this model was used to perform a number of scenario analyses to understand the feasibility of installing a flow barrier under realistic field conditions. In addition to confirm the viability of using Al-OM flocs to install a flow barrier in-situ, these scenario analyses were able to determine the realistic design parameters, the injection strategy as well as the expected changes in the system. Furthermore, the model implementation intentionally placed emphasis on the flexibility aspect. This is particularly important due to field applications often involved on-site adaptations. Later chapters will discuss in details about how the implementation scheme was adapted in response to these adaptations.

Two approaches for applying Al-OM flocs were studied with the model. The first approach, the in-situ mixing and reaction of Al and OM solutions, requires controlling the injection of the solutions. This was accurately regulated by the installation of injection/extraction wells and by adapting the injection strategy. The simulation results reveal that a cylindrical flow barrier can be created with this approach. However, as mentioned above, using dispersion to mix two components in-situ is not cost-effective: not all injected compounds are mixing and longer injection duration is needed to stimulate the spreading of the solutions. This is, nevertheless, not the case for the other approach. By utilising the shear-dependent transportation of Al-OM flocs, all injected compounds are theoretically contributing to reduce the soil permeability. The injection strategy we developed also requires a short injection duration to introduce the Al-OM flocs to the targeted zone. However, given the fact that no similar approaches have been applied before (to our knowledge), the controllability of this approach might not be as ideal as the simulations suggested. Evidence found from literature suggest that the breakage and re-

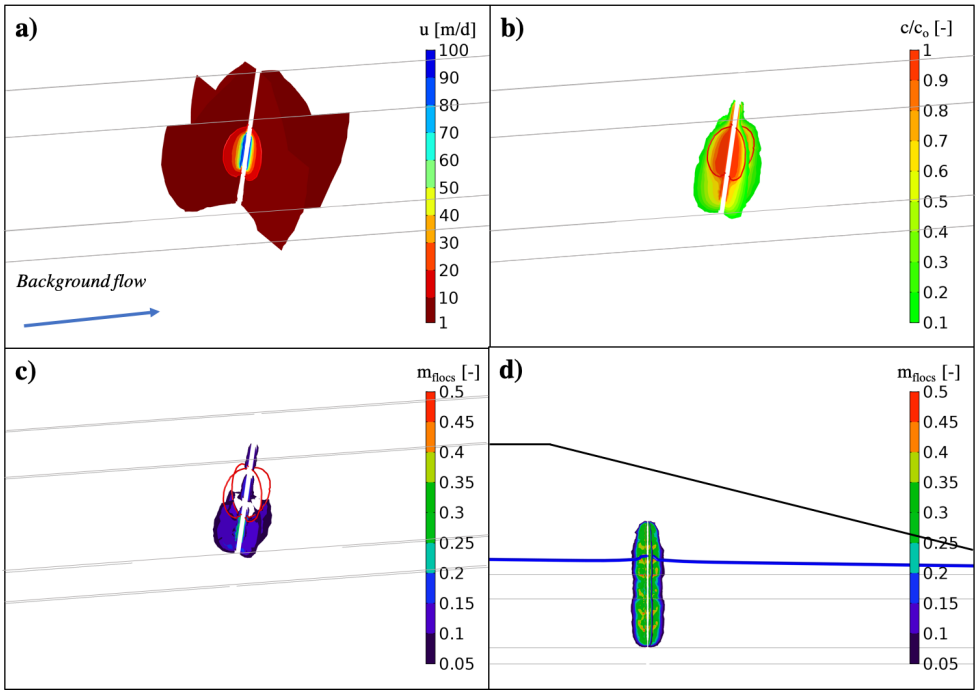

Figure 2.8: Illustration of the multi-level injection strategy using the second injection interval as an example, where a) and b) are the the Darcy velocity profile and the spatial distribution of mobile Al-OM flocs respectively, c) indicated the onset of the precipitation of injected Al-OM flocs and d) shows the final column after 7 intervals of injection. The grey lines denote the soil layering, the black solid line in d) denotes the dike profile and the dark blue line indicates the location of the water table. The colour bars in c) and d) represent the mass of precipitates (normalised to the concentration of injection solution).

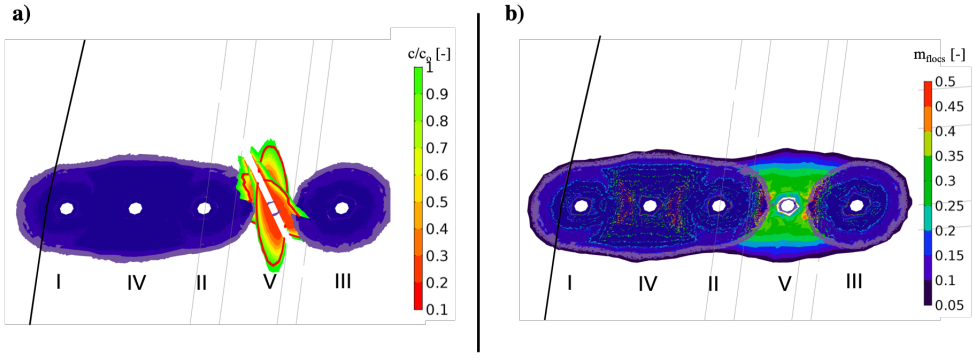

Figure 2.9: Illustration of the injection pattern using the the 5th injection as an example, where a) gives the spatial distribution of mobile Al-OM flocs during the injection and b) shows the final distribution of precipitated Al-OM flocs after this injection The roman number denotes the chronological sequence of the injection.

growth of Al-OM flocs depend on many other factors, such as the shear history [41], than purely shear-controlled.

The development of this model relies on some serious assumptions, which certainly introduce uncertainty to the simulation results. The reasons for adapting these assumptions are largely attributed to the absence of mechanistic knowledge of respective process. We therefore recommend additional laboratory tests to understand the interaction between Al and OM, the kinetics of the breakage of regrowth of Al-OM flocs and the exact mechanism of permeability reduction by Al-OM precipitates.

ACKNOWLEDGEMENT

This work is part of the research programme Water2014 with project number 13883, which is financed by the Netherlands Organization for Scientific Research (NWO).

REFERENCES

[1] J. T. DeJong, B. M. Mortensen, B. C. Martinez, and D. C. Nelson, *Bio-mediated soil improvement,* Ecological Engineering **36**, 197 (2010).

[2] M. G. Gomez, B. C. Martinez, J. T. DeJong, C. E. Hunt, L. A. DeVlaming, D. W. Major, and S. M. Dworatzek, *Field-scale bio-cementation tests to improve sands,* Proceedings of the Institution of Civil Engineers - Ground Improvement **168**, 206 (2015).

[3] C. J. Proto, J. T. DeJong, and D. C. Nelson, *Biomediated permeability reduction of saturated sands,* Journal of Geotechnical and Geoenvironmental Engineering **142**, 4016073 (2016).

[4] H. A. Anderson, M. L. Berrow, V. C. Farmer, A. Hepburn, J. D. Russell, and A. D. Walker, *A reassessment of podzol formation processes,* Journal of Soil Science **33**, 125 (1982).

[5] U. Lundström, N. van Breemen, and D. Bain, *The podzolization process. A review,* Geoderma **94**, 91 (2000).

[6] D. Sauer, H. Sponagel, M. Sommer, L. Giani, R. Jahn, and K. Stahr, *Podzol: Soil of the year 2007. A review on its genesis, occurrence, and functions,* Journal of Plant Nutrition and Soil Science **170**, 581 (2007).

[7] P. Jarvis, B. Jefferson, and S. A. Parsons, *Breakage, regrowth, and fractal nature of natural organic matter flocs,* Environmental Science & Technology **39**, 2307 (2005).

[8] M. Sharma and Y. Yortsos, *Transport of particulate suspensions in porous media - model formulation,* AICHE Journal **33**, 1636 (1987).

[9] J. N. Ryan and M. Elimelech, *Colloid mobilization and transport in groundwater,* Colloids and Surfaces A: Physicochemical and Engineering Aspects **107**, 1 (1996).

[10] T. Li, Z. Zhu, D. Wang, C. Yao, and H. Tang, *Characterization of floc size, strength and structure under various coagulation mechanisms,* Powder Technology **168**, 104 (2006).

[11] P. Jarvis, B. Jefferson, and S. A. Parsons, *Floc structural characteristics using conventional coagulation for a high doc, low alkalinity surface water source,* Water Research **40**, 2727 (2006).

[12] W.-Z. Yu, J. Gregory, and L. Campos, *Breakage and regrowth of Al-Humic flocs - Effect of additional coagulant dosage,* Environmental Science & Technology **44**, 6371 (2010).

[13] M. R. Wiesner, M. C. Grant, and S. R. Hutchins, *Reduced permeability in groundwater remediation systems: Role of mobilized colloids and injected chemicals,* Environmental Science & Technology **30**, 3184 (1996).

[14] V. I. Syngouna and C. V. Chrysikopoulos, *Transport of biocolloids in water saturated columns packed with sand: Effect of grain size and pore water velocity,* Journal of Contaminant Hydrology **129-130**, 11 (2012).

[15] T. Tosco and R. Sethi, *Transport of non-Newtonian suspensions of highly concentrated micro- and nanoscale iron particles in porous media: A modeling approach,* Environmental Science & Technology **44**, 9062 (2010).

[16] S. E. Trumbore, *Potential responses of soil organic carbon to global environmental change,* Proceedings of the National Academy of Sciences **94**, 8284 (1997).

[17] J. Lehmann and M. Kleber, *The contentious nature of soil organic matter,* Nature **528**, 60 (2015).

[18] J. Adusei-Gyamfi, B. Ouddane, L. Rietveld, J.-P. Cornard, and J. Criquet, *Natural organic matter-cations complexation and its impact on water treatment: A critical review,* Water Research **160**, 130 (2019).

[19] E. Tipping, *Cation binding by humic substances*, Vol. 12 (Cambridge University Press, 2002).

[20] A. van Zomeren and R. N. J. Comans, *Measurement of Humic and Fulvic acid concentrations and dissolution properties by a rapid batch procedure,* Environmental Science & Technology **41**, 6755 (2007).

[21] K. A. Rittle, J. I. Drever, and P. J. S. Colberg, *Precipitation of arsenic during bacterial sulfate reduction,* Geomicrobiology Journal **13**, 1 (1995).

[22] L. Weng, E. P. M. J. Fest, J. Fillius, E. J. M. Temminghoff, and W. H. Van Riemsdijk, *Transport of Humic and Fulvic acids in relation to metal mobility in a copper-contaminated acid sandy soil,* Environmental Science & Technology **36**, 1699 (2002).

[23] M. Baalousha, M. Motelica-Heino, and P. L. Coustumer, *Conformation and size of humic substances: Effects of major cation concentration and type, pH, salinity, and residence time,* Colloids and Surfaces A: Physicochemical and Engineering Aspects **272**, 48 (2006).

[24] A. Chappaz and P. J. Curtis, *Integrating empirically dissolved organic matter quality for WHAM VI using the DOM optical properties: A case study of Cu-Al-DOM interactions,* Environmental Science & Technology **47**, 2001 (2013).

[25] D. G. Kinniburgh, W. H. Van Riemsdijk, L. K. Koopal, M. Borkovec, M. F. Benedetti, and M. J. Avena, *Ion binding to natural organic matter: competition, heterogeneity, stoichiometry and thermodynamic consistency,* Colloids and Surfaces A: Physicochemical and Engineering Aspects **151**, 147 (1999).

[26] C. J. Milne, D. G. Kinniburgh, W. H. Van Riemsdijk, and E. Tipping, *Generic NICA-Donnan model parameters for metal-ion binding by humic substances,* Environmental Science & Technology **37**, 958 (2003).

[27] J. Duan and J. Gregory, *Coagulation by hydrolysing metal salts,* Advances in Colloid and Interface Science **100-102**, 475 (2003).

[28] J. C. L. Meeussen, *ORCHESTRA: an object-oriented framework for implementing chemical equilibrium models.* Environmental science & technology **37**, 1175 (2003).

[29] E. Tipping, *Humic ion-binding model VI: an improved description of the interactions of protons and metal ions with humic substances,* Aquatic geochemistry **4**, 3 (1998).

[30] D. G. Kinniburgh, C. J. Milne, M. F. Benedetti, J. P. Pinheiro, J. Filius, L. K. Koopal, and W. H. Van Riemsdijk, *Metal ion binding by humic acid: application of the NICA-Donnan model,* Environmental Science & Technology **30**, 1687 (1996).

[31] K. G. Nierop, B. Jansen, and J. M. Verstraten, *Dissolved organic matter, aluminium and iron interactions: Precipitation induced by metal/carbon ratio, pH and competition,* Science of the Total Environment **300**, 201 (2002).

[32] B. Jansen, K. G. J. Nierop, and J. M. Verstraten, *Mobility of Fe(II), Fe(III) and Al in acidic forest soils mediated by dissolved organic matter: Influence of solution pH and metal/organic carbon ratios,* Geoderma **113**, 323 (2003).

[33] B. Jansen, *The mobility of aluminium, iron and organic matter in acidic sandy soils* (2003) pp. 1– 187.

[34] L. Weng, E. J. Temminghoff, and W. H. Van Riemsdijk, *Interpretation of humic acid coagulation and soluble soil organic matter using a calculated electrostatic potential,* European Journal of Soil Science **53**, 575 (2002).

[35] E. L. Sharp, P. Jarvis, S. A. Parsons, and B. Jefferson, *The impact of zeta potential on the physical properties of ferric-NOM flocs,* Environmental Science & Technology **40**, 3934 (2006).

[36] X. Wu, X. Ge, D. Wang, and H. Tang, *Distinct mechanisms of particle aggregation induced by alum and PACl: Floc structure and DLVO evaluation,* Colloids and Surfaces A: Physicochemical and Engineering Aspects **347**, 56 (2009).

[37] D. Ghernaout and B. Ghernaout, *Sweep flocculation as a second form of charge neutralisation—a review,* Desalination and Water Treatment **44**, 15 (2012).

[38] C. T. Tanneru, J. D. Rimer, and S. Chellam, *Sweep flocculation and adsorption of viruses on aluminum flocs during electrochemical treatment prior to surface water microfiltration,* Environmental Science & Technology **47**, 4612 (2013).

[39] D. G. Lee, J. S. Bonner, L. S. Garton, A. N. Ernest, and R. L. Autenrieth, *Modeling coagulation kinetics incorporating fractal theories: A fractal rectilinear approach,* Water Research **34**, 1987 (2000).

[40] T. Scheel, L. Haumaier, R. H. Ellerbrock, J. Rühlmann, and K. Kalbitz, *Properties of organic matter precipitated from acidic forest soil solutions,* Organic Geochemistry **39**, 1439 (2008).

[41] P. T. Spicer, S. E. Pratsinis, J. Raper, R. Amal, G. Bushell, and G. Meesters, *Effect of shear schedule on particle size, density, and structure during flocculation in stirred tanks,* Powder Technology **97**, 26 (1998).

[42] N. Tufenkji and M. Elimelech, *Deviation from the classical colloid filtration theory in the presence of repulsive DLVO interactions,* Langmuir **20**, 10818 (2004).

[43] D. G. Lee, J. S. Bonner, L. S. Garton, A. N. Ernest, and R. L. Autenrieth, *Modeling coagulation kinetics incorporating fractal theories: Comparison with observed data,* Water Research **36**, 1056 (2002).

[44] Y. Wang, B.-Y. Gao, X.-M. Xu, W.-Y. Xu, and G.-Y. Xu, *Characterization of floc size, strength and structure in various aluminum coagulants treatment,* Journal of Colloid and Interface Science **332**, 354 (2009).

[45] M. Yan, D. Wang, J. Ni, J. Qu, C. W. Chow, and H. Liu, *Mechanism of natural organic matter removal by polyaluminum chloride: Effect of coagulant particle size and hydrolysis kinetics,* Water Research **42**, 3361 (2008).

[46] J. Bear, *Dynamics of Fluids in Porous Media,* Soil Science **120**, 162 (1975).

[47] G. F. Pinder and M. A. Celia, *Subsurface Hydrology* (John Wiley & Sons, 2006) pp. 1–468.

[48] T. Tosco, M. Petrangeli Papini, C. Cruz Viggi, and R. Sethi, *Nanoscale zerovalent iron particles for groundwater remediation: A review,* Journal of Cleaner Production **77**, 10 (2014).

[49] T. P. Clement, B. S. Hooker, and R. S. Skeen, *Macroscopic Models for Predicting Changes in Saturated Porous Media Properties Caused by Microbial Growth,* (1996).

[50] J. Islam and N. Singhal, *A one-dimensional reactive multi-component landfill leachate transport model,* Environmental Modelling and Software **17**, 531 (2002).

[51] S. A. Bradford, J. Simunek, M. Bettahar, M. T. Van Genuchten, and S. R. Yates, *Significance of straining in colloid deposition: Evidence and implications,* Water Resources Research **42**, 1 (2006).

[52] F. Gastone, T. Tosco, and R. Sethi, *Guar gum solutions for improved delivery of iron particles in porous media (Part 1): Porous medium rheology and guar gum-induced clogging,* Journal of Contaminant Hydrology **166**, 23 (2014).

[53] C. R. Fitts, *Groundwater science* (Academic Press, 2002).

[54] C. Z. Qin and S. M. Hassanizadeh, *Pore-network modeling of solute transport and biofilm growth in porous media,* Transport in Porous Media **110**, 345 (2015).

[55] P. F. Hudak, *Locating groundwater monitoring wells near cutoff walls,* Advances in Environmental Research **5**, 23 (2001).

[56] E. I. Anderson and E. Mesa, *The effects of vertical barrier walls on the hydraulic control of contaminated groundwater,* Advances in Water Resources **29**, 89 (2006).

3

APPLYING ALUMINIUM-ORGANIC MATTER PRECIPITATES TO REDUCE SOIL PERMEABILITY IN-SITU: A FIELD AND MODELLING STUDY

This chapter have been published in Science of the Total Environment **662**, 99-109 (2019) [1].

Using naturally occurring processes to modify the engineering properties of the subsurface has received increasing attention from industry and research communities as they aid in the development of cost-effective, robust and sustainable engineering technologies. In line with this trend, we propose to use precipitates of aluminium (Al) and organic matter (OM) to reduce soil permeability in-situ. This process is inspired by Podzolization: a soil stratification process where a layer with low permeability is developed at depth via the precipitation of metal-OM complexes.

In this study, the concept of applying Al-OM precipitates for in-situ soil permeability reduction was for the first time applied in the field. The aim of the field experiment was to create a cylindrical flow barrier in a sand layer at depth. In order to design and engineer the field application, we performed a series of scenario analyses with a site-specific 3D reactive transport model. This led to an in-situ engineering approach where a flow barrier was created by separate injection of Al and OM using a combined injection/extraction strategy. During the field application, the local variation of soil conditions required significant modifications to the design. Further scenario analyses with the model were conducted to adapt the original design and to understand the consequences of these modifications.

The results show that a cylindrical flow barrier was created after an injection period of 8 days. The precipitation of Al-OM is a highly localised process, where large amount of precipitates is formed in the close vicinity of the injection filter screens. Evaluation of pumping tests that were performed after the injection activities revealed that the permeability of the treated sand was reduced to 2 % of its original value. This first full-scale field test demonstrates that applying Al-OM precipitates is a suitable nature-based engineering tool to reduce soil permeability in-situ.

3.1. INTRODUCTION

The permeability of soil is an important factor controlling the flow of water through the subsurface. Being able to reduce the permeability can provide a solution to a wide range of problems such as reducing the spreading of contaminants in soil and groundwater [2], preventing seepage into building pits [3, 4], or in the case presented in this paper, improving the stability of dikes [5–7]. High permeability layers at shallow depths below a dike can cause stability problems at high water levels. Due to an increase in pore water pressure in the dike body, failure of the dike by slope sliding and heaving of the top soil may occur [8]. Conventional methods to increase the stability of the dike often take away this effect by adding large amounts of mass to the landside of the dike or by blocking the water flow using impermeable sheet pile barriers within the dike [9]. In densely populated countries like The Netherlands, it is becoming more and more difficult to find support for such invasive methods. One appealing alternative is the creation of a flow barrier in the highly permeable soil layers using in-situ processes. The appeal lies in the promise that such techniques are potentially efficient and cost-effective, have minimal environmental impact, and provide long-term stability of the dike.

One example of such in-situ processes is microbially induced calcite precipitation (MICP). This technique has been studied extensively in the past decade as a nature-based alternative to modify soil properties [10–12]. In most applications of MICP, the soil is treated by the injection of ureolytic bacteria, together with urea- and calcium-rich solutions. The in-situ calcite precipitation leads to a permeability reduction and also an increase in strength of the soil [13, 14]. Laboratory scale experiments have demonstrated that MICP can decrease the permeability of porous media by two orders of magnitude [15, 16]. Several field-scale trials have been carried out, and results indicate that MICP is an effective nature-based tool to reduce the permeability of porous/fractured media under field conditions [17–19].

In this study we present a different approach to reduce soil permeability, which is inspired by the natural soil formation process Podzolization. This process leads to the formation of a nearly impermeable spodic B-horizon [20, 21]. Although still under debate, it is commonly accepted that the formation of the B-horizon is caused by the complexation of organic matter (OM) with polyvalent metals, such as iron (Fe) and aluminium (Al), and subsequent precipitation of these organo-metallic complexes deeper in the soil profile [22, 23]. These organo-metallic precipitates have proven to be stable in soils over centuries [21, 24]. Although this is the first study, to our knowledge, which applies organo-metallic precipitates to reduce soil permeability, a lot of research has been carried out on OM-metal interaction in the water treatment and soil science communities [25–27]. Researchers from both fields showed that organo-metallic precipitates occur as floc-like structures with sizes ranging from 17 µm [28] up to 1000 µm [29], depending on the environmental conditions. Due to this broad size range, metal-OM flocs have the potential to be more efficient in reducing soil permeability than mineral crystals, such as calcite. Crystals reduce the permeability of a porous medium by filling up the pores [30, 31], while the larger-sized metal-OM flocs can cover the pore throat as the mechanism to reduce permeability [32, 33]. This would imply that less mass of metal-OM flocs is needed, compared to calcite crystals, to achieve the same permeability reduction.

In this paper we present the first field experiment on the in-situ formation and pre-

cipitation of metal-OM complexes as a method to reduce the soil permeability. We used aluminium as the cation in this study [34]. The formation of Al-OM precipitates was induced by separate injection of Al and OM solutions into the subsurface and where dispersion resulted in sufficient mixing of the components. The field site is in the flood plain along a dike stretch that is prone to failure by heaving. The aim of the field test is to create a vertical flow barrier in a sand layer at depth.

The objectives of the field experiment were 1) to test whether the concept of in-situ Al-OM precipitation is a suitable engineering tool and 2) to quantify the extent of permeability reduction that can be achieved under field conditions. The design and implementation of the field experiment are done using an iterative method where numerical modelling is integrated with data acquired from the field. Additional information about the soil conditions obtained during the drilling and installation of the infrastructure required fast on-site changes to the original design. The site-specific numerical model was used to develop multiple scenarios in order to understand the consequences of these adaptations and to re-design the field experiment.

3.2. MATERIALS AND METHODS

3.2.1. WORKFLOW AND SITE INFORMATION

The sequence of activities carried out for this full-scale field test is given in Figure 3.1. The implementation is based on an active iteration between numerical simulations and field activities. The model was first used to check the feasibility of the newly developed experimental design. Subsequently, additional information acquired during field activities was incorporated into the model in order to adapt the plan for the next engineering activities on site.

The field site is located at a dike along the river Lek, The Netherlands. The site covers a surface area of 100 m^2. Earlier site investigations in the close vicinity revealed the presence of a confined Holocene sand aquifer located between 6 and 8 m below ground surface (bgs). According to the regional groundwater flow model, the hydraulic conductivity of the Holocene sand is around 10^{-4} m/s. This highly permeable sand layer causes the toe of the dike to be prone to heaving, which means that the overburden soil pressure is not sufficient to resist an increase in pore water pressure that is induced by high water levels in the adjacent river [35]. The implementation of a vertical flow barrier, in the upstream direction (i.e., in the flood plain), is a way to mitigate this failure mechanism as the barrier can effectively retain the water pressure at a location where sufficient overburden soil pressure is present and therefore protect the dike.

To test the feasibility of using in-situ Al-OM precipitation to reduce soil permeability in full-scale field conditions, we decided on a cylindrical structure of the flow barrier because: 1) a cylindrical flow barrier diverges the ambient flow and leads to distinct hydraulic signals which can be monitored at wells located at different locations surrounding the barrier, and 2) being able to construct a complex structure demonstrates the flexibility of the hereby proposed approach to reduce the permeability. A cylindrical flow barrier is, in our opinion, the most favourable structure to detect the reduction in permeability on a small scale.

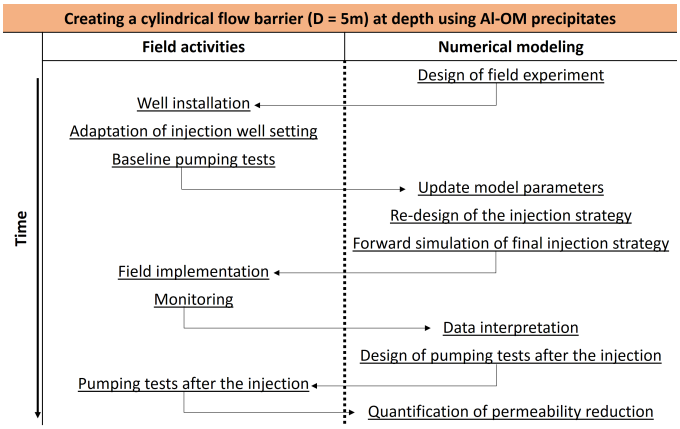

Figure 3.1: Sequence of activities carried out in the full-scale field test.

3.2.2. CHEMICALS AND PREPARATION OF SOLUTIONS

In this field experiment aluminium chloride ($AlCl_3 \cdot 6H_2O$, Alfa Aesar, Germany) and humic acid (HUMIN P775, Humintech, Germany) were selected as aluminium and organic matter sources. Both are commercially available and have a high water solubility. The solutions of aluminium chloride and humic acid are later in the text referred to as Al solution and OM solution.

Prior to the field experiment, a number of laboratory experiments were carried out to identify the Al and OM concentrations that are needed in the field. According to Jansen *et al.* [36] the reaction between Al and OM has a critical molar metal to carbon (M/C) ratio, above which the insoluble Al-OM complexes precipitate. For the aluminium and organic matter sources used in this experiment, the critical molar M/C ratio was determined to be 0.06 (data not shown). At molar M/C ratios higher than 0.06, floc-like precipitates are formed instantaneously.

In the field, 1 m^3 stock solutions of Al and OM were prepared with concentrations of approximately 1 g/l of Al and 11 g/l of C. The stock solutions were mixed with extracted groundwater from the site in order to prepare the injection solutions. Two vessels, each containing around 12.5 m^3 of injection solution, were equipped with a circulation system to homogenise the solutions. Daily measurements of Al and OM concentration were carried out during the implementation. The OM injection solution had a total organic carbon (TOC) concentration ranging between 0.5 and 0.74 g/l. The Al injection solution contained Al in the range of 0.09 to 0.11 g/l. The molar M/C ratio ranged between 0.06 and 0.10, indicating that the conditions were always favourable for precipitation. This was also daily checked on site by mixing of the two solutions and visually inspecting the development of flocs.

3.2.3. MODELLING

The aim of the field experiment is to create a cylindrical flow barrier in-situ using separate injection of Al and OM solutions. Mixing and reaction of the two injected solutions results in the formation of Al-OM precipitates and thus reduces the soil permeability. In

terms of model development, this requires a coupled description of water flow, solute transport, precipitation, and the permeability reduction induced by the precipitates. A 3D reactive transport model was implemented in COMSOL Multiphysics (v5.2), coupling Darcy's law and solute transport. The precipitation of Al-OM precipitates and its impact on the permeability are explicitly defined with empirical relationships based on earlier laboratory experiments.

The simulated domain is cube-shaped and covers an area of 50 m (length) by 50 m (width). Two opposite boundary surfaces adhere to the river and the ditch and the other two are no-flow boundaries as they are parallel to the flow field. A detailed overview of the applied boundary conditions can be found in Figure A2 of the Appendix A. Injection and extraction wells are specified in the domain at their corresponding locations with realistic length and diameter. Initial concentrations for Al and OM are set to zero as their background concentrations are orders of magnitude lower than that of the injected solutions. The soil layering together with corresponding transport properties are in accordance with information derived from either drillings carried out in the field or earlier site investigations in the close vicinity.

The simulation is specified by defining boundary conditions and model parameters. In this study, model parameters either came from lab/field activities or representative values from literature. The scenario analysis was carried out by varying the boundary conditions. The design of the field experiment was based on adjusting parameters related to the boundary conditions, such as the location of the injection/extraction wells, the injection/extraction rate, duration of injection/extraction, and the concentration of the reactive components.

Groundwater flow in the model is described by Darcy's law, for which the governing equations are given in Equation 3.1 and 3.2.

$$\frac{\partial}{\partial t}(\varepsilon_p \rho) + \nabla \cdot (\rho \mathbf{u}) = Q_m \tag{3.1}$$

In which

$$\mathbf{u} = \frac{\mathbf{K}}{\mu}(\nabla p + \rho g \nabla z) \tag{3.2}$$

where t is time $[T]$; ε_p is the porosity $[L^3/L^3]$; ρ is the fluid density $[M/L^3]$; $\mathbf{u}$ is the Darcy velocity $[L/T]$; Q_m is the volumetric source/sink term $[L^3/L^3T]$; $\mathbf{K}$ is the hydraulic conductivity tensor $[L/T]$; p indicates the pressure head $[L]$; μ is dynamic viscosity of the fluid $[M/LT]$; g is the gravity acceleration constant $[L/T^2]$ and z is the vertical direction assumed positive upwards $[L]$.

Equation 3.3 is used to describe the solute transport.

$$\frac{\partial \theta c_i}{\partial t} - \nabla \cdot \mathbf{D}_i \nabla \theta c_i + \nabla \cdot \mathbf{u} \theta c_i = R_i + S_i \tag{3.3}$$

where c_i is the concentration of solute i $[M/L^3]$; θ is the volumetric water content $[L^3/L^3]$; $\mathbf{D}_i$ is the dispersion tensor $[L^2/T]$, and it consists of molecular diffusion ($\mathbf{D}_{D,i}$) and hydrodynamic dispersion ($\mathbf{D}_{e,i}$); R_i is the reaction term of solute i $[M/L^3T]$ and S_i is the volumetric source/sink term of solute i $[M/L^3T]$.

The complexation of Al and OM is the most important reaction in this experiment. In this model, this reaction is implemented as a two-component reaction (Equation 3.4). The fast reaction kinetics are approximated by adjusting the rate parameters in Equation 3.5, and the occurrence of the precipitation reaction is determined by the M/C ratio.

$$a\mathrm{Al}_{(aq)} + b\mathrm{OM}_{(aq)} \rightarrow c\text{Al-OM}_{(s)} \tag{3.4}$$

$$R_p = \begin{cases} k_p c_{\mathrm{OM}} & \mathbf{c}_{\mathrm{Al}}/\mathbf{c}_{\mathrm{OM}} \geqq 0.06 \\ 0 & \mathbf{c}_{\mathrm{Al}}/\mathbf{c}_{\mathrm{OM}} < 0.06 \end{cases} \tag{3.5}$$

where a, b and c are stoichiometric coefficients, in this study we assumed $b = c = 1$ and $a = 0.06$; R_p is the precipitation rate $[M/TL^3]$; k_p is the rate constant for precipitation $[1/T]$; c_{Al} and c_{OM} are the concentration of Al and OM respectively. For the permeability reduction induced by the precipitation of Al-OM complexes, an embedded ramp function is used to correlate the mass of Al-OM precipitates to the permeability reduction empirically. To be consistent with laboratory observations, a threshold precipitate mass level is specified in the ramp function as the mass needed to trigger the permeability reduction (Figure A3 in Appendix A). The model assumed 4 orders of magnitude as the maximum permeability reduction.

3.2.4. DESIGN OF THE FIELD EXPERIMENT AND BASELINE SCENARIO ANALYSIS

The baseline scenario analysis demonstrated the feasibility of creating a cylindrical flow barrier (inner diameter of 5 m) across the height of the sand layer using separate injection of Al and OM solutions. The design of the field experiment was therefore based on the baseline analysis. In total 20 injection wells, ten wells for the injection of each solution, are needed and placed in a unique well arrangement: in two circles with a radius of 2.5 m for the Al injection wells (Al1-10) and 3 m for the OM injection wells (C1-10). The spacing between any neighbouring Al and OM injection well is approximately 1 m (shown Figure 3.2 b)). The baseline scenario analysis further suggested that an extraction well (Pw) installed in the centre of the two injection circles can enhance the mixing between Al and OM and confine the injected solutions within the test site. Eight monitoring wells (M1-8) surrounding the two injection circles were proposed. The filter screen of all wells is located at a depth of 6-8 m bgs which covers the Holocene sand layer. The Al solution and OM solution are injected via the two injection circles simultaneously at 0.5 m^3/d per well. During injection, groundwater is continuously extracted via the extraction well (Pw) at 10 m^3/d. The baseline scenario analysis indicated that the flow barrier can be completed after 3 days of injection.

Figure 3.2: Illustration of the design of the field experiment a) profile view and b) top view.

3.2.5. WELL INSTALLATION

Well installation took place in July 2016. In total, 29 boreholes were drilled to approximately 15 m bgs by sonic drilling. Soil profiles were recorded at selected well locations and are provided in the Appendix A (i.e., at well Pw, M1, and M8). The soil layering at this particular site differed considerably from the available data in the close vicinity. The Holocene sand layer was 6 m thick instead of the expected 2 m. It consists of a 2 m thick fine sand at a depth of 7 to 9 m bgs which is underlain by a 4 m thick medium to coarse sand layer reaching to a maximum depth of around 13 m bgs. Falling head tests were performed in the lab using KSAT (KSAT, UMS GmbH, Germany) on samples recovered from the drilling and revealed that the fine sand has a hydraulic conductivity of 4 m/d and the coarse sand of 20 m/d. These differences in the soil layering imposed a challenge for the well installation as filter screens were prepared for a 2 m thick sand layer. In order to prevent any additional costs, it was decided on site that the installation was to be continued with the materials at hand and the original design needed to be adapted:

Instead of one injection well, two wells (32 mm outer diameter) were installed at each of the 20 injection points: one in the coarse sand with a filter screen from 9 to 12 m bgs and the other in the fine sand layer with a filter screen from 7 to 8 m bgs (illustrated in Figure 3.2 a)). It was expected that the vertical dispersion in the soil would allow injected solutions to diffuse between the two filter screens [37]. Moreover, the assumption was made that the injected solutions would, to some degree, change their transport pattern during the course of injection due to the induced changes in permeability, which means that the injected solutions are directed towards the least resistant soil layers and fill the gaps without filter screens. A similar idea has been reported by DeJong *et al.* [11] in their discussion of using MICP to change soil permeability. In each of the eight monitoring wells (M1-8) a single tube (32 mm outer diameter) with a filter screen from 9 to 12 m bgs was installed. The extraction well (Pw) was installed with a single tube (125 mm outer diameter) that has a filter screen from 9 to 13 m bgs.

Based on the additional soil information from the drilling, some of the model parameters were also updated, i.e., the the soil profile, the transport properties and the injection well setting. A new scenario analysis with the model was carried out in order to adapt the injection strategy. This included alteration of the injection and extraction rate, change to a sequential injection strategy, and a longer injection time. These adaptations resulted in significant modifications to the original design of the field experiment discussed in Section 2.4.

3.2.6. FIELD IMPLEMENTATION AND MONITORING

The injection started in September 2016. During a period of 8 days, a total volume of 17ăm^3 of Al and OM solutions was injected into the sand layer, from which 6ăm^3 of each injection fluid was injected via the deep wells and 2.5 m^3 via the shallow wells. This corresponds to a total injected mass of around 12 kg aluminium chloride and 25 kg OM in the coarse sand and 5 kg and 10 kg of the two components in the fine sand layer. The injection system was equipped with an online system that continuously recorded the injection rates and injection back-pressure.

In total twelve pressure sensors (CTD diverső, Van Essen Instruments, The Netherlands) were used to monitor the changes in hydraulic head on site. The divers were in-

stalled in the eight monitoring wells (M1-8), the extraction well (Pw), and in three varying injection wells (depending which ones were in use for injection). The measurement interval of the CTD divers was set to be 30 s. Before the injection phase, constant-rate pumping tests were performed at well Pw using pumping rates of 10 m^3/d and 20 m^3/d. The results were used to derive the background hydraulic situation of the site.

3.2.7. PUMPING TESTS AFTER THE INJECTION AND WELL HYDRAULICS

To facilitate the quantification of the reduction in permeability, additional scenario analyses with the model have been carried out. These analyses gave insight in where and how to implement pumping tests after the injection. Based on this information a series of constant-rate pumping tests were performed at well Pw immediately after the implementation, after 1 month, and after 6 months using pumping rates of 20 m^3/d and 40 m^3/d. Two additional constant-rate pumping tests were conducted at well C3 and C8 with a pumping rate of 10 m^3/d. Data from the pumping tests were used to derive the transmissivity at the site via the Thiem equation (Equation 4.2) [38].

$$s = \frac{Q}{2\pi T} \ln(\frac{r_e}{r}) \tag{3.6}$$

where s is the hydraulic drawdown $[L]$; Q is the pumping rate $[L^3/T]$; T is the transmissivity $[L^2/T]$, and $T = KB$, K is the hydraulic conductivity $[L/T]$ and B is the thickness of the aquifer $[L]$; r_e is a sufficiently far distance from the pumping well, which is undisturbed by the pumping $[L]$ and r is the radial distance from the pumping well $[L]$. For a multiple-layer aquifer, its lumped transmissivity is calculated as $T = \sum_{i=1}^{n} T_i$, where T_i is the transmissivity of each layer [39].

The pumping tests provide information on the local hydraulic conductivity rather than the permeability. The relation between hydraulic conductivity and permeability is given in Equation 3.7 [40]. In this field experiment, the injected Al and OM solutions have approximately the same rheological properties and density as the groundwater. Although the permeability is not directly characterised, the measured reduction in hydraulic conductivity is considered to be identical to the reduction in permeability.

$$\kappa = K \frac{\mu}{\rho g} \tag{3.7}$$

where κ is the permeability $[L^2]$.

3.3. RESULTS AND DISCUSSION

3.3.1. DESIGN OF THE FIELD EXPERIMENT AND ADAPTATIONS TO THE INJECTION STRATEGY

The original design of the field experiment is described in Section 2.4. Due to the fact that the thickness of the aquifer was larger than expected, some adaptations had to be made to the original design and especially the injection strategy. Originally the injection strategy assumed simultaneous injection of the Al and OM solutions in all 20 injection wells. In the modified system with two wells installed per injection point, this was not

feasible anymore because the hardware available for the injection did not have sufficient capacity. A four step rotating injection strategy was developed in order to meet the hardware capacity and still achieve the objectives of the field test. The strategy starts with the injection of the Al and OM solutions in 10 wells located in the upstream direction of the circle at a rate of 0.5 m^3/d per well. In the following second step, the injection sector, consisting of 10 wells, is rotated by 90 degrees anti-clock wise. The 90 degrees rotation of the injection sector is continued into the third and forth step. Alongside with the injection, extraction of groundwater at well Pw is maintained at a rate of 6 m^3/d. Figure 3.3 gives the simulated spatial distribution of injected Al and OM solutions at various injection steps, from which sub-figures a)-d) give an illustration of the four step rotating injection strategy. The simulation results show that the sequential injection creates a circular mixing zone of the two components between all adjacent injection points. In addition, Al is well contained within the test site due to the extraction in Pw.

The four step injection strategy was first applied three times (i.e., three full circles of injection) in the deep wells that are located in the coarse sand layer, and then repeated another two times in the shallow wells in the fine sand layer. Consequently, less mass of the two components is injected in the shallow sand layer. This is due to the fact that less area is needed to be treated in this layer. Also the lower permeability of the fine sand implies that less precipitates are required to reduce its permeability to the same level as in the coarse sand. Given the short spacing between the injection wells, the lower permeability of the fine sand layer is considered favourable for the application. As illustrated in Figure 3.3 f), the spreading of the injected solutions is less profound in the fine sand layer compared to the coarse sand layer (Figure 3.3 d)). This results in a more concentrated mixing band and a higher efficiency of material usage in this area.

This is confirmed by the simulated spatial distribution of Al-OM precipitates in the 3D domain, shown in Figure 3.4. The band of Al-OM precipitates is thinner and with less mass in the fine sand layer compared to the precipitates band in the coarse sand layer. The simulation results further demonstrate that the precipitation of Al-OM is a highly localised process, which occurs mainly in the close vicinity of the injection wells. As a consequence, a very limited amount of precipitates is formed at the depths without filter screen (i.e., 8-9 m bgs and 12-13 m bgs). This indicates that the extent of vertical dispersion is not sufficient to create adequate mixing over a height of 1 m. The other assumption, i.e., optimisation of the transport pattern due to the reduced permeability, is also less favourable than expected. Instead of changing the flow path, after the formation of the precipitates, the solutions, which were still introduced via the injection wells, experienced local immobilisation and little further mixing was taking place (as shown in Figure 3.3 e)). According to the simulation, two gaps with little Al-OM precipitates will therefore remain in the flow barrier at the depth without filter screen (Figure 3.4 d)). Figure 3.4 also shows the effect of the background groundwater flow on the location of the flow barrier. The barrier is shifted towards the downstream direction. The extraction of groundwater in the centre of the two injection circles even increased this effect for the upstream part. In addition, relatively large amounts of precipitates are located in the two areas where the injection wells are aligned along the groundwater flow direction. In this case hydrodynamic dispersion favours mixing of the two components.

The results presented above imply a large variability in the achieved reduction in

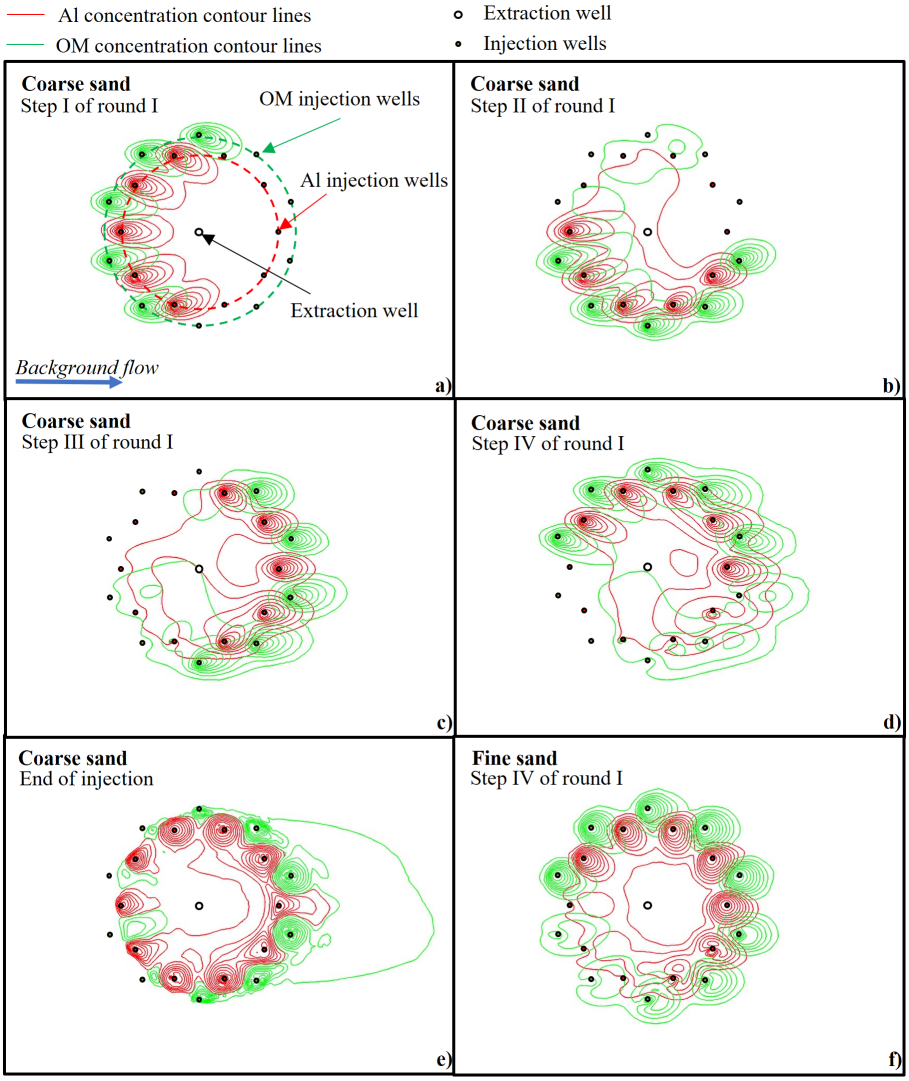

Figure 3.3: Simulated Al and OM concentration contours after specific injection steps, where a)-d) illustrate the first four injection steps applied in the coarse sand, e) represents the final status in the coarse sand at the end of injection, and f) shows the completion of the first four injection steps in the fine sand. Red and green contour lines indicate $c_{\mathrm{Al}}/c_{\mathrm{Al}_o}$ and $c_{\mathrm{OM}}/c_{\mathrm{OM}_o}$, in which c_{Al_o} and c_{OM_o} are the input concentrations of the two injection solutions. The contour lines are scaled from 0.1 to 1.0 with a spacing of 0.1, where the highest values are found at the corresponding injection wells and attenuate with further distance. Locations of Al and OM injection wells are given in red and green dots and the black circle indicates the location of the extraction well Pw.

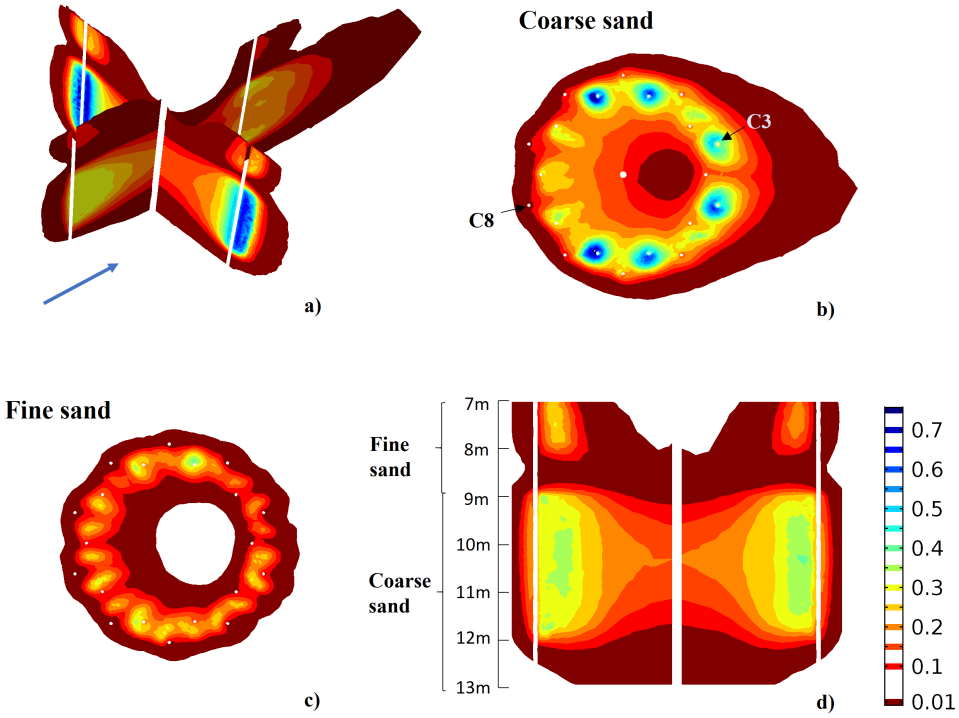

Figure 3.4: Simulated spatial distribution of the Al-OM precipitates after the injection, where b) and c) are horizontal cross sections in the middle of the coarse sand and fine sand; d) is the vertical cross section cutting through Pw and which is perpendicular to the flow direction. The colour bars represent the mass of precipitates (normalised to the concentration of injection solution).

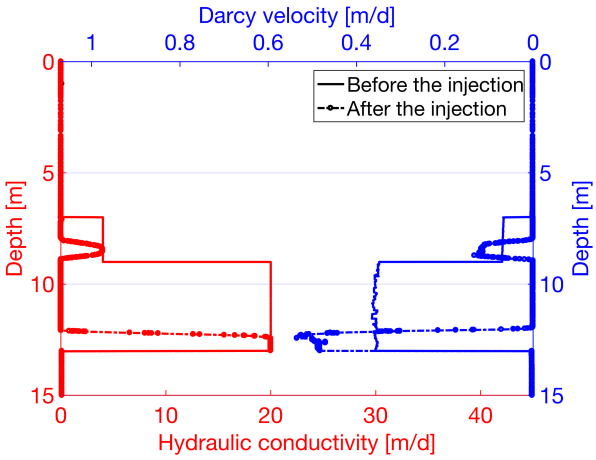

Figure 3.5: Comparison of simulated hydraulic conductivity profiles and Darcy velocity profiles under ambient flow condition at the location of the flow barrier before and after the injection.

permeability in the sand layer. Most permeability reduction occurs in zones where large amounts of Al-OM complexes have been precipitated. The lowest permeability is found in the area that was not covered by the injection wells. This is illustrated in Figure 3.5, in which the simulated hydraulic conductivity profiles before and after the formation of the flow barrier are compared. The two gaps at a depth of 8-9 m bgs and 12-13 m bgs complicate the measurement of the permeability reduction as groundwater will preferentially flow through these gaps. The quantification of permeability is based on Darcy's law, where the permeability is determined by the ratio between the Darcy velocity and the hydraulic gradient. To demonstrate the impact of the two gaps, a scenario analysis was performed in which the Darcy velocity field before and after the injection were compared under natural background flow conditions. There is no noticeable difference between the overall Darcy velocity integrated over the complete depth of the aquifer before and after the injection due to the preferential flow through the two gaps (Figure 3.5). The consequence is that quantifying the reduction in permeability due to the Al-OM precipitates is a challenge and not as straight forward as initially hoped for.

3.3.2. PERMEABILITY REDUCTION INDUCED BY AL-OM INJECTION AND PRECIPITATION

The impact of the formed Al-OM precipitates on the permeability of the sand layer was quantified using field measurements. The first set of data was derived from measurements conducted during the injection, where the temporal variation of hydraulic head in the monitoring wells and the adjacent river are recorded (shown as Figure A4 in Appendix A). During the injection, groundwater was extracted from well Pw at a constant rate of 6 m^3/d. A reduced permeability at the location of the flow barrier should lead to an increase in hydraulic gradient. This means that the measured head differences between monitoring wells (M1-8) and well Pw should gradually increase along with the

formation of the flow barrier. Nevertheless, the variation in head caused by the tide is approximately 20 cm (Figure A4 in Appendix A) which complicates the identification of these changes in head difference over the course of the injection. When analysing the measured data in detail, a very gentle increase, in the order of 1-2 cm, of head differences is noticed at the end of the injection period. This increase is however subjected to a high level of uncertainty and can not be regarded as solid evidence of a permeability reduction.

A second set of data consists of the injection rate and the back-pressure during the injection. While maintaining roughly a constant injection rate of 5 m^3/d, the injection back-pressure for the Al solution increased from 0.5 bar in the first injection step to 0.95 bar in the last step in the coarse sand layer. At the same time, the back-pressure at the OM injection wells increased from 0.4 to 0.9 bar (Figure A5 in Appendix A). This increase is attributed to the fact that the injection system has to overcome a higher resistance in order to maintain the same injection rate. The growing resistance is a consequence of the reduction in permeability that occurred in the close vicinity of the injection wells.

In order to quantify the integrated effect of the reduction in permeability on the groundwater flow, pumping tests were carried out after all injection activities were completed. These pumping tests had to be designed in a way that the measured differences in hydraulic head are distinct from the effect caused by the tide and the presence of the two gaps within the flow barrier. This was done using scenario analyses with the 3D model. By applying a constant-rate pumping test, the hydraulic gradient across the barrier must become steeper regardless how the Darcy velocity distributes over the depth. The steepness of this hydraulic gradient is proportional to the imposed flow rate at the pumping well. This implies that with a sufficiently high pumping rate, a distinct signal should be detectable with the given well arrangement. Figure 3.6 gives the simulated distribution in drawdown from pumping tests at well Pw applying various pumping rates (i.e., 10, 20 and 40 m^3/d). The hydraulic gradient across the zone with reduced permeability becomes steeper as the pumping rate is increased. The difference in drawdown before and after the formation of the flow barrier at radial distances larger than 3 m from the extraction well is 10 cm at a pumping rate of 20 m^3/d and 20 cm at a pumping rate of 40 m^3/d. These differences are considered to be measurable in the field. It was therefore decided to perform pumping tests in Pw using rates of 20 m^3/d and 40 m^3/d.

Results from these pumping tests corroborate the results of the scenario analysis. The drawdown measured from pumping tests after the injection is noticeably less than the one measured before the injection (Figure 3.6). This demonstrates that the hydraulic gradient becomes steeper at the location of injection and that the local permeability was reduced. Nevertheless, the measured differences in drawdown are smaller than expected from the model simulation. Instead of 10 cm and 20 cm, the differences in drawdown at radial distance larger than 3 m are 5 cm and 12 cm for pumping tests at 20 m^3/d and 40 m^3/d respectively. This discrepancy is most likely a result of the overall permeability reduction assumed by the model, which is based on laboratory experiments. Apparently in this field test, the achieved permeability reduction is less than 4 orders of magnitude.

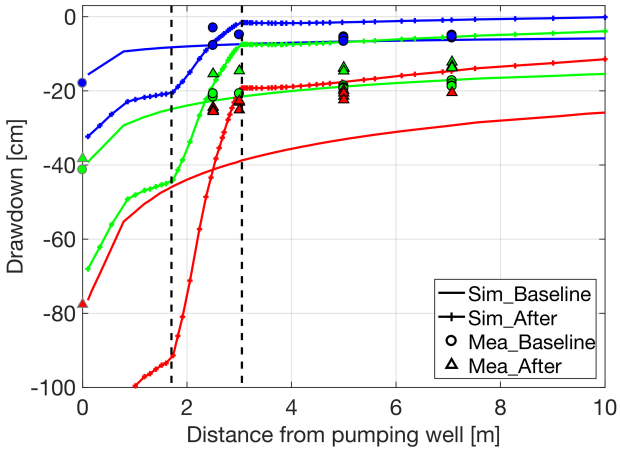

Figure 3.6: Simulated and measured drawdown distribution from pumping tests performed before and after the injection at well Pw using constant rates of 10, 20 and 40 m^3/d (marked in blue, green and red respectively). The area defined by the two dashed lines indicates the location of the flow barrier (based on model simulation).

3.3.3. QUANTIFICATION OF THE PERMEABILITY REDUCTION

In order to determine the permeability of the flow barrier, a transmissivity analysis was applied. The analysis was based on the hypothesis that the injection led to a decrease in the local transmissivity, while prior to the injection the transmissivity of the aquifer is homogeneous in the planar direction. The transmissivity analysis is coupled with results from the forward simulation, i.e. the location of reduced transmissivity was based on the simulated spatial distribution of the Al-OM precipitates.

Data was derived from the pumping tests performed before and after the injection. The background transmissivity of the aquifer was determined to be 88 m^2/d. As shown in Figure 3.4, this background transmissivity gives a good match between the measured and calculated drawdowns for various pumping tests performed before the injection. For pumping tests after the injection, the background transmissivity is kept the same for the area that is not affected by the injection. At the location of the flow barrier the reduced transmissivity is quantified by fitting against the measured drawdown. The best fit for the transmissivity at the location of the barrier is determined to be 25.5 m^2/d, which is 28% of the background transmissivity. s

It should be noticed however that the transmissivity at the location of the flow barrier is the vertical average over the entire height of the aquifer and therefore also includes the two gaps in the flow barrier at the bottom and in the middle part of the aquifer. As illustrated in Figure 3.8, the injection decreased the permeability at two different depths along the aquifer, creating a flow barrier of 3 m thickness in the coarse sand layer and 1 m thickness in the fine sand. In order to understand to what extent the Al-OM precipitates reduced the permeability in these two barriers, it was assumed that the permeability in both layers was reduced by the same extent (N). Accordingly, we were able to quantify the extent of permeability reduction (N) to be 42.7 times lower than the original perme-

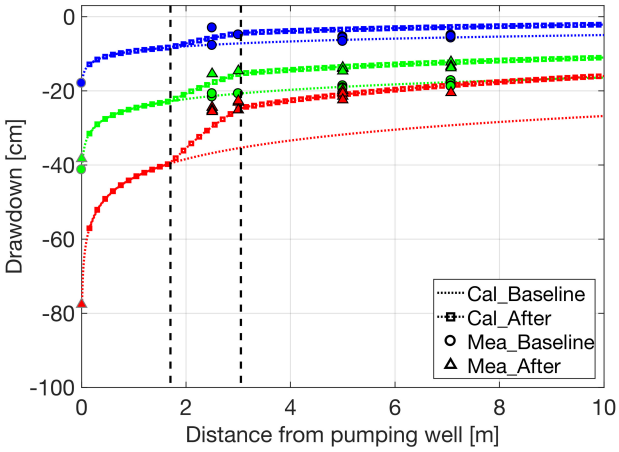

Figure 3.7: Calculated and measured drawdown distribution from pumping tests performed before and after the injection at well Pw using constant rates of 10, 20 and 40 m^3/d (marked in blue, green and red respectively). The drawdown calculation is based on Thiem's solution.

ability. This implies that the Al-OM precipitates reduced the permeability of the sand to 2% of the background permeability.

3.3.4. VERIFICATION OF THE SPATIAL DISTRIBUTION OF AL-OM PRECIPITATES AND UNCERTAINTIES IN THE QUANTIFICATION

The modelled spatial distribution of reduction in permeability was verified with additional data from constant-rate pumping tests at C3 and C8 (pumping rate 10 m^3/d). Due to the effect of background flow on the location of the precipitation zones, which is illustrated in Figure 3.4 b), it is expected that OM injection wells located in the downstream direction (i.e., C3) will have a higher reduction in permeability than those located in the opposite direction (i.e., C8). Measured drawdowns, given in Figure A7 in Appendix A, confirm that the hydraulic gradient resulting from pumping at C3 is much steeper in the close vicinity of the well compared to the one from pumping at well C8. The results therefore corroborate the spatial distribution of the precipitates derived from the 3D modelling.

The uncertainty in the quantification of permeability reduction is largely related to the spatial distribution of Al-OM precipitates. The knowledge of the spatial distribution of Al-OM precipitates in this study is derived from 3D process-orientated modelling, which greatly mitigates the uncertainty involved in the calculation. Although the modelling results are heavily influenced by the used model parameters, the parameters used in this study either came from lab/field experiments or representative values from literature. As the modelled spatial distribution of the precipitates was verified with field pumping tests, we are confident that the modelling results give a sufficient insight regarding the distribution of the Al-OM precipitates in the 3D domain.

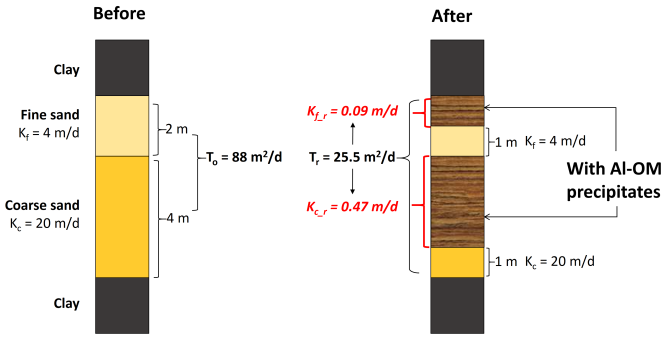

Figure 3.8: Soil profile and the hydraulic properties before and after the injection (K_f and K_c are the hydraulic conductivity of the fine and coarse sand before the injection, while K_{f_r} and K_{c_r} give the reduced hydraulic conductivity; T_o denotes the background transmissivity and T_r is the reduced transmissivity that caused by the injection).

3.4. IMPLICATIONS FOR FUTURE APPLICATIONS OF AL-OM PRECIPITATES AS A NATURE-BASED ENGINEERING TECHNIQUE

This field experiment is the first demonstration of the feasibility of using Al-OM precipitates as a geo-engineering tool to construct a flow barrier under field conditions. The results demonstrate that this concept can reduce the soil permeability to 2% of its original permeability, which is comparable to other nature-based techniques, such as MICP. In comparison with MICP, the use of Al-OM precipitates has several advantages. The application of MICP requires the injection of multiple components such as nutrients, urea, calcium, and bacteria. Research is still ongoing on the use of economically viable chemicals for large-scale application [41]. The Al and OM sources used in this study, however, are already available at relatively low costs and in large quantity. In addition, the application scheme of MICP is relatively complicated and often requires the circulation of solutions within the porous medium [18, 42]. This is mainly due to the production of ammonia as a by-product, which is subjected to strict regulations [10]. The hereby presented two component mixing concept uses a comparably straightforward application scheme. Due to the fact that both solutions have the same rheological properties as groundwater, the requirements for the equipment on site is also low. With respect to by-product management, spreading of ionic Al may raise environmental concerns. The spreading can, however, be controlled by proper design of the injection strategy. As in this experiment, groundwater analysis during and after the implementation demonstrated that no Al ions arrived at the extraction well or any of the surrounding monitoring wells (data not shown). In fact, given the high reactivity of Al ions, the residual of injected Al will either adsorb to the soil matrix or precipitate as aluminium hydroxide [43].

The major challenge encountered in this field experiment is the quantification of the achieved reduction in permeability. Understanding of the spatial distribution of the precipitates is the key element to interpret the field measurement data and further improve the application. Due to excessive costs in real engineering practices, installation of an extensive monitoring network is however not feasible. Future research on alternative

monitoring systems, preferably non-destructive, should be carried out, as they might provide a better insight in the spatial distribution of Al-OM precipitates at depth.

Another challenge in the hereby proposed geo-engineering technique is process control. The application of Al-OM precipitates depends on the mobility and reactivity of Al and OM in the subsurface and their mixing and reaction in-situ. The high reactivity of Al puts a limit on the spacing between Al and OM injection wells. In this field experiment, numerous injection wells and the adaptation of an injection-extraction strategy results in fast mixing of the Al and OM solutions. This reduces the impact of other processes, including the interaction with the soil skeleton, Al hydrolysis, and microbial degradation of OM. However, under circumstances where the time scale for mixing of the two components is larger, the impact of those processes needs to be taken into account.

Another practical concern is related to the efficiency of material usage. As earlier discussed in Section 3.1, the barrier that is formed in the mixing zone inhibits the further mixing of the two injected components, indicating that parts of the injected Al and OM are not contributing to create the flow barrier. Further research is therefore needed to use the materials as efficiently as possible.

In general, this full-scale field test represents a major step forward towards the application of Al-OM precipitates as a nature-based engineering tool to reduce soil permeability in-situ. Further studies are necessary to test this concept under different site conditions and using different implementation strategies. Additional laboratory tests are required to understand the interaction between Al and OM and the exact mechanism of permeability reduction by Al-OM precipitates. The model we developed in this field experiment adopts empirical correlations to represent our laboratory observations regarding these two processes. With more detailed knowledge available, mechanistic models of these two processes can be developed and improve the model capacity. In addition, such knowledge would help to investigate alternative sources of Al and OM, which may further enhance the suitability and flexibility of the hereby presented nature-based engineering technique.

ACKNOWLEDGMENT

We would like to thank Heijmans, Tauw, Waterschap Rivierenland, De Vries en van den Wiel, and Movares for partially financing the field experiment and for providing support during the entire course of this research. This work is part of the research programme Water2014 with project number 13883, which is financed by the Netherlands Organisation for Scientific Research (NWO).

REFERENCES

[1] J. Zhou, S. Laumann, and T. J. Heimovaara, *Applying aluminum-organic matter precipitates to reduce soil permeability in-situ: A field and modeling study,* Science of the Total Environment **662**, 99 (2019).

[2] C. N. Mulligan, R. N. Yong, and B. F. Gibbs, *Remediation technologies for metal-contaminated soils and groundwater: An evaluation,* Engineering Geology **60**, 193 (2001), arXiv:04 .

[3] N. Benmebarek, S. Benmebarek, and R. Kastner, *Numerical studies of seepage failure of sand within a cofferdam,* Computers and Geotechnics **32**, 264 (2005).

[4] Y. Wang, B.-Y. Gao, X.-M. Xu, W.-Y. Xu, and G.-Y. Xu, *Characterization of floc size, strength and structure in various aluminum coagulants treatment,* Journal of Colloid and Interface Science **332**, 354 (2009).

[5] M. E. Reid, *Slope instability caused by small variations in hydraulic conductivity,* Journal of Geotechnical and Geoenvironmental Engineering **123**, 717 (1997).

[6] C. W. Ng and Q. Shi, *A numerical investigation of the stability of unsaturated soil slopes subjected to transient seepage,* Computers and Geotechnics **22**, 1 (1998).

[7] S. van Baars and I. M. van Kempen, *The causes and mechanisms of historical dike failures in the Netherlands,* E-WAter **2009**, 1 (2009).

[8] V. M. van Beek, H. T. J. de Bruijn, J. G. Knoeff, A. Bezuijen, and U. Förster, *Levee failure due to piping: A Full-Scale Experiment,* in *Scour and Erosion*, November (American Society of Civil Engineers, Reston, VA, 2010) pp. 283–292.

[9] J. M. Duncan, S. G. Wright, and T. L. Brandon, *Soil Strength and Slope Stability (2nd Edition)* (John Wiley & Sons, 2014).

[10] J. T. DeJong, B. M. Mortensen, B. C. Martinez, and D. C. Nelson, *Bio-mediated soil improvement,* Ecological Engineering **36**, 197 (2010).

[11] J. T. DeJong, K. Soga, E. Kavazanjian, S. Burns, L. A. van Paassen, A. Al Qabany, A. Aydilek, S. S. Bang, M. Burbank, L. F. Caslake, C. Y. Chen, X. Cheng, J. Chu, S. Ciurli, A. Esnault-Filet, S. Fauriel, N. Hamdan, T. Hata, Y. Inagaki, S. Jefferis, M. Kuo, L. Laloui, J. Larrahondo, D. A. C. Manning, B. Martinez, B. M. Montoya, D. C. Nelson, A. Palomino, P. Renforth, J. C. Santamarina, E. A. Seagren, B. Tanyu, M. Tsesarsky, and T. Weaver, *Biogeochemical processes and geotechnical applications: progress, opportunities and challenges,* Géotechnique **63**, 287 (2013), arXiv:9809069v1 [arXiv:gr-qc] .

[12] V. P. Pham, A. Nakano, W. R. L. van der Star, T. J. Heimovaara, and L. A. van Paassen, *Applying MICP by denitrification in soils: a process analysis,* Environmental Geotechnics , 1 (2016).

[13] M. G. Gomez, B. C. Martinez, J. T. DeJong, C. E. Hunt, L. A. DeVlaming, D. W. Major, and S. M. Dworatzek, *Field-scale bio-cementation tests to improve sands,* Proceedings of the Institution of Civil Engineers - Ground Improvement **168**, 206 (2015).

[14] C. J. Proto, J. T. DeJong, and D. C. Nelson, *Biomediated permeability reduction of saturated sands,* Journal of Geotechnical and Geoenvironmental Engineering **142**, 4016073 (2016).

[15] A. Al Qabany and K. Soga, *Effect of chemical treatment used in MICP on engineering properties of cemented soils,* Géotechnique **63**, 331 (2013).

[16] B. C. Martinez, J. T. DeJong, T. R. Ginn, B. M. Montoya, T. H. Barkouki, C. Hunt, B. Tanyu, and D. Major, *Experimental optimization of microbial-induced carbonate precipitation for soil improvement,* Journal of Geotechnical and Geoenvironmental Engineering **139**, 587 (2013).

[17] l. A. van Paassen, R. Ghose, T. J. M. van der Linden, W. R. L. van der Star, and M. C. M. van Loosdrecht, *Quantifying biomediated ground improvement by ureolysis: large-scale biogrout experiment,* Journal of Geotechnical and Geoenvironmental Engineering **136**, 1721 (2010).

[18] M. O. Cuthbert, L. A. McMillan, S. Handley-Sidhu, M. S. Riley, D. J. Tobler, and V. R. Phoenix, *A field and modeling study of fractured rock permeability reduction using microbially induced calcite precipitation,* Environmental Science & Technology **47**, 13637 (2013).

[19] A. J. Phillips, A. B. Cunningham, R. Gerlach, R. Hiebert, C. Hwang, B. P. Lomans, J. Westrich, C. Mantilla, J. Kirksey, R. Esposito, and L. Spangler, *Fracture sealing with microbially-induced calcium carbonate precipitation: A field study,* Environmental Science & Technology **50**, 4111 (2016).

[20] H. A. Anderson, M. L. Berrow, V. C. Farmer, A. Hepburn, J. D. Russell, and A. D. Walker, *A reassessment of podzol formation processes,* Journal of Soil Science **33**, 125 (1982).

[21] U. Lundström, N. van Breemen, and D. Bain, *The podzolization process. A review,* Geoderma **94**, 91 (2000).

[22] U. S. Lundström, N. van Breemen, D. C. Bain, P. A. van Hees, R. Giesler, J. P. Gustafsson, H. Ilvesniemi, E. Karltun, P. A. Melkerud, M. Olsson, G. Riise, O. Wahlberg, A. Bergelin, K. Bishop, R. Finlay, A. G. Jongmans, T. Magnusson, H. Mannerkoski, A. Nordgren, L. Nyberg, M. Starr, and L. Tau Strand, *Advances in understanding the podzolization process resulting from a multidisciplinary study of three coniferous forest soils in the Nordic Countries,* Geoderma **94**, 335 (2000).

[23] D. Sauer, H. Sponagel, M. Sommer, L. Giani, R. Jahn, and K. Stahr, *Podzol: Soil of the year 2007. A review on its genesis, occurrence, and functions,* Journal of Plant Nutrition and Soil Science **170**, 581 (2007).

[24] M. von Lützow, I. Kögel-Knabner, B. Ludwig, E. Matzner, H. Flessa, K. Ekschmitt, G. Guggenberger, B. Marschner, and K. Kalbitz, *Stabilization mechanisms of organic matter in four temperate soils: Development and application of a conceptual model,* Journal of Plant Nutrition and Soil Science **171**, 111 (2008).

[25] P. A. van Hees and U. S. Lundström, *Equilibrium models of aluminium and iron complexation with different organic acids in soil solution,* Geoderma **94**, 201 (2000).

[26] K. G. Nierop, B. Jansen, and J. M. Verstraten, *Dissolved organic matter, aluminium and iron interactions: Precipitation induced by metal/carbon ratio, pH and competition,* Science of the Total Environment **300**, 201 (2002).

[27] P. Jarvis, B. Jefferson, and S. A. Parsons, *Floc structural characteristics using conventional coagulation for a high doc, low alkalinity surface water source,* Water Research **40**, 2727 (2006).

[28] T. Scheel, L. Haumaier, R. H. Ellerbrock, J. Rühlmann, and K. Kalbitz, *Properties of organic matter precipitated from acidic forest soil solutions,* Organic Geochemistry **39**, 1439 (2008).

[29] P. Jarvis, B. Jefferson, and S. A. Parsons, *Breakage, regrowth, and fractal nature of natural organic matter flocs,* Environmental Science & Technology **39**, 2307 (2005).

[30] P. Baveye, P. Vandevivere, B. L. Hoyle, P. C. DeLeo, and D. S. de Lozada, *Environmental Impact and Mechanisms of the Biological Clogging of Saturated Soils and Aquifer Materials,* Critical Reviews in Environmental Science and Technology **28**, 123 (1998), arXiv:arXiv:1011.1669v3 .

[31] S. Emmanuel and B. Berkowitz, *Mixing-induced precipitation and porosity evolution in porous media,* Advances in Water Resources **28**, 337 (2005).

[32] M. Sharma and Y. Yortsos, *Transport of particulate suspensions in porous media - model formulation,* AICHE Journal **33**, 1636 (1987).

[33] J. N. Ryan and M. Elimelech, *Colloid mobilization and transport in groundwater,* Colloids and Surfaces A: Physicochemical and Engineering Aspects **107**, 1 (1996).

[34] B. Jansen, K. G. J. Nierop, and J. M. Verstraten, *Mobility of Fe(II), Fe(III) and Al in acidic forest soils mediated by dissolved organic matter: Influence of solution pH and metal/organic carbon ratios,* Geoderma **113**, 323 (2003).

[35] H. G. B. Allersma, A. Rohe, and O. Dupont, *Centrifuge tests on the failure of dikes caused by uplift pressure,* International Journal of Physical Modelling in Geotechnics **3**, 747 (2002).

[36] B. Jansen, K. G. J. Nierop, and J. M. Verstraten, *Influence of pH and metal/carbon ratios on soluble organic complexation of Fe(II), Fe(III) and Al(III) in soil solutions determined by diffusive gradients in thin films,* Analytica Chimica Acta **454**, 259 (2002).

[37] L. W. Gelhar, C. Welty, and K. R. Rehfeldt, *A critical review of data on fieldâĂŘscale dispersion in aquifers,* Water Resources Research **28**, 1955 (1992), arXiv:arXiv:1011.1669v3 .

[38] G. P. Kruseman and N. A. de Ridder, *ILRI publication*, 47 (1991) p. 377.

[39] A. J. Desbarats, *Spatial averaging of transmissivity in heterogeneous fields with flow toward a well,* Water Resources Research **28**, 757 (1992).

[40] G. F. Pinder and M. A. Celia, *Subsurface Hydrology* (John Wiley & Sons, 2006) pp. 1–468.

[41] A. Cunningham, A. Phillips, E. Troyer, E. Lauchnor, R. Hiebert, R. Gerlach, and L. Spangler, *Wellbore leakage mitigation using engineered biomineralization,* Energy Procedia **63**, 4612 (2014).

[42] J. T. DeJong, B. C. Martinez, T. R. Ginn, C. Hunt, D. Major, and B. Tanyu, *Development of a scaled repeated five-spot treatment model for examining microbial induced calcite precipitation feasibility in field applications,* Geotechnical Testing Journal **37** (2014), 10.1520/GTJ20130089.

[43] J. Duan and J. Gregory, *Coagulation by hydrolysing metal salts,* Advances in Colloid and Interface Science **100-102**, 475 (2003).

4

DIRECT INJECTION OF AL-OM FLOCS TO REDUCE SOIL PERMEABILITY AND CREATE A VERTICAL FLOW BARRIER IN-SITU

This chapter is submitted to Water Resource Research.

Being able to reduce the permeability of soil is a way to control the groundwater flow and thus can provide a solution to various engineering challenges. We developed a nature-based approach that uses precipitates of aluminium (Al) and organic matter (OM) to reduce soil permeability. The viability of this approach has been demonstrated in a previous study, where the results showed that the in-situ mixing and reaction of Al and OM components produce Al-OM flocs and thus can effectively reduce the soil permeability. In order to further improve the efficiency of the technique, a revised approach is developed and presented in this study, namely shear-controlled direct floc injection.

The direct floc injection makes use of the shear-dependent size of Al-OM flocs and the linear correlation between Darcy velocity and shear. During the injection, and therefore under high-flow and high-shear conditions, the Al-OM flocs are small and mobile enough to be transported through the soil. As soon as the injection stops and low-shear conditions prevail, the Al-OM flocs re-grow in size and subsequently deposit in the porous medium. The deposition of Al-OM flocs ultimately leads to a reduction in soil permeability.

The new approach was applied for the first time in a dike section that is surrounding a water reservoir in the Netherlands. The aim of the field experiment is to create a continuous 70 m long and 7 m tall vertical flow barrier in the dike body. During the experiment, Al-OM flocs were prepared ex-situ and the floc suspension was injected directly to the dike body to reduce the local permeability. The implementation was divided into two zones (A and B), where different Al-OM floc concentrations, 3 g/l OM in zone A (covers 30m) and 5 g/l OM in zone B (covers 40m), were applied.

The results show that the direct floc injection can successfully reduce the permeability of soil under field conditions. Field monitoring data suggest that a continuous flow barrier is created in zone A, while in the zone with a higher OM input concentration (zone B) the injection led to spot-wise reduction in permeability. This indicates that controlling the spatial distribution of Al-OM flocs in-situ requires a better understanding in the kinetics of flocs breakage and regrowth and the transport of flocs in porous media.

4.1. INTRODUCTION

The permeability of a soil is a crucial property that controls groundwater flow in the subsurface. Highly permeable soil layers often lead to high seepage flow and can cause a variety of problems from the spreading of contaminants [1] to excessive uplift pressure underneath dikes [2] or slope instability [3]. A solution to tackle these problems lies in the reduction of the soil permeability. Techniques like jet grouting, colloidal-silica injection, and the installation of sheet-pile walls have been successfully applied to reduce soil permeability in many cases [4–6]. Many of these traditional approaches, however, face challenges with respect to their environmental impact as well as high energy and labor costs [7]. So there is a demand for alternative engineering solutions that are both economically effective and have a minimal environmental impact. We developed a nature-based geo-engineering technique to reduce soil permeability that is inspired by the soil stratification process: known as Podzolization. During Podzolization, precipitation and accumulation of organo-metallic precipitates result in a distinct soil horizon that can have a significantly reduced permeability [8].

Organo-metallic precipitates occur as floc-like structures [9] and consist in our case of aluminium (Al) and organic matter (OM). Al-OM flocs are several hundred micrometers in size [10, 11], which is significantly larger than the pore size in many soils [12]. Due to their large size, these flocs are filtered from the system after formation and as a consequence, reduce the permeability [13]. The approach of using Al-OM flocs has been previously applied in a field experiment for the first time [14]. In that case study the in-situ precipitation of Al-OM flocs was induced by separate injection of Al and OM solutions into the subsurface. The results show that the in-situ production of Al-OM flocs can reduce the soil permeability up to a factor of around 50 [14]. It was, however, also concluded that in-situ mixing and reaction of Al and OM is not very efficient since not all material injected in to the soil led to the formation of flocs. In addition, the reliance on in-situ mixing and reaction required a relatively long injection time in order to maintain the production of Al-OM flocs in-situ, and the installation of numerous injection wells for both components. All these aspects make this solution less economically attractive, particularly for large-scale applications.

In this study we present an alternative approach that originated from detailed analysis of the first field test, and is based on ex-situ production of Al-OM flocs, followed by the injection of a floc suspension. This has significant engineering advantages since in-situ mixing and reaction are no longer required. The direct injection of Al-OM flocs makes use of the fact that the size of the flocs is shear-dependent, which is well known from water treatment literature [11, 15, 16]. Under high shear conditions, flocs break into colloids that are in the low μm range [10]. Flocs of this size can be transported through a porous medium for a certain distance [12, 17, 18]. Floc size and transport can be controlled by manipulating the flow field since the shear is linearly correlated to the Darcy flow velocity [19]. Injection usually creates a radial flow field, where the flow velocity deceases significantly with radial distance from the injection point [20]. This means that the Al-OM flocs are mobile in the close vicinity of the injection point, where a sufficiently high flow velocity is achieved. As soon as low-shear conditions prevail, i.e., at larger radial distance from the injection point or after injection has ceased, the Al-OM flocs re-grow in size and subsequently are trapped in the porous medium.

We applied this direct Al-OM floc injection for the first time in a full-scale field experiment at a dike that surrounds a water reservoir in the Netherlands. This experiment was part of a research program aiming to assess the feasibility of direct injection of Al-OM flocs to reduce soil permeability and to quantify the achieved reduction in permeability. Doing the experiment at full-scale also gives the opportunity to study the spatial distribution of the reduction in permeability. During the experiment, Al-OM flocs were prepared on site and injected into the dike body using direct-push injection. The aim of this field experiment is to create a 70 m long vertical flow barrier with a height of 7 m in the dike body by reducing the local soil permeability. The flow barrier is expected to reduce the groundwater flow, which leads to a head drop at its location. According to Darcy's law the magnitude of this head drop is linear to the permeability of the flow barrier if the background flow rate stays constant. The effectiveness of the flow barrier to reduce groundwater flow, however, is not only dependent on its permeability but also on its continuity [2]. As stated in our previous study [14], gaps within the flow barrier lead to the occurrence of preferential flow and subsequently diminish the effectiveness of the barrier. This has a large consequence on the quantification of the permeability reduction as a discontinuity may result in unchanged hydraulic signals despite the locally reduced soil permeability.

In this study, we compare the results obtained from two different injection scenarios applied during this experiment, where the concentration of the Al-OM flocs was varied. In order to determine the hydraulic characteristics of the site before, during and after the experiment, monitoring wells were installed and used to perform field hydraulic tests. Monitoring data are analysed together with simulation results that are generated by a site-specific groundwater flow model.

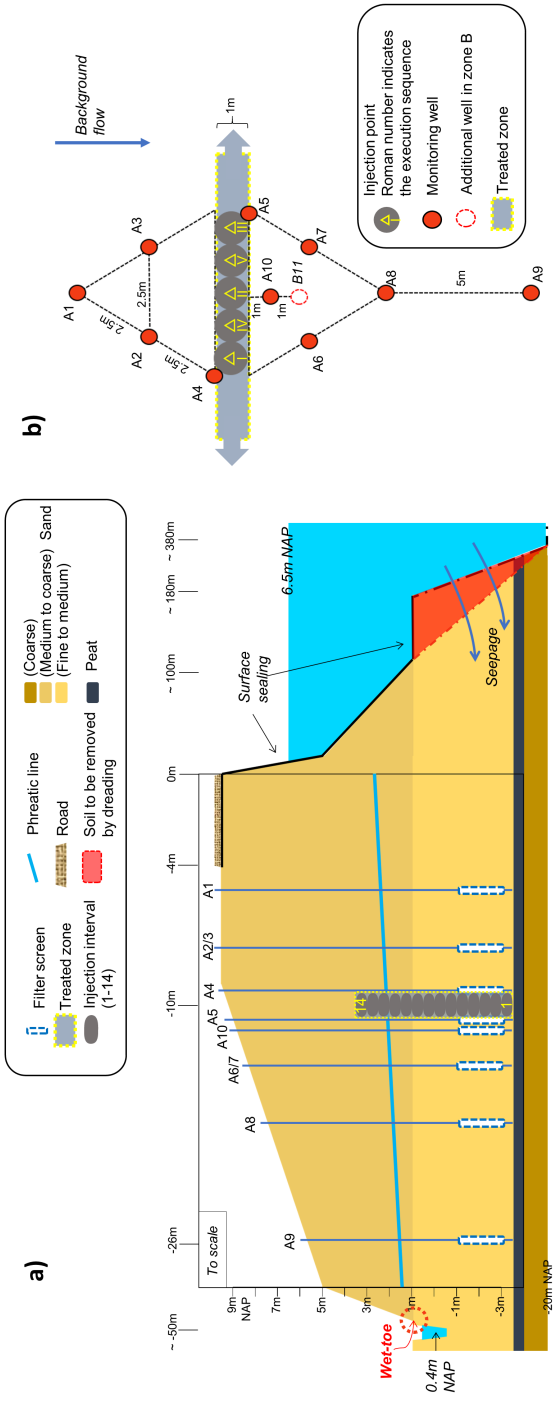

Figure 4.1: Illustration of the site a) profile view, please note that only a section of this figure is plotted to scale and b) top view. An example of the injection sequence is illustrated in b), in which the roman number denotes the chronological sequence of the injection.

4.2. MATERIALS AND METHODS

4.2.1. SITE DESCRIPTION

The field site is part of an 8 km long dike that surrounds the water reservoir de Gijster in the Biesbosch (Figure B1 in Appendix B) of which the construction was finalised in 1979. The dike was built on top of the former ground surface (1 m NAP (Dutch reference system)) up to a height of 9.5 m NAP using medium to coarse sand that became available during the reservoir construction. Site investigation revealed that the soil layer underneath the dike consists of fine to medium sand that reaches to a depth of approximately -3.5 m NAP and which is underlain by a peat layer with varying thickness (up to 1.5 m) (illustrated in Figure 4.1 a). The pilot site covers a surface area of 1260 m^2 and is located at the east side of the water reservoir. At this point excessive seepage flow occurs, which leads to fully saturated soil conditions at the toe of the dike. The high water content does not raise any concerns regarding dike stability but results in high maintenance costs due to muddy conditions and a limited bearing capacity of the top soil.

The water level in the reservoir is usually maintained at 6.50 m NAP, while the water level in the adjacent ditch, at a distance of about 50 m from the reservoir, fluctuates around 0.40 m NAP. At the reservoir side, the dike is sealed until the former ground surface by asphalt and clay. Due to this surface sealing, the hydraulic head measured in the middle of the dike ranges between 2.20 to 2.80 m NAP. During the field experiment (in the summer of 2018) the hydraulic boundary conditions changed due to dredging activities in the reservoir basin, which started in the same period as our field experiment. During the dredging work parts of the former top soil still present in the basin was removed in order to adapt the profile of the water reservoir so that it meets the original design criteria (Figure 4.1 a).

4.2.2. DESIGN OF THE FIELD EXPERIMENT AND IMPLEMENTATION

A site-specific groundwater flow model (described in Section 4.2.4) was developed in order to determine the reason for the high water content at the toe of the dike. This analysis confirmed that the excessive seepage originates from the water reservoir where water infiltrates in the sand layers above the peat layer and is transported towards the ditch (Figure 4.1 a). A measure to reduce the water content of the soil at the toe of the dike is to create an up-gradient vertical flow barrier that covers the entire transport path of the seepage. The flow barrier lowers the groundwater table in its downstream direction and also reduces the groundwater discharge rate [21]. As a consequence, the top soil will become drier which reduces the maintenance effort at the site.

The design of the flow barrier is based on a scenario analysis using the site-specific flow model. The permeability reduction that is induced by the Al-OM flocs is set to 50 times based on previous experiments [14]. According to the simulation results, a sufficiently lowered groundwater table at the toe of the dike requires the flow barrier to be at least 1 m thick. In order to prevent vertical overflow, the barrier needs to be higher than the current groundwater table. We designed the height of the flow barrier to be 7 m (5-12 m below ground surface (bgs)) where 1.5 m is located above the original water table in the dike (Figure 4.1 a). The whole pilot area is 70 m long and the implementation is carried out parallel to the dike structure at 10 m distance from the top of the dike (Figure

4.1). According to the simulation results and existing literature [21, 22], the dewatering effect of a finite flow barrier decreases at further down-gradient distances, which would make a location closer to the toe of the dike the preferred option. However, this is not feasible due to the limitations of the machine used to inject the flocs and the slope of the dike.

The machine (MDE Drive, Heijmans bv, The Netherlands) is equipped with a direct-push system and uses an injection rod (33 mm diameter and 20 cm long) with 4 annular distributed injection ports for the injection of the Al-OM floc suspension. A picture of the machine and the setup of the equipment is given in the Appendix B(Figure B2). The injection location, depth, rate, and duration are programmed beforehand and recorded continuously. The radius of influence (ROI) of the Al-OM flocs is targeted at 0.5 m. Assuming full displacement of groundwater (expressed in Equation 4.1 [23, 24]) and a safety margin of 10%, the injection volume for the 7 m high barrier at each injection point should be 1.82 m^3 (1.1 pore volume). With a ROI of 0.5 m, 70 injections are needed to complete the 70 m long flow barrier.

$$PV = \varepsilon_p \cdot \pi \cdot ROI^2 \cdot L_s \tag{4.1}$$

where PV stands for the pore volume of the aquifer [L^3]; ε_p is the porosity [L^3/L^3] (assumed to be 0.3 based on the characteristics of the sand) and L_s is the length of well screen [L], which in this study is equivalent to the height of the flow barrier.

In order to create a 7 m high flow barrier with the direct-push system, the injection at each injection point is divided into 14 vertical intervals of 0.5 m. This execution routine is considered favourable for a uniform distribution of Al-OM flocs [24]. The injection rod was first pushed down to 11.75 m bgs, followed by the 1st injection interval (illustrated in Figure 4.1 a). After injecting 0.13 m^3 of Al-OM floc suspension at a rate of 60 m^3/d, the injection rod was lifted by 0.5 m for the following interval. A target volume of 1.82 m^3 is injected throughout 14 intervals at each injection point. The injection sequence was designed to minimise the impact of ongoing injection on the earlier injected Al-OM flocs. In order to guarantee that the injected Al-OM flocs have sufficient time to re-grow and deposit (which lasts not longer than a few minutes according to literature [10, 25, 26]), a back and forth injection pattern was implemented (illustrated in Figure 4.1 b), ensuring that no neighbouring injections were implemented sequentially in time.

The field site was sub-divided in two zones, in order to test two injection scenarios, where different Al-OM floc concentrations were applied. A humic acid input concentration of 3 g/l was applied in zone A (covers a length of 30 m), and 5 g/l OM input was used in zone B (40 m long). The Al-OM floc suspension is prepared daily on site, by mixing aluminum chloride ($AlCl_3 \cdot 6H_2O$, Alfa Aesar, Germany) with humic acid (HUMIN P775, Humintech, Germany) in a continuously stirred reactor (volume of 9 m^3/d). Water for preparing the suspension was taken from the reservoir. Jansen *et al.* [27] demonstrated that insoluble Al-OM flocs are formed when the molar metal to carbon (M/C) ratio is above certain threshold. In this experiment, Al-OM flocs are formed as soon as the molar M/C ratio is above 0.05 using the water extracted from the reservoir. The appearance of flocs was inspected daily by taking a small sample before the injection started. During a period of 10 working days 54.6 and 72.8 m^3 of the Al-OM floc suspension was injected in zone A and B respectively. This corresponds to a total injected mass of around 49.2 kg

aluminium salt and 163.8 kg OM in zone A and 116.4 kg and 354 kg of the two components in zone B. The injection went smoothly and without any major difficulties.

4.2.3. MONITORING AND DATA ANALYSIS

In total, 21 monitoring wells (50 mm outer diameter) were installed (illustrated in Figure 4.1) in the middle of both zone A (10 wells) and B (11 wells). The spatial distribution of each monitoring system consists of two triangles that are mirrored with respect to the injection line. At the down-gradient side of the injection line, additional wells were installed to monitor the background flow. The filter screen of each well (2 m long) was placed at approximately -3 to -1 m NAP, which is 0.5 m above the peat layer (Figure 4.1 a).

Monitoring at the site was carried out using 17 pressure, electrical conductivity and temperature sensors (CTD divers, Van Essen Instruments, The Netherlands). These were used to monitor the changes in hydraulic head and electrical conductivity (EC) on site. The time interval for measurement and the location of the divers were varied depending on the field activities: while monitoring the natural hydraulic gradient, the time interval was set to 10 mins and locations of the divers were switched bi-weekly to ensure the complete coverage of all wells; during injection and pumping tests, the time interval was shortened to 10 s and full coverage of all wells was ensured in the respective zone.

In order to characterise the hydraulic properties of the site and understand the impact of the injection, constant-rate pumping tests, with a pumping rate of around 30 m^3/d, were performed in wells A9 and B9 before, immediately after and three months after the injection. We applied Dupuit-Thiem's solution (Equation 4.2) [32] in order to estimate the hydraulic conductivity of the site from the pumping test data.

$$h_2^2 - h_1^2 = \frac{Q}{\pi K} \ln(\frac{r_2}{r_1}) \tag{4.2}$$

where h is the hydraulic head in the piezometer $[L]$; Q is the pumping rate $[L^3/T]$; K is the hydraulic conductivity $[L/T]$; r is the radial distance from the pumping well $[L]$.

Dupuit-Thiem's solution is based on the radial distribution of the drawdown and can therefore be applied to determine the spatial distribution of the reduction in hydraulic conductivity. The change in hydraulic conductivity is closely related to the reduction in permeability, due to the similarity in density and viscosity between the injected suspension and the groundwater [14].

Due to the depth of the groundwater table and the narrow filter tubes (Figure 4.1 a), no pumping tests were performed in the upper wells. Instead, in selected upper wells (i.e., A/B 3, A7, and B10) constant-rate infiltration tests (infiltration rate around 25 m^3/d) were performed before and after the injection. As reported by Payne *et al.* [23], hydraulic equations used for pumping test cannot provide accurate hydraulic characteristics under infiltration conditions. In this study, the results from the infiltration test are therefore only used qualitatively to verify the results obtained from other data sets.

Groundwater sampling and analysis were performed at pre-defined well locations (i.e., A/B 2,4,5,8,9 &10 and B11) on selected dates. Baseline measurements were performed in June 2018. After the injection phase, the groundwater sampling was performed on weekly-basis for a month and continued with monthly monitoring for ad-

ditional 6 months. The samples were analysed for total organic carbon (TOC), Al (after filtration), chloride, and potassium (after filtration).

4.2.4. SITE-SPECIFIC FLOW MODEL

A site-specific flow model is implemented in COMSOL Multiphysics (v5.3) in order to design the installation of the flow barrier and to understand the impact of the changing hydraulic boundary conditions which are related to the dredging activities. Groundwater flow in the model is described by Darcy's law, and the governing equations are Richards' equation combined with the extended version of Darcy's law:

$$\frac{\partial}{\partial t}(\varepsilon_p \rho S_w) + \nabla \cdot (\rho \mathbf{u}) = \rho Q_m \tag{4.3}$$

in which

$$\mathbf{u} = \frac{\mathbf{K}\mathbf{k_r}(\mathbf{S_e})}{\mu}(\nabla p + \rho g \nabla z) \tag{4.4}$$

where t is time $[T]$; ρ is the fluid density $[M/L^3]$; S_w is the saturation degree $[L^3/L^3]$; $\mathbf{u}$ is the Darcy velocity $[L/T]$; Q_m is the volumetric source/sink term $[L^3/L^3T]$; k_r is the relative permeability $[-]$, which is a function of effective saturation degree S_e, $[L^3/L^3]$; p indicates the pressure head $[L]$; μ is dynamic viscosity of the fluid $[M/LT]$; g is the gravity acceleration constant $[L/T^2]$ and z is the vertical direction assumed positive upwards $[L]$.

The model was used to simulate the hydraulic conditions in the profile shown in Figure 4.1 a). The soil layering and corresponding transport properties were derived from site investigations and baseline pumping tests (before the injection of the Al-OM flocs). The hydraulic boundaries (the water reservoir and the ditch) were implemented as Robin-type boundary conditions:

$$\mathbf{u} = R_c(H_{ext} - H) \tag{4.5}$$

where H_{ext} is the known external hydraulic head $[L]$; H is head at the boundary $[L]$ and R_c is the conductance term $[1/T]$.

In this way the entry resistance at the boundary can be denoted as the conductance term R_c. The determination of the conductance term was done by fitting against field monitoring data. The geometry, location, and permeability of the flow barrier were specified in the domain in the respective scenario analysis.

4.3. RESULTS

4.3.1. EFFECT OF THE DIRECT FLOC INJECTION ON THE HYDRAULIC GRADIENT

The presence of a continuous flow barrier can be identified by looking at changes in the hydraulic gradient before and after the direct Al-OM floc injection. The hydraulic gradient before the injection was determined by averaging the hydraulic head data that are monitored at all wells over a period of three months. The averaged hydraulic heads in zone A and B are presented in Figure 4.2. A nearly straight phreatic line is observed in both zones. The hydraulic gradients measured are relatively high, namely 0.05 m/m and

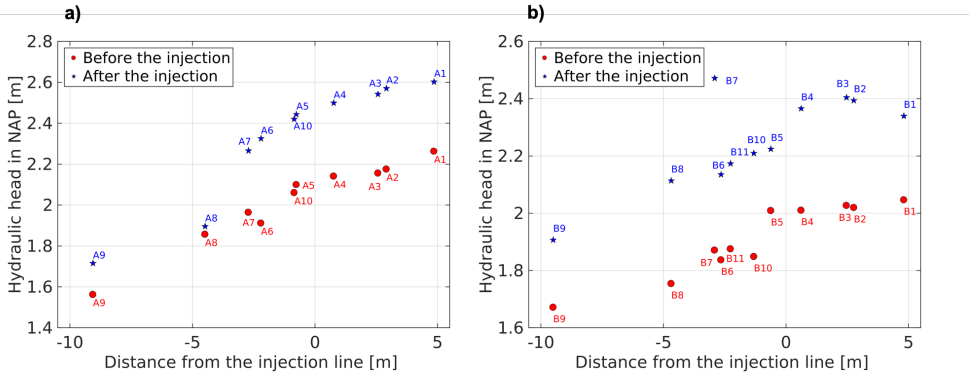

Figure 4.2: Comparison on hydraulic gradient that measured before and after the injection in zone A (a) and B (b).

0.028 m/m in zone A and B respectively. This is the consequence of the large difference between water levels in the water reservoir (6.5 m NAP) and the ditch (0.4 m NAP).

After the injection, the hydraulic gradient was again determined (over a period of three months) and distinct changes were noticed. The hydraulic head measured at all wells in zone B indicate an increase of approximately 30 cm. The only exception is well B7 where the measured head after the injection was abnormally high (Figure 4.2 b). However, the evenly distributed increase in hydraulic head shows that the injection did not result in any change in the hydraulic gradient.

A similar increase in hydraulic head is measured in zone A, but with variations in its magnitude depending on the location of the monitoring well. The increase in hydraulic head at the wells which are the furthest downstream from the injection line (i.e., A8 and A9) is 20 cm less than at all other wells in zone A (shown in Figure 4.2 a), where the increase in hydraulic head is around 35 cm. This result demonstrates that the hydraulic gradient between monitoring wells A6/7 and A8 became steeper after the injection, while it is comparable to the one measured before the injection in the rest of the domain. This change in hydraulic gradient was consistently observed throughout the entire year after the injection (latest data was collected on summer 2019).

4.3.2. HYDRAULIC CHARACTERISATION BY PUMPING AND INFILTRATION TESTS

In order to quantify the effect of the direct floc injection on the soil permeability, the spatial drawdown distributions during a pumping test performed before and after the injection are compared. Results from the pumping tests in zone A and B before the injection (shown in Figure 4.3 and 4.4) show a well shaped cone of depression, where the drawdown decreases with increasing radial distance from the pumping well. This indicates that the initial permeability of the two zones is rather homogeneous. The background hydraulic conductivity of zone A and B is determined to be 6.3 m/d and 7.6 m/d using Dupuit-Thiem's solution (Equation 4.2). As shown in Figure 4.3 and 4.4, the calculated drawdown distribution using the background hydraulic conductivity matches the

measured data very well.

After the injection the most profound difference in drawdown in zone B is measured at monitoring wells B7 and B8. At these two locations the drawdown is significantly lower than at the other wells (Figure 4.4). If monitoring points B7 and B8 are, however, excluded, the cone of depression after the injection is comparable to that measured before the injection in zone B.

The results from the pumping test in well A9 show that the cone of depression in zone A changed after the direct floc injection (Figure 4.3). It is no longer uniformly distributed over the entire domain, but shows a distinct pattern change between monitoring wells A6/7 and A8. At monitoring wells A1-7 and A10 the pumping test performed after the injection led to a drawdown that is 6 cm less than before the injection. At well A8, on the other hand, the drawdown increased by 4 cm. The change of measured drawdown across wells A6/7 and A8 is consistent with the hydraulic gradient in this area (Figure 4.2 a).

The results from infiltration tests at various well locations before the injection (presented in Figure B3 and B4 in Appendix B) show that the magnitude of the head change primarily depends on the radial distance from the infiltration well. This corroborates the results from the pumping tests before the injection in zone A and B. The same consistency when comparing infiltration and pumping tests is also found after the injection. In zone A, the difference of measured head change between wells A6/7 and A8 increased noticeably during the infiltration tests performed in well A3 and A7 after the injection (Figure B3 in Appendix B). The difference between infiltration tests before and after the injection in zone B is mainly identified at monitoring wells B7 and B8. The head change at these locations was considerably less than that measured in the test before the injection (Figure B4 in Appendix B).

4.3.3. TRANSPORT OF THE INJECTION FLUID

Continuous EC measurement in the monitoring wells allowed us to monitor the propagation of the injection fluid in the subsurface. It should be noted that the EC is mainly influenced by the concentrations of ions (Cl^- and K^+) in the injected suspension. The transport of Al-OM flocs is not necessarily the same due to filtration and deposition.

As shown in Figure 4.5 a) and b), the transport of the injection fluid in zone B was subject to preferential flow. Shortly after the start of the injection at point I44, the EC value measured at wells B7 and B8 significantly increased to about 2.75 mS/cm. This corresponds with the EC of the injection fluid applied in this zone. At well locations in the closer proximity to injection point I44 (i.e., B5, B6, and B10) the increase in EC was much less pronounced or even unnoticeable (well B6). The change in hydraulic head (dH) is in line with the EC data (Figure 4.5 c and d). The change in head measured at wells B7 and B8 was so prominent that the linear interpolation (Figure 4.5) suggests a large area with a significant increase in head. It should be noted that this can not reflect the actual head in this area since the injected volume is not enough to result in such a rise in water table over a large area. The EC data also revealed a down-gradient transport of the injection suspension. At well B9, which is located approximately 10 m away from the injection line, the EC peaked at 2 mS/cm, while in the opposite direction (against the natural groundwater flow) only a gentle rise in EC was detected (the highest EC mea-

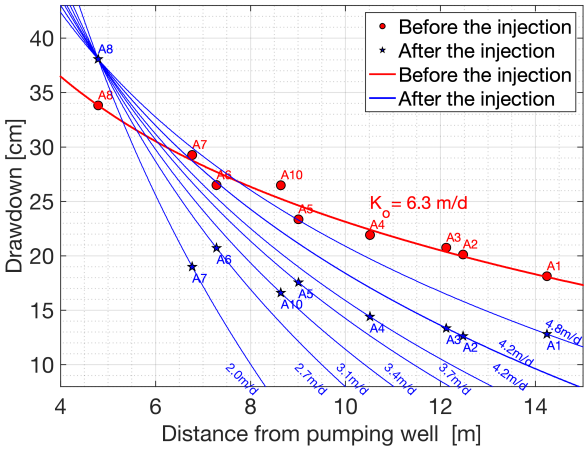

Figure 4.3: Measured and calculated drawdown distribution from the pumping test performed in well A9 before and after the injection (pumping rate of 30 m^3/d). Circles and stars indicate measured data and the lines represent the drawdown distribution calculated with Dupuit-Thiem's solution. K_o is the background hydraulic conductivity (before the injection). Values of equivalent hydraulic conductivity are stated next to the respective calculated drawdown distribution. With a larger distance between the data points selected for determining the equivalent hydraulic conductivity, a larger proportion of unreduced hydraulic conductivity is integrated into the respective equivalent hydraulic conductivity (since the flow barrier is present between A6/7 and A8). A larger equivalent hydraulic conductivity therefore coincides with a larger distance between the two data points.

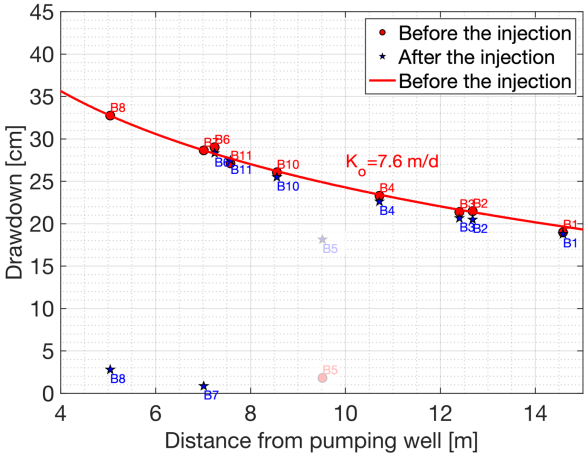

Figure 4.4: Measured and calculated drawdown distribution from the pumping test performed in well B9 before and after the injection (pumping rate of 30 m^3/d). Circles and stars indicate measured data and the line represents the drawdown distribution calculated with Dupuit-Thiem's solution. Data from well B5 is regarded as outlier and not included in the calculation

sured at well B3 is 0.7 mS/cm). In zone A (results presented in Appendix B, Figure B5) a similar trend was observed. Preferential flow led to a sharp rise of EC and dH firstly at well A8, followed by an increase at A6 and A7. In contrast to zone B, no increase in EC at well A9 was noticed during the entire monitoring period.

Results from the chemical analysis of groundwater samples corroborate the field-measured EC data. Samples taken from well A8 and B8 on the 6th of July 2018 contained 0.42 g/l and 0.7 g/l of Cl^-, and 0.25 g/l and 0.44 g/l of K^+. Both are comparable to that of the injection suspension used in the respective zones. The measured Al and TOC concentrations, however, were far lower. TOC concentrations of 19 mg/l and 60 mg/l were measured at well A8 and B8, which are higher than the background (around 5 mg/l) but not even close to the TOC concentrations in the injection suspension. Measured Al concentrations were consistently below 50 μg/l (detection limit), expect for one measurement in well B8 directly after the injection where a concentration of 400 μg/l was measured. This is again much lower than the Al concentration in the injection suspension.

4.4. DISCUSSION

4.4.1. PERMEABILITY OF THE FLOW BARRIER IN ZONE A

The results presented in Chapter 3 all indicate that a flow barrier has been created in zone A between wells A6/7 and A8. The hydraulic gradient is noticeably steeper between wells A6/7 and A8 even under ambient flow conditions. The head difference between those points increased from 10 cm (before) to 37 cm (after the injection, Figure 4.2). This shows that the barrier is continuous throughout a relevant part of zone A. Otherwise the measured signal would be less pronounced due to water bypassing the barrier, especially under steady state conditions [1, 21, 29]. The presence of the flow barrier is further confirmed by the results obtained from the pumping and infiltration tests. Literature shows that the presence of a flow barrier leads to distinct effects on either sides of the barrier during a pumping event [1, 23, 30]. The low permeability of the flow barrier widens the capture zone of the pumping at the well. As a consequence, a decrease in the streamline density is observed at the side across the flow barrier and thus a reduced drawdown, while at the side of the pumping well, the density of streamline is locally enhanced and this results in an increase in drawdown (illustrated by Figure B6 in Appendix B). This is exactly what has been observed during the pumping and infiltration tests in zone A (described in Section 4.3.2 and shown in Figure 4.3 and B3 in Appendix B).

We applied a hydraulic conductivity analysis to quantify the reduction in permeability of the flow barrier in zone A. An equivalent hydraulic conductivity (K_{eq}) was derived from the pumping test results after the injection using Dupuit-Thiem's solution. The derivation of the equivalent hydraulic conductivity is based on measured drawdowns from two monitoring points at both sides of the flow barrier (i.e., A8 and any other well downstream). The equivalent hydraulic conductivity is therefore an integrated hydraulic conductivity over the area that is not affected by the injection of Al-OM flocs (with a background hydraulic conductivity K_o) and the flow barrier itself (with a reduced hydraulic conductivity K_r). We assume that the geometry of the flow barrier is linear with a sufficient lateral extension and that it extends over the entire saturated height of the aquifer. Consequently we calculated eight equivalent hydraulic conductivities in zone

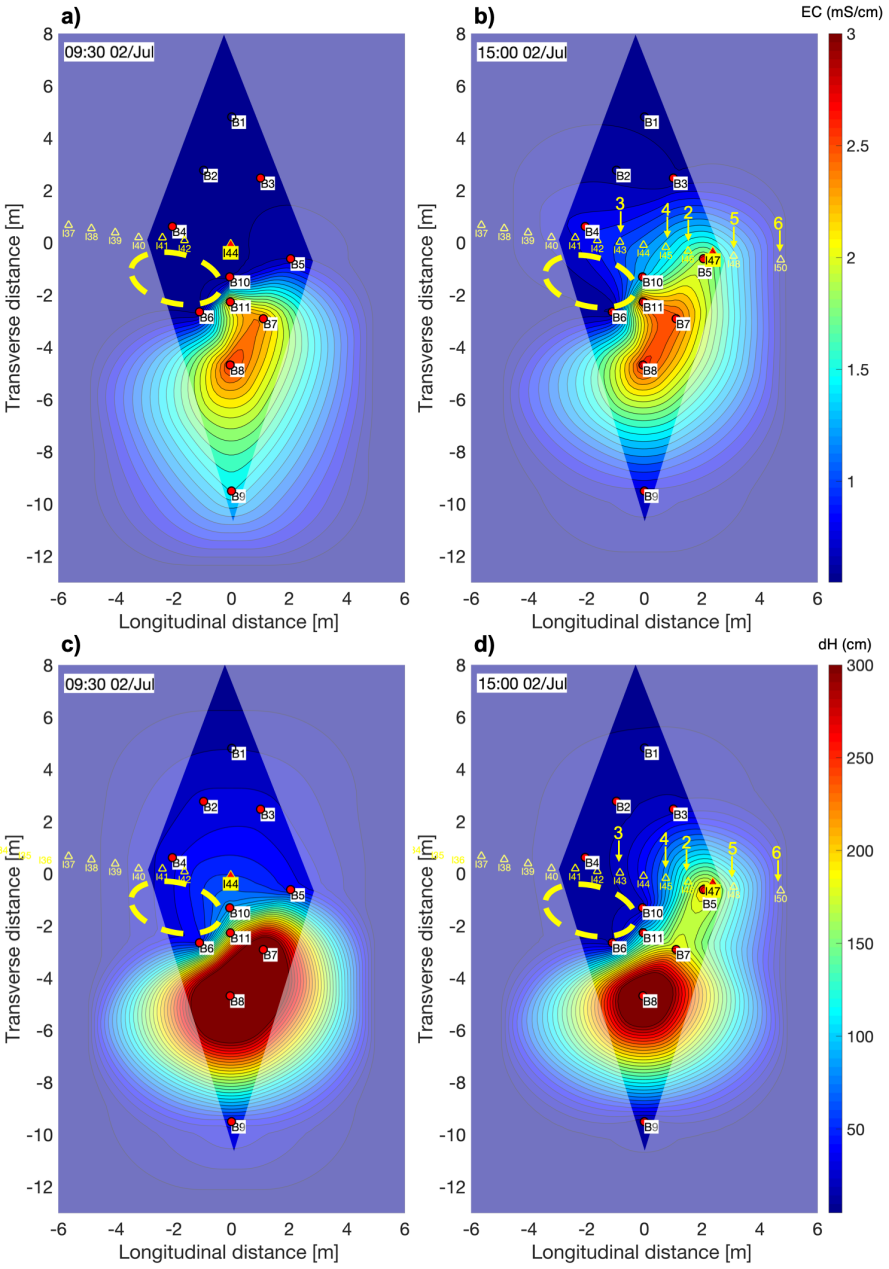

Figure 4.5: Measured EC (a and b) and dH (c and d) during the injection of the Al-OM flocs suspension. Figures a) and c) show the results at the end of the first injection of a day (I44), and b) and d) show the last injection of the day (I47). The empty yellow triangles indicate the location of completed injections, while a filled triangle shows the location of the on-going injection. The monitoring wells are denoted as circles (filled means equipped with diver). The dashed oval indicates a spot with reduced permeability that was created by earlier injections. Linear interpolation was applied to the EC and pressure data to create the contour maps. In the area where the confidence level is limited (because of extrapolation)the results are shadowed. In this interpolation the data from well B2 was disregarded due to abnormally high values even before the start of the injection. The entire time-lapse of the data is provided in the Appendix B (Figure B7).

A, which are presented in Figure 4.3.

The hydraulic conductivity of the flow barrier (K_r) is determined based on the assumption that the flow direction is perpendicular to the orientation of the flow barrier. Thus, the equivalent hydraulic conductivity is the harmonic mean [31] (Equation 4.6):

$$K_{eq} = \frac{\sum_{i=1}^{n} L_i}{\sum_{i=1}^{n} (L_i / K_i)} \tag{4.6}$$

where L_i is the thickness of layer i [L]; T_i is hydraulic conductivity of layer i [L^2/T].

The average of all eight calculations was taken as the final hydraulic conductivity. One important variable that needs to be considered in this calculation is the thickness of the various layers. The flow barrier is located between wells A6/7 and A8, which means that it is not thicker than 2 m. We therefore conducted a series of calculations assuming the thickness of the flow barrier to vary from 0.1 m to 2 m. The corresponding hydraulic conductivity of the flow barrier is shown in Figure B7 in the Appendix. Based on the results, the effectiveness of the flow barrier is controlled by its thickness and its hydraulic conductivity. For example, a flow barrier with hydraulic conductivity of 0.6 m/d and a thickness of 1 m is as efficient in reducing the groundwater flow as a barrier with a hydraulic conductivity of 0.15 m/d and a thickness of 0.2 m.

It should be noticed that the hydraulic conductivity is vertically lumped over the saturated thickness of the treated dike body. As stated earlier, the continuity, both planar and vertical, is essential in determining the effectiveness of the flow barrier. Based on available data we cannot judge the vertical variability of the permeability in the flow barrier. For this reason, we assume that the Al-OM floc injection decreased the soil permeability homogeneously in the vertical direction. This implies that the factor of reduction calculated using the hydraulic conductivity is identical to that of the factor of permeability reduction (Section 4.2.3). By assuming the thickness of the flow barrier created in zone A is the same as it was designed (1 m), it can therefore be concluded the direct floc injection reduced the permeability of the soil by 11 times. However, it should be noted that this quantification might considerably underestimate the true impact of the injected Al-OM flocs on soil permeability since the actual thickness of the flow barrier is highly uncertain and the results from zone B (Figure 4.4) clearly indicate that a significant reduction in soil permeability was locally achieved. Results from our previous study [14], on the other hand, showed that the flow barrier created by in-situ production of Al-OM flocs results in a permeability reduction of 50 times. If this value is assumed for the reduction in permeability in zone A, the flow barrier would have a thickness of approximately 0.15 m, which is thinner than designed.

4.4.2. VERIFICATION OF THE QUANTIFICATION AND THE IMPACT OF DREDGING

The analysis presented in Section 4.4.1 is verified with the site-specific flow model, which also includes the change in hydraulic boundary conditions after the injection due to the dredging activities (Section 4.2.1). The elevation in hydraulic head in zone A and B (Figure 4.2) is the direct consequence of the dredging since the removal of the top soil reduced the resistance for water to enter the soil body and subsequently enhanced the discharge.

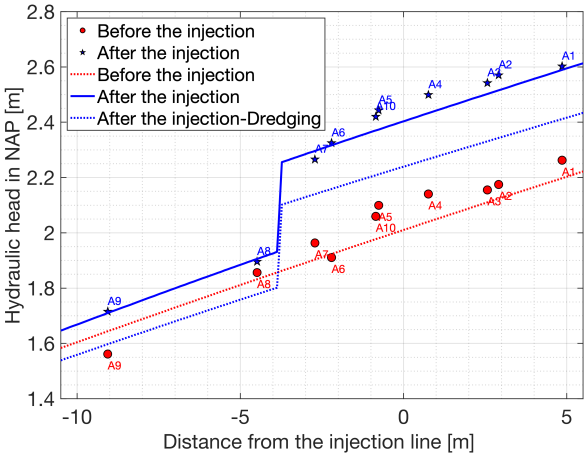

Figure 4.6: Measured and simulated hydraulic gradient in zone A, where circles and stars indicate measured data and the lines represent the simulated results with the site-specific flow model. After the injection-Dredging denotes the result from the scenario where effect of the dredging activities on the flow barrier is removed.

The initial conductance terms on both boundaries, i.e., the water reservoir and the ditch, were determined in the baseline scenario (before the injection) by calibrating against the phreatic line measured before the injection (Figure 4.6). The conductance term assigned to the water reservoir boundary was increased for the analysis after the injection in order to account for the dredging. In addition, the flow barrier (i.e., assumed to be 0.15 m thick with the permeability reduced by 50 times and located between wells A6/7 and A8) was added to this scenario. Simulated results match the measured data well in both scenarios (shown in Figure 4.6) and therefore provide credibility to the quantification described in the previous section. This analysis additionally confirms entry resistance in the water basin has been reduced and that, therefore, the dredging activities are the cause of the elevated groundwater table after the creation of the low permeability barrier.

A scenario analysis was constructed in order to remove the effect of the dredging activities. This was done by using the same conductance terms on both boundaries as in the baseline scenario for the situation after the injection. As shown in Figure 4.6, the flow barrier in zone A would have lowered the groundwater table at its downstream side by 5 cm. The simulation results also indicate that the creation of the flow barrier would reduce the discharge from the water reservoir by approximately 3.5% as the flow barrier provides additional resistance to the seepage flow that originates from the water reservoir. The reduction in groundwater table and in discharge would in that case both contribute to reduce the water content of the soil at the toe of the dike.

4.4.3. LOCALISED REDUCTION IN PERMEABILITY IN ZONE B

There is little to no difference in the hydraulic gradient in zone B after the injection compared to the one measured before (Figure 4.2 b). This implies that no continuous flow barrier is created. Nevertheless, there is some evidence of localised reduction in permeability. Both pumping and infiltration tests that were performed after the injection (Figure 4.4 and Figure B4 in Appendix B) show that the hydraulic head at wells B7 and B8 are not affected by the pumping/infiltration. Clearly, the permeability in the close vicinity of these wells was significantly reduced. The identification of this spot with reduced permeability is only possible due to its location between two monitoring wells. As discussed earlier, spot-wise reduction in permeability is not expected to deliver field-detectable signals. It is, therefore, possible that other spots with reduced permeability were created by the injection.

One additional spot in zone B is identified based on the monitoring during the injection of the Al-OM flocs. Given the fact that chloride ions were co-injected with the Al-OM flocs, every injection step can also be considered as a tracer test. Following changes in EC offers an insight in to the transport pattern of the tracer and therefore into the soil permeability. The preferential transport of the injection fluid led to an immediate breakthrough of EC at wells A8 and B8 during the respective injection. In zone A a pronounced increase in EC was subsequently also measured at wells A6 and A7 (Figure B5 in Appendix B). The injected suspension in zone B however did not spread over well B6. This is most likely the result of a reduced permeability in the area around B6 and B10 due to earlier injections (illustrated as dashed oval in Figure 4.5). The low permeability of this spot diverted the injected suspension towards well B7 and led to an asymmetric distribution of measured EC. Hydraulically, the change in head at this spot was also lower than at other locations, confirming the previous results (Figure 4.5 c and d).

4.4.4. CHALLENGES IN PROCESS CONTROL AND IMPLEMENTATION

OCCURRENCE OF PREFERENTIAL FLOW

The flow barrier created in zone A is located between wells A6/7 and A8, which is 3 m further downstream than originally designed. This is partially attributed to the fact that the hydraulic gradient at this site is relatively high, leading to pore water velocities above 1 m/d (Section 4.3.1). This forces the transport of flocs towards the downstream direction. There has to be, however, another transport mechanism that explains the preferential flow towards monitoring wells A8 and B8 (which are located 5 m away from the injection line). Full groundwater displacement can not be the case since the injected volume is far from sufficient to reach well A8 or B8. Additionally no breakthrough was observed in other wells that are located closer to the injection line.

We hypothesise that the preferential flow is a combination of ambient groundwater flow, the installation of monitoring wells, and the occurrence of micro-hydraulic fracturing. Even though the wells were installed with a small diameter (OD 50 mm), the amount of monitoring wells is relatively large. Water can move freely in the open monitoring well compared to the transport in the soil. This is particularly relevant when the flow rate is high [32, 33]. The rise in water table in the wells will attract the flow during the injection of Al-OM flocs. The ambient flow enhanced this effect towards the down–gradient side of the injection, which leads to a concentration of injection fluid downstream of the

injection line. Hydraulic fracturing is initiated if the vertical effective stress of the soil is exceeded by the applied injection pressure [23, 24]. The lowest overburden pressure, among the down-gradient wells, is found at the location of wells A8 and B8. The vertical effective stress at well A8 is nearly 1 bar less than at well A7, which makes this location most prone for fracturing. The high injection pressure used was intended to ensure the spreading of Al-OM flocs, and it seems like this triggered micro-fracturing. Once the fracture channel is established, it will serve as the least-resistant path [34]. It has to be noted that there is no evidence of extensive fracturing or structural failure of the soil matrix, as the measured pressures during the injection indicated no sudden drop and injection rates remained constant [23].

PRODUCTION RECIPE OF AL-OM FLOCS

The permeability reduction caused by the Al-OM flocs is the result of filtration and deposition, which takes place when the size of the flocs exceeds a certain threshold limit defined by the properties of the porous medium [13, 35–37]. This is confirmed by the difference between the TOC concentration and ion concentrations measured in well A8 and B8 (Section 4.3.3), which indicates that most of the Al-OM flocs were filtered and immobilised along the transport path.

In addition to challenges related to the transport of the injection fluid, the input concentration clearly plays a role in distributing the Al-OM flocs in-situ. A higher concentration corresponds to a larger probability for soil pores to be blocked by the flocs and thus a faster permeability reduction rate [13, 19, 38]. In addition, the research from Yan *et al.* [39] suggests that a high OM concentration leads to a faster regrowth rate of the Al-OM flocs as well as larger floc sizes. The concentration applied in zone B might be overly effective in reducing the soil permeability. In addition to the preferential flow, the high injected mass of Al-OM flocs resulted in the clogging of the soil along the transport path. As a result, the injected Al-OM flocs led to the creation of localised spots with significantly reduced soil permeability in zone B (i.e., the spot around well B7 and B8). This was not the case in zone A where a lower injection concentration was applied. The achieved reduction in permeability is shown to be more continuous, which demonstrates that the injected Al-OM flocs had a larger extent of spreading. This suggests that a lower concentration favours the spreading of Al-OM flocs in-situ.

Besides the input concentration, fundamental understanding of the breakage and regrowth kinetics of Al-OM flocs in porous media is essential to control the spatial distribution of the Al-OM flocs. In fact, most of available knowledge from water treatment literature so far is derived from batch experiments [10, 11, 40], where the impact of the interaction between Al-OM flocs with the soil matrix as well as their transport are not addressed.

4.5. CONCLUSIONS

This is the first full-scale experiment in which direct Al-OM floc injection was applied to reduce soil permeability in-situ. Field measured data demonstrate that this approach is viable in reducing the soil permeability and that a continuous flow barrier can be created in a dike body. The advantages of this approach are apparent. Direct-push injection requires no installation of injection wells, which is often a significant cost factor for

large-scale applications [7]. In addition, this approach relies only on a single component injection. The effort for preparing and managing the injection solution on site is minimal. The field experiment demonstrated that the ease of field implementation and efficiency of this approach are both deemed to be high, meaning that this newly developed approach is more friendly and economically feasible for large-scale applications.

The remaining challenges in process control also demonstrate the versatility of this approach. The breakage and regrowth kinetics of Al-OM flocs are influenced by factors including the source and dosage of Al, the source of OM, and the applied injection method. With a more detailed knowledge available, we believe that the direct injection of Al-OM flocs has the potential to be applicable in reducing permeability under a wide range of environmental conditions. Besides laboratory studies, field studies would be recommended in order to test the viability of this approach under different site conditions.

ACKNOWLEDGMENT

We would like to thank our industrial partners, Evides Waterbedrif N.V., Tauw bv and Heijmans N.V., for financing the field experiment and for providing valuable support during the entire course of this research. This work is part of the research programme Water2014 with project number 13883, which is financed by the Netherlands Organisation for Scientific Research (NWO).

REFERENCES

[1] P. Bayer, M. Finkel, and T. Georg, *Combining pump-and-treat and physical barriers for contaminant plume control,* Ground Water **42**, 856 (2004).

[2] Y. Yihdego, *Evaluation of Flow Reduction due to Hydraulic Barrier Engineering Structure: Case of Urban Area Flood, Contamination and Pollution Risk Assessment,* Geotechnical and Geological Engineering **34**, 1643 (2016).

[3] A. T. Papagianakis and D. G. Fredlund, *A steady state model for flow in saturated-unsaturated soils,* Canadian Geotechnical Journal **21**, 419 (2009).

[4] C. N. Mulligan, R. N. Yong, and B. F. Gibbs, *Remediation technologies for metal-contaminated soils and groundwater: An evaluation,* Engineering Geology **60**, 193 (2001), arXiv:04 .

[5] L. Shen, Q. Du, H. Wang, W. Zhong, and Y. Yang, *In situ polymerization and characterization of polyamide-6/silica nanocomposites derived from water glass,* Polymer International **53**, 1153 (2004).

[6] B. Nikbakhtan and M. Osanloo, *Effect of grout pressure and grout flow on soil physical and mechanical properties in jet grouting operations,* International Journal of Rock Mechanics and Mining Sciences **46**, 498 (2009).

[7] P. Suer, N. Hallberg, C. Carlsson, D. Bendz, and G. Holm, *Biogrouting compared to jet grouting: Environmental (LCA) and economical assessment,* Journal of Environmental Science and Health - Part A Toxic/Hazardous Substances and Environmental Engineering **44**, 346 (2009).

[8] D. Sauer, H. Sponagel, M. Sommer, L. Giani, R. Jahn, and K. Stahr, *Podzol: Soil of the year 2007. A review on its genesis, occurrence, and functions,* Journal of Plant Nutrition and Soil Science **170**, 581 (2007).

[9] T. Scheel, L. Haumaier, R. H. Ellerbrock, J. Rühlmann, and K. Kalbitz, *Properties of organic matter precipitated from acidic forest soil solutions,* Organic Geochemistry **39**, 1439 (2008).

[10] Y. Wang, B.-Y. Gao, X.-M. Xu, W.-Y. Xu, and G.-Y. Xu, *Characterization of floc size, strength and structure in various aluminum coagulants treatment,* Journal of Colloid and Interface Science **332**, 354 (2009).

[11] W.-Z. Yu, J. Gregory, and L. Campos, *Breakage and regrowth of Al-Humic flocs - Effect of additional coagulant dosage,* Environmental Science & Technology **44**, 6371 (2010).

[12] J. T. DeJong, B. M. Mortensen, B. C. Martinez, and D. C. Nelson, *Bio-mediated soil improvement,* Ecological Engineering **36**, 197 (2010).

[13] J. N. Ryan and M. Elimelech, *Colloid mobilization and transport in groundwater,* Colloids and Surfaces A: Physicochemical and Engineering Aspects **107**, 1 (1996).

[14] J. Zhou, S. Laumann, and T. J. Heimovaara, *Applying aluminum-organic matter precipitates to reduce soil permeability in-situ: A field and modeling study,* Science of the Total Environment **662**, 99 (2019).

[15] T. Li, Z. Zhu, D. Wang, C. Yao, and H. Tang, *Characterization of floc size, strength and structure under various coagulation mechanisms,* Powder Technology **168**, 104 (2006).

[16] P. Jarvis, B. Jefferson, and S. A. Parsons, *Floc structural characteristics using conventional coagulation for a high doc, low alkalinity surface water source,* Water Research **40**, 2727 (2006).

[17] M. R. Wiesner, M. C. Grant, and S. R. Hutchins, *Reduced permeability in groundwater remediation systems: Role of mobilized colloids and injected chemicals,* Environmental Science & Technology **30**, 3184 (1996).

[18] V. I. Syngouna and C. V. Chrysikopoulos, *Transport of biocolloids in water saturated columns packed with sand: Effect of grain size and pore water velocity,* Journal of Contaminant Hydrology **129-130**, 11 (2012).

[19] T. Tosco and R. Sethi, *Transport of non-Newtonian suspensions of highly concentrated micro- and nanoscale iron particles in porous media: A modeling approach,* Environmental Science & Technology **44**, 9062 (2010).

[20] T. Tosco, M. Petrangeli Papini, C. Cruz Viggi, and R. Sethi, *Nanoscale zerovalent iron particles for groundwater remediation: A review,* Journal of Cleaner Production **77**, 10 (2014).

[21] E. I. Anderson and E. Mesa, *The effects of vertical barrier walls on the hydraulic control of contaminated groundwater,* Advances in Water Resources **29**, 89 (2006).

[22] P. F. Hudak, *Locating groundwater monitoring wells near cutoff walls,* Advances in Environmental Research **5**, 23 (2001).

[23] F. Payne, S. Potter, and J. Quinnan, *CRC Press*, Vol. 126 (CRC Press, 2008) p. 21.

[24] H. Sapion, J. Gemoets, T. Tosco, R. Muyshondt, L. Bastiaens, R. Sethi, F. Gastone, N. Klaas, M. Velimirovic, and M. Luna, *Pressure-controlled injection of guar gum stabilized microscale zerovalent iron for groundwater remediation,* Journal of Contaminant Hydrology **181**, 46 (2015).

[25] X. C. Wang, P. K. Jin, and J. Gregory, *Structure of Al-humic flocs and their removal at slightly acidic and neutral pH,* Water Science and Technology: Water Supply **2**, 99 (2002).

[26] Y. X. Zhao, B. Y. Gao, H. K. Shon, B. C. Cao, and J. H. Kim, *Coagulation characteristics of titanium (Ti) salt coagulant compared with aluminum (Al) and iron (Fe) salts,* Journal of Hazardous Materials **185**, 1536 (2011).

[27] B. Jansen, K. G. J. Nierop, and J. M. Verstraten, *Influence of pH and metal/carbon ratios on soluble organic complexation of Fe(II), Fe(III) and Al(III) in soil solutions determined by diffusive gradients in thin films,* Analytica Chimica Acta **454**, 259 (2002).

[28] A. Zech, C. L. Schneider, and S. Attinger, *The Extended Thiem's solution: Including the impact of heterogeneity,* Water Resources Research **48**, 1 (2012).

[29] J. A. Cunningham and M. Reinhard, *Injection-extraction treatment well pairs: An alternative to permeable reactive barriers,* (2002).

[30] EPA (U.S. Environmental Protection Agency), *A systematic approach for evaluation of capture zones at pump and treat systems,* Tech. Rep. January (U.S. Environmental Protection Agency, Washington, DC, EPA/600/R-08/003, 2008., 2008).

[31] P. Renard and G. de Marsily, *Calculating equivalent permeability: A review,* Advances in Water Resources **20**, 253 (1997).

[32] G. F. Pinder and M. A. Celia, *Subsurface Hydrology* (John Wiley & Sons, 2006) pp. 1–468.

[33] R. P. Chapuis and D. Chenaf, *Detecting a hydraulic short circuit along a monitoring well with the recovery curve of a pumping test in a confined aquifer: method and example,* Canadian Geotechnical Journal **35**, 790 (2011).

[34] A. J. Phillips, E. Lauchnor, J. J. Eldring, R. Esposito, A. C. Mitchell, R. Gerlach, A. B. Cunningham, and L. H. Spangler, *Potential CO2 leakage reduction through bbiofilm-induced calcium carbonate precipitation,* Environmental Science & Technology **47**, 142 (2013).

[35] S. A. Bradford, J. Simunek, M. Bettahar, M. T. Van Genuchten, and S. R. Yates, *Significance of straining in colloid deposition: Evidence and implications,* Water Resources Research **42**, 1 (2006).

[36] S. Xu, B. Gao, and J. E. Saiers, *Straining of colloidal particles in saturated porous media,* Water Resources Research **42**, 1 (2006).

[37] I. L. Molnar, W. P. Johnson, J. I. Gerhard, C. S. Willson, and D. M. O'Carroll, *Predicting colloid transport through saturated porous media: A critical review,* Water Resources Research **51**, 6804 (2015).

[38] M. Sharma and Y. Yortsos, *Transport of particulate suspensions in porous media - model formulation,* AICHE Journal **33**, 1636 (1987).

[39] M. Yan, D. Wang, J. Ni, J. Qu, C. W. Chow, and H. Liu, *Mechanism of natural organic matter removal by polyaluminum chloride: Effect of coagulant particle size and hydrolysis kinetics,* Water Research **42**, 3361 (2008).

[40] J. Duan and J. Gregory, *Coagulation by hydrolysing metal salts,* Advances in Colloid and Interface Science **100-102**, 475 (2003).

5

A MECHANISTIC UNDERSTANDING OF THE FLOCCULATION OF ORGANIC MATTER INDUCED BY ALUMINIUM IONS

This chapter is ready to be submitted.

The interaction between organic matter (OM) and metal cations and the resulted flocculation of OM are important for both fields of soil science and water treatment. Though semi-mechanistic understanding of the metal-OM interaction has been developed, the subsequent flocculation process is not well understood. This therefore limits the development of a quantitative description of the OM flocculation. We hereby present our conceptual model that aims to provide a mechanistic framework to address the flocculation of OM.

In line with DLVO theory, this conceptual model adapts charge neutralisation of OM molecules as the mechanism for the flocculation of OM, while quantifies the change in charge by assessing the amount of cations bound to the surface of OM. Accordingly, a numerical model was built in MATLAB environment by coupling the the NICA-Donnan model (addressing metal ion-OM interaction), chemical equilibrium calculator, and empirically defined flocculation relations. Scenario analyses were performed using the model to provide detailed insight into the OM flocculation induced by Al^{3+} ions, in which the role of the type of OM and pH on the OM flocculation with Al^{3+} ions was examined.

The results reveal that the competition between cations for binding with OM together with the background pH is crucial in the flocculation of OM. A low pH-level (<4) enhances the protonation of functional groups on OM, as such limits the site-specific binding of Al^{3+} ions to OM molecules. At pH-levels above 6, the availability of ionic Al^{3+} is capped by the precipitation of aluminium hydroxides and consequently deteriorates the effectiveness of Al^{3+} as the coagulant. The optimal pH for Al^{3+} ions to coagulate OM is found between 5 and 6, in which range the Al^{3+} ions out competes H^{+} for binding with OM molecules and thus can lower the surface change on OM adequately to induce flocculation.

5.1. INTRODUCTION

The interaction between OM (organic matter) and metal ions plays an important role in many processes. Transport of contaminants (i.e., metal ions) through soils is widely recognised to be strongly controlled by metal-OM interactions [1–3], where the formation of organo-metallic complexes can either enhance the mobility of the metal ions (if the soluble complexes are formed) or lead to the retardation of the contaminants (when the complexes are insoluble). Physical soil properties can also be affected by metal-OM interactions. For instance, during Podzolization, the localised precipitation and accumulation of organo-metallic precipitates result in a distinct soil horizon that is considerably stiffer with a significantly lower permeability [4]. In the field of water treatment, metal-OM interactions are used as a well-established process to remove natural organic matter (NOM) from the water stream. The addition of metal salts (mostly based on aluminium or iron) induces the flocculation and sedimentation of OM, thus removing pollutants from the liquid phase [5–7].

Metal-OM interactions have been extensively studied in both soil science and water treatment, but with different focus. The primary interest of soil scientists is to assess the dual effect of OM in determining the free metal ion concentrations, which is relevant to bioavailability and toxicity studies, in a natural environment [8–10]. Consequently, researchers from soil science often view the metal-OM interaction in the context of geochemistry. As such OM is considered to be a mixture of organic compounds with distinct chemical characteristics and the focus is on its ion-binding behaviour [10–14]. Researchers revealed that the metals show preferential ion-binding to OM, where metal cations, such as Al^{3+}, $Fe^{2/3+}$, Cu^{2+} and Ca^{2+}, bind strongly with OM [1, 15, 16]. Semi-mechanistic models, such as the NICA-Donnan model [11, 17] and Model VI [18], are readily available to describe the metal ion-binding to OM under various environmental conditions (i.e., varying pH and ionic strength) in an aquatic system. The flocculation and subsequent precipitation of OM as a result of its interaction with metal ions have been, to our knowledge, not yet studied in detail in soil science. This might be attributed to the intrinsic complexity of soils, where other processes, such as the adsorption to mineral surfaces and biodegradation, are co-occurring and also affect the solubility of OM. As such the extent of the flocculation/precipitation of OM becomes difficult to evaluate [4].

Flocculation of OM is an important topic in the water treatment practice. Researchers in this field often interpret the flocculation of OM from the perspective of colloidal stability, where OM is conceptualised as negatively charged particles [5, 6, 19]. Due to the electrical repulsion, these OM particles are stabilised in suspension. In line with classical DLVO theory [5, 19–21], the flocculation mechanism of OM by metal ions is considered to be induced by the charge neutralisation of OM particles: the addition of positively charged metal cations neutralises the negative charge of OM particles and subsequently destabilises the suspension.

The DLVO theory primarily addresses the electrical and physical interactions. However, the extent of the metal-OM interaction is actually determined by the chemical characteristics of OM [12–14]. Instead of being purely controlled by electrostatics, the interaction between OM and metal cations is highly specific, where site-specific binding to functional groups on OM and electrostatic interaction occur simultaneously [12, 17]. We

aim to integrate the concept of charge neutralisation which induces flocculation with the description of site specific binding on functional groups of the OM. This integrated approach allows for a quantitative description of the metal-OM flocculation process.

A conceptual model is introduced with the aim to quantitatively describe the flocculation mechanism of OM. This model is consistent with the current state of the art. The conceptual model integrates the NICA-Donnan model to describe the metal ion-OM interaction, and the extent of metal ion-OM interaction is interpreted in line with DLVO theory in order to assess the flocculation potential. The conceptual model is implemented in MATLAB [22] and is coupled with the chemical equilibrium simulator ORCHESTRA [23]. In order to obtain a quantitative understanding of the conceptual model, a number of scenario analyses were performed to study OM flocculation induced by Al^{3+} ions. The scenario analyses examined the impact of the type of OM and pH on the OM flocculation with Al^{3+} ions where the values for the parameters in the model were obtained from literature.

5.2. MATERIAL AND METHODS

5.2.1. BATCH EXPERIMENT

In order to gain understanding in the pH-dependence of the flocculation of dissolved organic matter, a batch experiment was carried out. The dissolved organic matter used in this batch experiment is the same as for our field experiments [24]. This organic matter, potassium humate (HUMIN P775, Humintech, Germany; later on referred to as HPA), is commercially available for industrial applications. HPA was extracted from leonardite and reacted with potassium compounds to obtain high solubility in water (information provided by the producer). The batch experiment was performed with a HPA concentration of 3 g/L, which contains approximately 0.1 mol/L of dissolved carbon. The initial pH of the HPA solution is around 9.5, and batches were adjusted to 15 different pH-values in the interval between 9 and 2 using a HCl solution. These solutions were vigorously shaken and then placed stilly for 24 hours at 25 ^{o}C. Samples were then taken from the supernatant (if flocculation occurred) or the suspension (if no flocculation took place) in order to quantify the dissolved fraction of OM using UV-VIS spectroscopy at 254 nm wavelength.

5.2.2. MODELLING APPROACH

CONCEPTUAL MODEL

The prerequisite of a quantitative description of the OM flocculation is the development of a conceptual model. The developed conceptual model is illustrated in Figure 5.1, where its development began with understanding why OM molecules can remain dissolved in solution. The dissociation of the functional groups on OM molecules leads to the development of a net negative surface charge [14]. This negative surface charge is compensated by cations attracted electrically in the double layer. A high negative surface charge corresponds to a large electrical repulsion, and a sufficient separation between OM molecules in order to prevent the occurrence of other short range interactions (illustrated in Figure 5.1 a). Instead of using charge neutralisation, we use a more precise approach to assess the flocculation of OM. Site-specific binding of cations on these

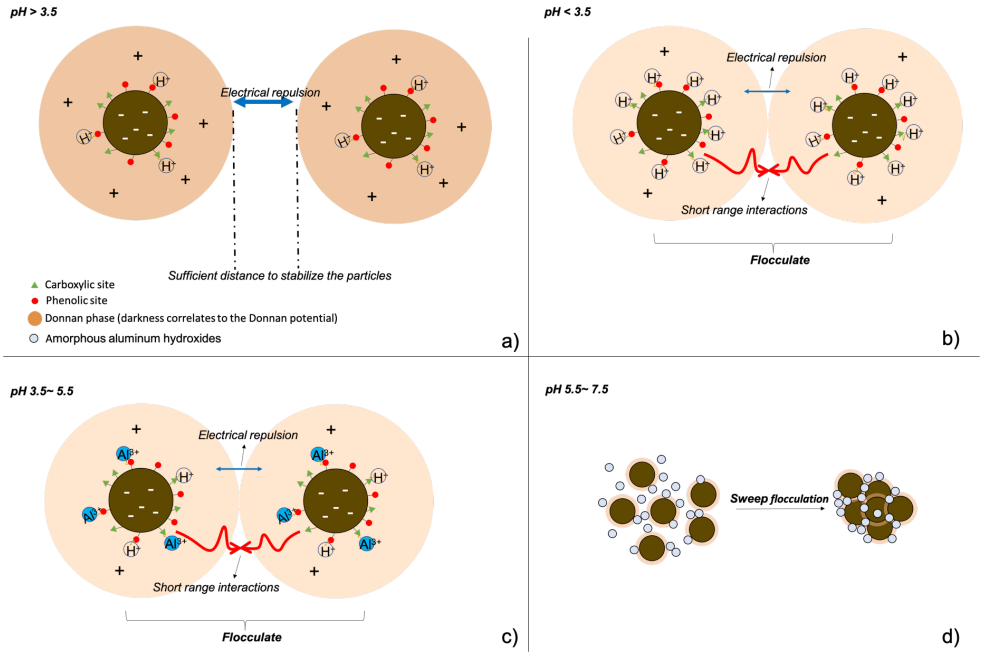

Figure 5.1: Conceptual model of OM flocculation. a) shows a stable OM suspension, where electrical repulsion is sufficiently high due to the high negative charge on the OM molecules; b) indicates the flocculation of OM induced by reducing the pH where protonation of functional groups on the OM molecule reduces the negative surface charge and thus lowers the electrical repulsion; c) shows the flocculation of OM induced by the addition of Al^{3+} ions, where site-specific binding of Al^{3+} to OM causes the reduction of the surface charge on OM; and d) illustrates the sweep flocculation of OM caused by precipitation of amorphous aluminium hydroxides from solution, in which OM co-precipitates. The pH ranges in a), b) and c) are derived from our batch experiment and are specific for the type of OM we used.

functional groups decreases the net negative surface charge of the OM molecules, which decreases the electrical repulsion and leads to a condition that favours the occurrence of other short range interactions. Flocculation of OM takes place when the net negative surface charge is sufficiently reduced. Taking the site-specific binding into account enables the differentiation of the flocculation behaviour of OM with respect to different coagulants (illustrated in Figure 5.1 b for binding of only protons and c for competitive binding of both protons and Al^{3+}).

In addition, at high pH-values, amorphous aluminium hydroxides will be formed and this affects the solubility of OM via another mechanism, namely sweep flocculation. As reported in the literature [5, 25, 26], owing to their small size, amorphous aluminium hydroxides have a very large surface area. As such, when the amount is adequate, they co-precipitate with OM molecules. Although the sweep flocculation involves little interaction between Al^{3+} ions with OM molecules, which is the primary focus of this study, it should certainly be a part of the conceptual model for addressing OM flocculation with aluminium. Accordingly, sweep flocculation is incorporated into the conceptual model (Figure 5.1 d). As sweep flocculation is based on a completely different mechanism, which is beyond the scope of studying the impact of surface charge on the flocculation of OM, we have not attempted to develop a quantitative description for sweep flocculation in this study.

The conceptual model is implemented in a simulation code where the semi-mechanistic NICA-Donnan model [17] is adapted to describe the metal ion-OM interaction and the potential of flocculation is assessed in line with DLVO theory. This allows for a quantitative description of the flocculation mechanism of OM as a function of pH and metal cation concentration in solution. We implemented this model in MATLAB [22] where we coupled the NICA-Donnan model (describing the ion-binding behaviour of OM) [17] with the geochemistry calculator (ORCHESTRA) that evaluates multi-phase speciation [23]. The model output was processed and plotted using the available tools in the MATLAB environment.

NICA-DONNAN MODEL

The NICA-Donnan model takes the intrinsic heterogeneity of OM, the competition of ions for the binding sites on OM and the electrostatic interaction between charged ions into account [11, 17]. In order to implement this model, we distinguish two types of ion-OM binding: site-specific binding (NICA, non-ideal competitive adsorption, model) and non-specific coulombic binding (Donnan model). The derivation of NICA-Donnan model (especially NICA model) involves a number of empirical 'fitting' parameters that are required to capture the 'non-ideal' behaviour as well as the intrinsic complexity of OM [11, 17]. This use of empirical parameters allows for the description of ion-OM interaction under a wide range of environmental conditions [3, 27]. Milne *et al.* [28] parameterised the NICA-Donnan model by re-analysing an extensive dataset of metal-OM binding experiments. The NICA-Donnan model has become one of the most applied models in simulating the interaction between OM and metal ions.

In our conceptual model we assume that two of the functional groups on OM, carboxylic and phenolic groups, are dominant for binding metal cations [14, 29]. This is reflected in the NICA model (Equation 5.1).

$$Q_i = Q_{\max 1} \cdot \frac{n_{i1}}{n_{\mathrm{H1}}} \cdot \frac{(\widetilde{K}_{i1} C_{iD})^{n_{i1}}}{\sum (\widetilde{K}_{i1} C_{iD})^{n_{i1}}} \cdot \frac{\left\{(\widetilde{K}_{i1} C_{iD})^{n_{i1}}\right\}^{p_1}}{1 + \left\{(\widetilde{K}_{i1} C_{iD})^{n_{i1}}\right\}^{p_1}} + Q_{\max 2} \cdot \frac{n_{i2}}{n_{\mathrm{H2}}} \cdot \frac{(\widetilde{K}_{i2} C_{iD})^{n_{i2}}}{\sum (\widetilde{K}_{i2} C_{iD})^{n_{i2}}} \cdot \frac{\left\{(\widetilde{K}_{i2} C_{iD})^{n_{i2}}\right\}^{p_2}}{1 + \left\{(\widetilde{K}_{i2} C_{iD})^{n_{i2}}\right\}^{p_2}} \tag{5.1}$$

where the subscripts 1 and 2 refer to the carboxylic and phenolic sites respectively; Q_i expresses the amount of ion i bound to OM via site-specific binding [mol/kg]; $Q_{\max}$ denotes the density of the sites [mol/kg]; $\widetilde{K}_i$ is the median affinity for ion i in regard to the respective site [-]; C_{iD} is the concentration of ion i in the Donnan phase [mol/L]; p and n_i are the fitting parameters, which reflect the heterogeneity of OM and non-ideality of ion i [-].

The proton dissociation from these two functional groups creates a net negative surface charge on OM. The maximum negative potential created by the respective dissociation is parameterised with $Q_{\max 1}$ and $Q_{\max 2}$. The occurrence of site-specific binding with cations neutralises the negative charge of the respective functional group and leads to a reduction in the net negative surface charge on OM (Equation 5.2).

$$q = -Q_{\max 1} + z_i \sum Q_{i1} - Q_{\max 2} + z_i \sum Q_{i2} \tag{5.2}$$

where q is the net negative surface charge [eq/kg]; Q_{i1} and Q_{i2} refer to the ion i bound to carboxylic and phenolic sites respectively; and z_i is the charge of ion i.

Electrostatic interaction occurs between charged molecules/ions in solution. This interaction is described with the Donnan model. In this model, the OM molecule is assumed to a sphere, where its negative charge (q) is compensated by the attraction of cations in its double layer [17, 30]. The corresponding electroneutrality is expressed in Equation 5.3.

$$q / V_D + \sum z_i (C_{iD} - C_i) = 0 \tag{5.3}$$

where V_D is the volume of water in the Donnan phase [L/kg] and C_i denotes the concentration of ion i in the liquid phase [mol/L]. In line with the finding from Benedetti *et al.* [31], the volume of this double layer (Donnan volume) is dependent on the background ionic strength, I (Equation 5.4).

$$\log_{10}(V_D) = a - b \log_{10}(I) \tag{5.4}$$

where a and b are constants.

In order to study the flocculation of different types of OM we chose to define reactive OM as a mixture of HA (humic acid) and FA (fulvic acid). This is in line with the research from van Zomeren and Comans [32], which shows that OM can be classified as being constituted by different proportions of HA, FA and Humin (which is an inert fraction). It should be realised that the distinction between HA and FA relies on an operational proxy, which is mostly based on the solubility of OM in alkaline extracts. How-

ever, OM especially NOM is known to be thoroughly mixed with various organic compounds ranging from plant residuals to highly oxidised carbon in carboxylic acids [33]. Lehmann and Kleber [13] argued that a fundamentally robust description of OM should be a continuum model. Indeed, a continuum model would address the nature of OM to a much better extent. However, the modelling development of such continuum model remains a challenge and requires extensive amounts of quantitative data which is not yet available. As such, Lehmann and Kleber [13] recognised that the humification theory is still the predominant theory in classifying OM, mainly because of the fact that a large quantitative dataset were adapted to this theory. As such the parameterisation of the NICA-Donnan model becomes possible [28]. Though we understand and acknowledge the limitations of the usage of HA and FA, we chose to model the complexity of OM by varying the proportion of HA and FA following others [3, 32].

CHEMICAL EQUILIBRIUM

In order to quantitatively describe the flocculation mechanism of OM that is induced by interaction with metal ions we need to describe the behaviour of metal cations in solution. Nearly all metal ions are hydrolysed in water. The OM binding characteristics of hydrolysed metal ions may be considerably different than those of non-hydrolysed ionic metal ions. As reflected in the formulation of the NICA model (Equation 5.1), the ion-binding with functional groups is highly specific. However, because of the limited availability of data, site-specific binding with hydrolysed metal ions is not considered explicitly in the parametrisation of NICA model [17, 28]. With respect to the Donnan model, the charge of hydrolysed ions is often less positive, indicating that electrostatic binding will also be influenced by hydrolysis.

In this study we focus on monomeric Al^{3+} ions. Some of successive hydrolysis reactions of Al^{3+} ions are shown in Table 5.1, where the equilibrium constants (K) are taken from the minteq.v4 database. Besides the speciation of Al^{3+} ions in the liquid phase, it is important to also include precipitation reaction of aluminium hydroxides. The corresponding mineral formation equation is given as Equation 5 in Table 5.1. Because all equilibrium reaction equations in Table 5.1 depend on the proton concentration, all reactions and as a result also the ion-binding with OM molecules depend strongly on pH. We use the ORCHESTRA simulator to calculate the concentrations of each hydrolysed Al species in the liquid solution as well as the amount of precipitated amorphous aluminium hydroxides as a function of pH. The fraction of Al-species versus pH for a fixed amount of Al in the system is shown in Figure C1 in Appendix C.

Table 5.1: Hydrolysis of Al^{3+} ions in an aqueous system

Liquid phase		
$Al^{3+} + H_2O \longleftrightarrow Al(OH)^{2+} + H^+$	$\log_{10} K_1 = -4.99$	(1)
$Al^{3+} + 2H_2O \longleftrightarrow Al(OH)_2^+ + 2H^+$	$\log_{10} K_2 = -10.09$	(2)
$Al^{3+} + 3H_2O \longleftrightarrow Al(OH)_{3(aq)} + 3H^+$	$\log_{10} K_3 = -16.79$	(3)
$Al^{3+} + 4H_2O \longleftrightarrow Al(OH)_4^- + 4H^+$	$\log_{10} K_4 = -22.60$	(4)
Solid phase		
$Al^{3+} + 3H_2O \longleftrightarrow Al(OH)_{3[am]} + 3H^+$	$\log_{10} K_{sp} = -10.80$	(5)

FLOCCULATION OF OM

The first step in the modelling of the flocculation is to define the critical surface charge level on OM molecules where flocculation occurs. The intrinsic complexity of OM requires that in order to model OM characteristics, serious simplifications have to be made [14]. This is also true for the modelling of OM flocculation. As stated in the conceptual model, the reduction of the net negative surface charge leads to a condition that favours other short-range interactions to take place which eventually lead to flocculation of OM. Though the surface charge is calculated with the NICA-Donnan model, other factors such as the structure and molecular weight of OM are also important but are not accounted for in the model. We thus assume that the critical surface charge depends on the source and type of OM, and it has to be identified individually. At the same time the critical charge should be independent from the ions which bind to the active sites on the OM. For HPA, used in this research, our experiments indicate that flocculation occurs when the pH is lowered below 3.5, which corresponds to a net negative surface charge that is less than 1.2 eq/kg (details will be elaborated on in the Results section of this paper).

We assume full chemical equilibrium during flocculation (described in Section 5.2.2), which implies that as soon as the surface charge reaches the critical level, flocculation of OM will be instantaneous. Even though the flocculation of OM is widely understood to be a fast process, our experimental results as well as data from literature [5, 15] indicate that flocculation in not completely instantaneous. In order to mimic the kinetic behaviour in the flocculation pattern, we use the following approach. The fraction of OM that flocculates is determined by the saturation of the surface charge:

$$f_F = \frac{q_{max} - q_{critical}}{q_{max}} \tag{5.5}$$

where f_F is the fraction of OM that flocculates [-]; $q_{critical}$ is the critical charge level [eq/kg] and q_{max} is the total charge capacity of the OM, which is the sum of both site densities (shown in Equation5.1) [eq/kg]. This implementation is consistent with DLVO theory, where electrostatic repulsion determines the extent of the energy barrier that particles have to overcome in order to flocculate. Tufenkji and Elimelech [34] concluded that a larger probability of particle collision coincides with a smaller energy barrier. In terms of flocculation of OM molecules, a low critical surface charge level indicates a lower repulsive energy barrier and therefore a more profound flocculation. Due to the assumed equilibrium, a more profound flocculation is approximated as a larger fraction of precipitated OM.

In order to calculate the amount of cations that co-precipitates with OM we use the results from the NICA-Donnan model which provides the amount of both site-specifically and electrically bound Al. We assume the same fraction (f_F) of bound Al will co-precipitate. However, it is also well known that free Al species participate in the bridging of OM molecules during the flocculation process [21], and this contribution is not included in the calculation of bound Al. If the bridging by free Al species is not taken in to account, the residual OM in the liquid phase will still be at the critical state and (according to our implementation) it will continue to flocculate regardless whether further Al^{3+} ions are added. In order to solve this problem, a correction term ($f_{bridging}$) is introduced and

the amount of co-precipitated Al is calculated as: $f_{\text{bridging}} * f_{\text{F}} * \text{Al}_{\text{bound}}$. This parameter , f_{bridging} has a value larger than 1 in order to ensure that more Al^{3+} ions are removed from the liquid phase and, consequently, the surface charge of the dissolved fraction OM is above the critical level. This is thermodynamically consistent because flocculation should result in a liquid phase that is stable [35]. The determination of f_{bridging} needs to be done experimentally. For this study, we assumed a constant value of 1.1.

5.2.3. THE IMPLEMENTATION

The simulation is performed in a MATLAB script that couples with ORCHESTRA calculator [23] as well as other user-programmed functions in MATLAB. A schematic illustration of the model structure is given in Figure 5.2. Specific adaptations to the ORCHESTRA calculator were made in this model. As shown in Figure 5.2, the model explicitly accounts for the contribution of the carboxylic, phenolic site binding and electrical attraction for all ions present in the system. Based on the outputs of the ORCHESTRA calculation, the flocculation of OM and the co-precipitation of ions are evaluated in the MATLAB environment. The flocculated mass, including OM and ions, is assumed to be non-reactive and is subsequently subtracted from the input mass for following calculations in ORCHESTRA. The complete data derived from the titration process is then processed and visualised in MATLAB.

Various scenario analyses were performed with the model as the way to generate insight into the flocculation process. The first scenario was designed to mimic the batch experiment, which is to simulate the acid titration of a HPA solution in a high background concentration of K^+ ions (0.1 mol/L). Titrations of $AlCl_3$ in HPA solution at various pH-levels (fixed throughout the titration process) were simulated with another scenario analysis. The binding characteristics of HPA in these two scenario analyses were assumed to be identical to that of HA. In order to study the effect of the type of OM on its flocculation process, the other titrations of $AlCl_3$ in OM were simulated, in which the composition of the OM varied: the FA fraction increased from 0% to 75% by a step of 25%.

5.3. RESULTS AND DISCUSSION

5.3.1. CONCEPTUAL MODEL OF OM FLOCCULATION

In order to understand the charge neutralisation of OM molecules, which is often used to explain the flocculation of OM [5, 21, 25], a batch experiment was performed. In this experiment, a solution of HPA was acidified using HCl in a high background concentration of K^+ ions (0.1 mol/L). The results from this batch experiment indicate that the presence of K^+ ions does not affect the solubility of OM which is also corroborated by results obtained by Benedetti *et al.* [36] and Kinniburgh *et al.* [17]. In the batch experiment, we clearly see that flocculation of OM occurs when the concentration of H^+ is sufficiently high (Figure 5.3). In this figure we also show the results calculated with our model, which resemble the similar flocculation pattern.

The above results corroborate with our conceptual model (illustrated in Section 5.2.2 and shown in Figure 5.1), in which the site-specific binding to the functional groups on OM molecules is identified as the driver for flocculation. A deeper insight into the role of

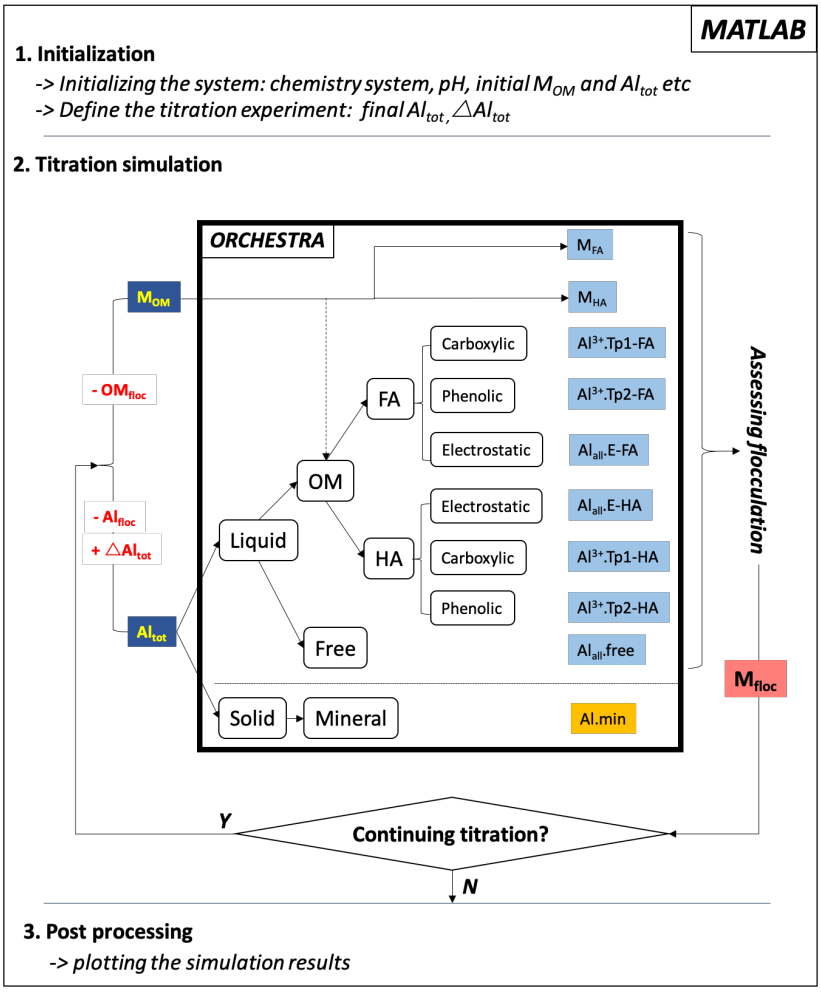

Figure 5.2: Schematic illustration of the model structure using Al^{3+} ions as example.

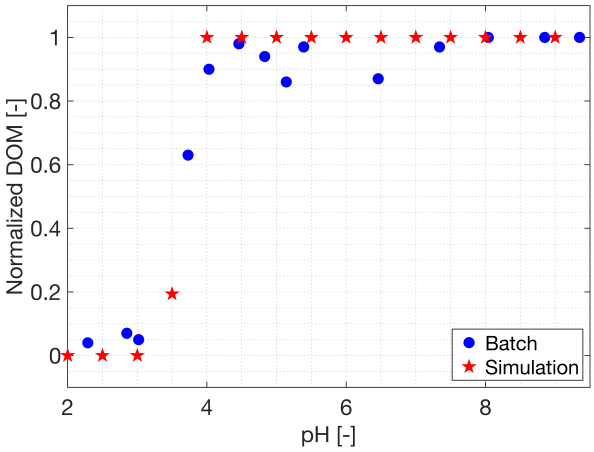

Figure 5.3: Measured and simulated dissolved fraction of HPA as a function of pH.

site-specific binding in the flocculation of OM was further obtained with the scenario analysis using the model, where our implementation explicitly accounts for different ion-OM binding mechanisms as well as multi-phase speciation of ions.

Figure 5.4 gives an insight in the species distribution for the acid titration of HPA. Though the total amount of bound cation remains constant throughout the titration, due to the decrease in pH, H^+ gradually replaces K^+ ions that were initially bound to OM. As expected, the charge-balance criterion requires the total charge in the bound cations to remain constant. However, the distribution of the cations over the different binding sites varies as a function of pH and consequently so did the electrostatic binding in the system. Increased availability of H^+ leads to the protonation of the carboxylic and phenolic groups, that are located on the surface of OM molecules (Figure 5.4 a), while the binding of K^+ is electrostatic only.

Protonation of the carboxylic and phenolic groups leads to a decrease in the negative surface charge of the OM molecules (Figure 5.4 b). As a consequence, less counter ions are required to balance charge in the double-layer [30, 31], corresponding to a decrease in the electric potential in the Donnan phase. This leads to a reduction in the electrical repulsion between OM molecules and thus a smaller separation distance [34]. When this separation distance becomes small enough, classical DLVO theory states that other short range interactions including hydrogen bonding, van de Waals attraction and the bridging by multivalent cations, become important and eventually leads to the flocculation of OM molecules [6, 37, 38]. This corroborates with the result of the batch experiment, where the flocculation takes place at pH-values between 3 and 4, which apparently correspond with a sufficiently reduced surface charge level as suggested by the model (Figure 5.4 b).

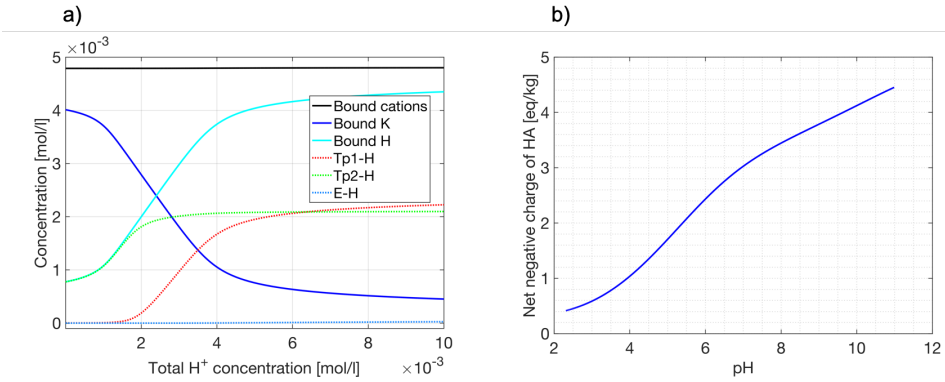

Figure 5.4: Proton binding to HPA in a 0.1 mol/L KNO_3 background electrolyte. Figure a) shows the partitioning of K^+ and H^+ over the various reactive complexes as a function of pH. The solid black line represents the total amount of bound cations (including H^+ and K^+ ions) throughout the titration; Tp-1 and Tp-2 stand for proton binding to carboxylic and phenolic group respectively; E-H denotes the proton binding to HPA electrically. Because phenolic site is weaker in terms of acidity than the carboxylic group, its protonation takes place at a significantly lower pH-values. b) indicates the corresponding change of the net negative surface change on HA during the titration process.

5

5.3.2. Al^{3+} AS THE COAGULANT

As shown in the results above, reducing the surface charge on OM using only H^+ requires a very low pH. Such low pH-levels are generally not found in the natural environment. Metal cations, such as Al^{3+}, $Fe^{2/3+}$, Cu^{2+} and Ca^{2+}, also bind to the functional groups on OM [11], and their concentrations can vary over a large range. Milne *et al.* [28] found that Al^{3+}, Fe^{3+} and Cu^{2+} have the highest affinities among other common metal ions. Because flocculation of OM depends on the reduction of surface charge, the charge of the metal ions is therefore important. Highly charged cations reduce the negative surface potential of OM more effectively and are therefore more efficient coagulants. The flocculation efficiency of Fe^{3+} is very good as it has both high binding affinity and high charge, the stability of the flocculant is a concern under reduced circumstances. The reduced form, Fe^{2+}, has poor binding affinity [28] and lower charge, making it a less desired flocculant. Consequently we consider Al^{3+} to be suitable for creating OM flocs. In fact, Al^{3+} is the most applied coagulant in wastewater treatment plant for removing OM pollutants [5, 19].

To demonstrate the effectiveness of Al^{3+} ions as the coagulant in inducing the flocculation of OM, titrations of HA (0.84 g/L) with Al^{3+} in 0.1 mol/L KNO_3 at fixed pH-levels of 4.5 and 5.5 are simulated. Reduction of the negative surface charge via site-specific binding is the driving force for the flocculation of OM. The simulation results (Figure 5.5 a), indicate competition between Al^{3+} and H^+ for the binding sites on the OM. Given that Al^{3+} ions have a higher binding affinity towards the phenolic group than H^+ [17], Al^{3+} ions replace protons that were associated with phenolic sites when its concentration is in the same order as that of H^+. Carboxylic sites appear to be less susceptible to an increased concentration of Al^{3+} ions. Only after the Al^{3+} concentration is nearly an order of magnitude higher than that of H^+, H^+ ions are replaced by Al^{3+} ions. The extent

of Al^{3+} binding on carboxylic sites is significantly smaller than Al^{3+} binding on phenolic groups (Figure 5.5 a).

The simulation also shows that the exchange ratio of Al^{3+} to H^+ is less than 1, implying that more H^+ ions are moved from the OM than Al^{3+} ions are bound. The net negative surface charge, however, decreases as more Al^{3+} ions are added, mainly because of the high positive charge of Al^{3+} ions (shown in Figure 5.5 b). This result is a strong indication that flocculation of OM molecules can be induced by adding Al^{3+} ions. Consequently, the conceptual model is expanded to address the OM flocculation induced by Al^{3+} ions (illustrated in Figure 5.1 c).

Because Al^{3+} is the most prominent species among all other hydrolysed aluminium species, in binding with functional groups on OM, Al^{3+} ion-binding should be highly dependent on pH because of the pH-dependency of Al-hydrolysis (described in Section 5.2.2). As a consequence it is important to include this pH-dependency in the modelling of the competition between Al^{3+} and H^+ for the binding sites. The mole fraction of free ionic Al^{3+} is reduced by a factor of three when the pH increases from 4.5 to 5.5 (Figure C1 in Appendix C). This implies that the site-specific binding of Al^{3+} ions at pH 4.5 should be more prominent than at pH 5.5. This is, however, not the case because the competition by H^+ is also more profound at lower pH-values. The simulations (shown in Figure 5.5 a), illustrate that the site-specific binding of Al^{3+} ions is more prominent at pH 5.5 than at pH 4.5. As a consequence, the reduction of negative surface charge at pH 5.5 is larger than that at pH 4.5 (Figure 5.5 b).

Even though the surface charge reduction is more profound at pH 5.5, the simulation shows that this reduction stops after the concentration of Al^{3+} ions reached a specific level. This stagnation is attributed to the hydrolysis of Al^{3+} ions, which leads to the precipitation of amorphous aluminium hydroxides at higher pH-levels (>5). The consequence of this precipitation is that the ionic Al^{3+} concentration in solution can no longer increase (Figure C1 in Appendix C and the mineral formation Equation is included in Table 5.1). The simulation results in Figure 5.5 a) demonstrate that the exchange between bound H^+ with Al^{3+} also ceases and consequently, the surface charge will no longer decrease (Figure 5.5 b).

These results clearly illustrate the significance of pH for Al^{3+} ion-binding on OM. In order to further demonstrate the effect of pH on the Al-OM binding, the simulated titration of OM solution with Al^{3+} ions is repeated at constant pH-values which range between 3 and 8. The results in Figure 5.6 a) show that Al^{3+} ions reduce the negative surface charge on OM most effectively at intermediate pH-values (5-6). A low pH-values the H^+ out competes Al^{3+} because of its high concentration in solution. At higher pH-values, the fraction of Al^{3+} ions in solution is limited due to the hydrolysis process.

The simulation results clearly show that the onset of stagnation in surface charge reduction is pH dependent. The reason for this is that the ion activity product of amorphous aluminium hydroxides depends both on the pH and the concentration of ionic Al^{3+} (Equation 5 in Table 5.1). Therefore, lower Al^{3+} concentrations are required to reach the saturation of amorphous aluminium hydroxides at higher pH-values. Deprotonation of functional groups at high pH-values also corresponds to a higher starting negative surface charge on OM (shown in Figure 5.4 and Figure 5.6). As identified in the conceptual model, the flocculation of OM molecules takes place when its surface charge is

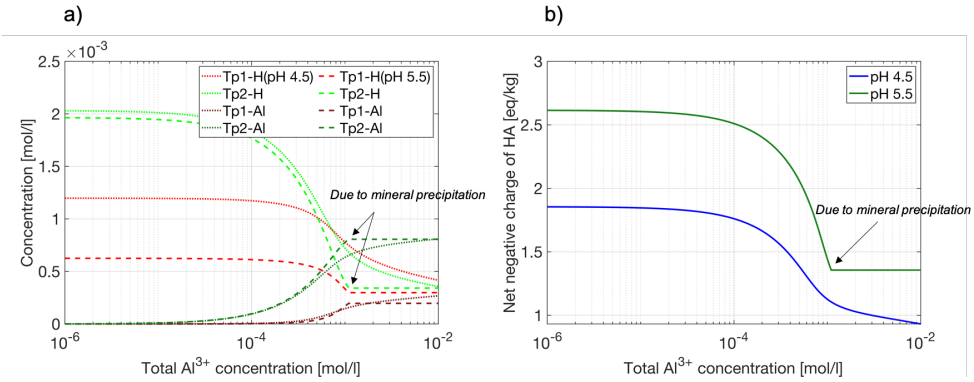

Figure 5.5: Simulated results of Al^{3+}-ion binding to HPA in a 0.1 mol/L KNO_3 background electrolyte at pH 4.5 and 5.5. a) shows the partitioning of various binding processes as a function of total Al in the system at fixed pH levels; b) indicates the corresponding change of the net negative surface change on HPA during the titration process.

5

sufficiently reduced. Limiting the surface charge reduction by the mineral precipitation implies that the charge level required for flocculation may not be reached at high pH-values (>6).

5.3.3. FLOCCULATION OF OM USING AL^{3+}

IMPACT OF THE IMPLEMENTATION

To demonstrate the impact of the implementation of the flocculation process, the titration of HPA (0.84 g/L) with Al^{3+} at pH = 4.5 is simulated. As stated in Section 5.2.2, the modelling of OM flocculation relies on the determination of the critical surface charge, which is identified as 1.2 eq/kg based on the results of our batch experiment (shown in Figure 5.3 and 5.4). The simulation (shown in Figure 5.7) clearly shows that flocculation occurs as soon as the calculated surface charge reaches the critical level. Further addition of Al^{3+} ions leads to a step-wise flocculation of the remaining dissolved fraction until no HPA is left in liquid phase. This step-wise pattern is the direct consequence of the inclusion of the correction term ($f_{bridging}$): the surface charge on the residual fraction of HPA in the liquid phase increases slightly after the occurrence of flocculation which corresponds to a stabile suspension. Qualitatively, this simulated flocculation pattern matches the data from the literature [5, 15].

THE PH-DEPENDENT M/C RATIO

In Figure 5.7 we use the molar metal to carbon ratio (M/C ratio) instead of the total amount of Al^{3+} in the system. A critical molar M/C ratio has often been used to describe the flocculation of OM induced by metal ions [16, 24, 39]. Our implementation of the flocculation process allows a quantitative analysis of the underlying principle behind this M/C ratio. The flocculation takes place at approximately the same M/C ratio (i.e., 0.027) regardless of the input OM concentration (the simulations are presented as Figure C2 in Appendix C). This result confirms the concept behind the critical molar M/C ratio.

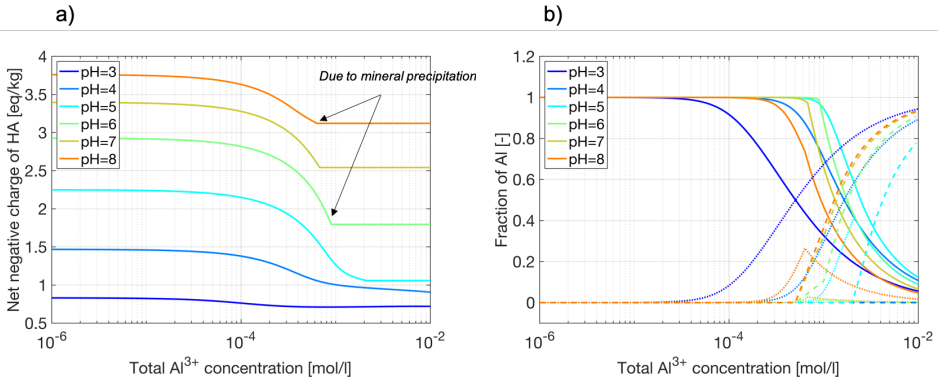

Figure 5.6: Adding Al^{3+} ions to HPA solution at various pH 3-8. a) change in the net negative surface change on HPA as function of total aluminium in system; b) fraction of Al: Al bound to HPA is denoted with solid lines; free Al fraction is shown as dotted lines; and dashed lines represent the Al in the mineral phase.

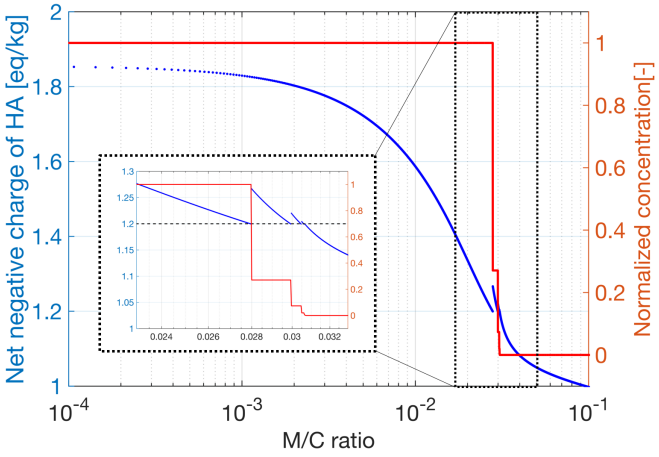

Figure 5.7: Simulated flocculation pattern in a titration of HPA with Al^{3+} at pH = 4.5. The blue dotted curve shows the net negative charge on HPA, the red solid curve shows the concentration of HPA in the liquid phase. The M/C ratio in the x-axis stands for molar metal to carbon ratio and the dashed black line represents the critical charge level at which flocculation of HPA will occur.

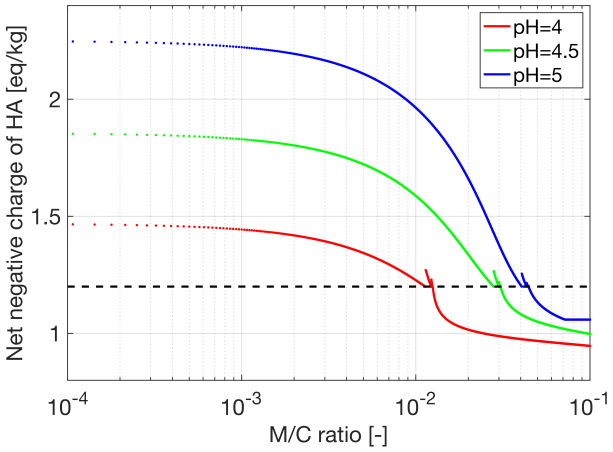

Figure 5.8: The simulated change in the net negative surface change during the titration of HPA using Al^{3+} at pH-values of 4, 4.5 and 5. The dashed black line shows the critical charge level.

However, our results also clearly show that value of the critical molar M/C ratio depends on the environmental conditions, where among others, the pH is most important. As discussed above, the interaction between Al^{3+} ions and OM is heavily influenced by the background pH. In order to obtain a deeper insight into the pH-dependency of the critical M/C ratio, a scenario analysis is performed where HPA is titrated with Al^{3+} at pH-values of 4, 4.5 and 5. The results from this scenario in Figure 5.8 show that an increase in pH leads to a larger value of the critical M/C ratio. The values for the critical M/C ratios are 0.011, 0.027, and 0.045 for pH-values of 4, 4.5 and 5 respectively. The origin of the dependency on pH is described in Section 5.3.2. At low pH-values, H^+ out competes Al^{3+} for binding at carboxylic sites, and as the consequence the starting surface charge on OM is lower than at higher pH-values. In this case, even though the binding efficiency of Al^{3+} ions is lower at low pH-values, a lower concentration of cations is required to bring the surface charge down to the critical level.

THE EFFECT OF THE TYPE OF OM

The effect of the type of OM on its flocculation behaviour is studied with a scenario analysis, where different types of OM are described using a mixture of HA and FA in different proportions (described in Section 5.2.3). The generic NICA-Donnan parameters (shown in Table C1 in Appendix C) were used for both HA and FA in order to capture the respective ion-binding characteristics. In order to describe flocculation, additional assumptions have to be made. The molecular weight of FA lies in the range of 1000 to 10000 which is an order of magnitude smaller than that of HA (10000 to 100000) [12, 14]. In addition, the composition of functional groups differs significantly between FA and HA. The carboxylic group accounts for 78%-90% of the total acidity of FA, while HA contains less carboxylic group (69-82%) [40]. Carboxylic groups are the major contribution of the net negative surface charge on OM molecules because of their high acidity (i.e., car-

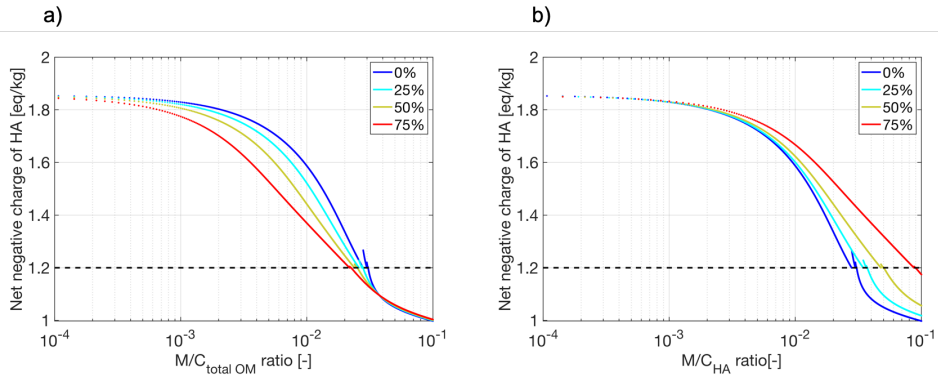

Figure 5.9: The critical M/C ratio for varying types of OM at pH = 4.5, where the fraction of FA increased from 0 to 75% with an interval of 25%. Because the FA fraction remains soluble at all pH values, the charge level on FA is not shown. The dashed black line shows the critical charge level. a) shows the net surface charge on HA as a function of the M/C ratio normalised by the carbon present in all OM dissolved, b) shows the surface charge on HA as function of the M/C ratio normalised by the carbon present in the HA fraction.

boxylic groups deprotonate at pH-values around 4.4 [41]). Therefore, due to the abundance of carboxylic groups in FA, these molecules have a larger negative surface charge compared with HA molecules. This is confirmed with the simulation shown in Figure C3 in the Appendix. According to the conceptual model, higher charge levels of FA indicates a stronger electrical repulsion compared to HA, and as a result larger separation distances between FA molecules. On the other hand, the smaller size of FA molecules makes it further difficult to form larger particles that are big enough to flocculate. Therefore, in our implementation, the FA fraction remains soluble at all conditions. This result is also consistent with the operational definition of FA, where FA stays soluble at all pH-values [12].

Results of this scenario analysis presented in Figure 5.9, indicate that the critical M/C ratio is a function of the type of OM. A higher fraction of FA leads to a lower value for the critical M/C ratio which is explained by the fact that carboxylic groups are the dominating functional group on FA and Al^{3+} ions bind strongly to phenolic functional groups [14] (Figure 5.5 a). Consequently, the binding capacity of FA is smaller than HA, meaning that a larger fraction of FA will increase the concentration of free Al^{3+} ions in the liquid phase (Figure C4 in Appendix C). As such the flocculation of the HA fraction occurs at a lower M/C ratios when the FA amount increases. Analysing the critical M/C ratio with respect to HA fraction present, competition between HA and FA for Al^{3+} ions becomes relevant. As shown in Figure 5.9 b), an increase in the FA fraction inevitably reduces the amount of Al^{3+} that can participate in the binding with HA. Furthermore, it is obvious that the total mass of OM that can be flocculated will decrease with increasing fractions of FA because we only take the HA fraction in to account for the precipitation process.

5.4. CONCLUSIONS AND IMPLICATIONS

Though the charge neutralisation has been widely understood as the mechanism for the flocculation of OM in the field of water treatment, the exact process that leads to the charge neutralisation is not specified. A process based conceptual model was developed for explaining flocculation of OM, in which the existing NICA-Donnan model is adapted to quantitively describe the site-specific binding of cations to OM. The model is implemented in a framework in which the ORCHESTRA chemical equilibrium simulator is integrated in the MATLAB computational environment.

Numerical scenario calculations describing the titration of OM solutions with Al^{3+} ions at fixed pH-values are used to obtain a quantitative understanding of concepts underlying the flocculation process. Competition between cations present in the liquid phase for binding sites on OM is a crucial aspect together with the pH of the solution. At low pH-values (<4) the H^+ ions out compete Al^{3+} ions for the binding sites on OM because of their relatively high concentration, so that extremely high concentrations of Al^{3+} ions are required to reduce the negative surface charge on OM. At pH-values above 6, the availability of ionic Al^{3+} is very low due to precipitation of aluminium hydroxides and consequently, Al^{3+} is no longer an effective coagulant. The optimal pH range for Al^{3+} ions to coagulate OM is between 5 and 6. This optimal pH ranges is related to the charge neutralisation mechanism. At pH-values larger than 7 sweep flocculation by fast precipitation of amorphous aluminium hydroxides may strip significant amounts of OM from the liquid phase.

Binding affinity of specific sites in OM is a crucial parameter controlling the ability to flocculate. More experimental data is required to quantify the critical surface charge values which determine the onset of flocculation. Experimental data are also required to quantify the the bridging factor introduced to quantify the amount of cation co-precipitated with OM.

The conceptual model and the numerical implementation of the coupled system of NICA-Donnan, chemical equilibrium and the semi-empirical flocculation process present a step forward toward a fully mechanistic quantitative description of OM flocculation. Using information (i.e, the critical charge level and the fraction of HA and FA) derived from lab experiments, this model can be used to engineer optimal flocculation approaches to induce the flocculation of OM under various pH-values.

ACKNOWLEDGEMENT

We would like to thank Max Veerkamp for his contribution in the lab work. This work is part of the research programme Water2014 with project number 13883, which is financed by the Netherlands Organisation for Scientific Research (NWO).

REFERENCES

[1] E. Tipping, C. Rey-Castro, S. E. Bryan, and J. Hamilton-Taylor, *Al (III) and Fe (III) binding by humic substances in freshwaters, and implications for trace metal speciation,* Geochimica et Cosmochimica Acta **66**, 3211 (2002).

[2] L. Weng, E. P. M. J. Fest, J. Fillius, E. J. M. Temminghoff, and W. H. Van Riemsdijk, *Transport of Humic and Fulvic acids in relation to metal mobility in a copper-contaminated acid sandy soil,* Environmental Science & Technology **36**, 1699 (2002).

[3] M. Ponthieu, O. Pourret, B. Marin, A. R. Schneider, X. Morvan, A. Conreux, and B. Cancès, *Evaluation of the impact of organic matter composition on metal speciation in calcareous soil solution: Comparison of Model VI and NICA-Donnan,* Journal of Geochemical Exploration **165**, 1 (2016).

[4] D. Sauer, H. Sponagel, M. Sommer, L. Giani, R. Jahn, and K. Stahr, *Podzol: Soil of the year 2007. A review on its genesis, occurrence, and functions,* Journal of Plant Nutrition and Soil Science **170**, 581 (2007).

[5] J. Duan and J. Gregory, *Coagulation by hydrolysing metal salts,* Advances in Colloid and Interface Science **100-102**, 475 (2003).

[6] E. L. Sharp, P. Jarvis, S. A. Parsons, and B. Jefferson, *The impact of zeta potential on the physical properties of ferric-NOM flocs,* Environmental Science & Technology **40**, 3934 (2006).

[7] P. Jarvis, B. Jefferson, and S. A. Parsons, *Floc structural characteristics using conventional coagulation for a high doc, low alkalinity surface water source,* Water Research **40**, 2727 (2006).

[8] P. A. van Hees and U. S. Lundström, *Equilibrium models of aluminium and iron complexation with different organic acids in soil solution,* Geoderma **94**, 201 (2000).

[9] E. R. Unsworth, K. W. Warnken, H. Zhang, W. Davison, F. Black, J. Buffle, J. Cao, R. Cleven, J. Galceran, P. Gunkel, E. Kalis, D. Kistler, H. P. van Leeuwen, M. Martin, S. Noël, Y. Nur, N. Odzak, J. Puy, W. van Riemsdijk, L. Sigg, E. Temminghoff, M.-L. Tercier-Waeber, S. Toepperwien, R. M. Town, L. Weng, and H. Xue, *Model predictions of metal speciation in freshwaters compared to measurements by in situ techniques,* Environmental Science & Technology **40**, 1942 (2006), arXiv:arXiv:1011.1669v3 .

[10] J. Xiong, L. Weng, L. K. Koopal, M. Wang, Z. Shi, L. Zheng, and W. Tan, *Effect of soil Fulvic and Humic acids on Pb binding to the goethite/solution interface: Ligand charge distribution modeling and speciation distribution of Pb,* Environmental Science & Technology **52**, 1348 (2018).

[11] D. G. Kinniburgh, C. J. Milne, M. F. Benedetti, J. P. Pinheiro, J. Filius, L. K. Koopal, and W. H. Van Riemsdijk, *Metal ion binding by humic acid: application of the NICA-Donnan model,* Environmental Science & Technology **30**, 1687 (1996).

[12] E. Tipping, *Cation binding by humic substances*, Vol. 12 (Cambridge University Press, 2002).

[13] J. Lehmann and M. Kleber, *The contentious nature of soil organic matter,* Nature **528**, 60 (2015).

[14] J. Adusei-Gyamfi, B. Ouddane, L. Rietveld, J.-P. Cornard, and J. Criquet, *Natural organic matter-cations complexation and its impact on water treatment: A critical review,* Water Research **160**, 130 (2019).

[15] L. Weng, E. J. Temminghoff, and W. H. Van Riemsdijk, *Interpretation of humic acid coagulation and soluble soil organic matter using a calculated electrostatic potential,* European Journal of Soil Science **53**, 575 (2002).

[16] K. G. Nierop, B. Jansen, and J. M. Verstraten, *Dissolved organic matter, aluminium and iron interactions: Precipitation induced by metal/carbon ratio, pH and competition,* Science of the Total Environment **300**, 201 (2002).

[17] D. G. Kinniburgh, W. H. Van Riemsdijk, L. K. Koopal, M. Borkovec, M. F. Benedetti, and M. J. Avena, *Ion binding to natural organic matter: competition, heterogeneity, stoichiometry and thermodynamic consistency,* Colloids and Surfaces A: Physicochemical and Engineering Aspects **151**, 147 (1999).

[18] E. Tipping, *Humic ion-binding model VI: an improved description of the interactions of protons and metal ions with humic substances,* Aquatic geochemistry **4**, 3 (1998).

[19] X. Wu, X. Ge, D. Wang, and H. Tang, *Distinct mechanisms of particle aggregation induced by alum and PACl: Floc structure and DLVO evaluation,* Colloids and Surfaces A: Physicochemical and Engineering Aspects **347**, 56 (2009).

[20] Y. Dudal and F. Gérard, *Accounting for natural organic matter in aqueous chemical equilibrium models: A review of the theories and applications,* Earth-Science Reviews **66**, 199 (2004).

[21] T. Li, Z. Zhu, D. Wang, C. Yao, and H. Tang, *Characterization of floc size, strength and structure under various coagulation mechanisms,* Powder Technology **168**, 104 (2006).

[22] MATLAB Release 2019a, *MATLAB Release 2019a* (2019).

[23] J. C. L. Meeussen, *ORCHESTRA: an object-oriented framework for implementing chemical equilibrium models.* Environmental science & technology **37**, 1175 (2003).

[24] J. Zhou, S. Laumann, and T. J. Heimovaara, *Applying aluminum-organic matter precipitates to reduce soil permeability in-situ: A field and modeling study,* Science of the Total Environment **662**, 99 (2019).

[25] D. Ghernaout and B. Ghernaout, *Sweep flocculation as a second form of charge neutralisationâĂŤa review,* Desalination and Water Treatment **44**, 15 (2012).

[26] C. T. Tanneru, J. D. Rimer, and S. Chellam, *Sweep flocculation and adsorption of viruses on aluminum flocs during electrochemical treatment prior to surface water microfiltration,* Environmental Science & Technology **47**, 4612 (2013).

[27] L. Weng, E. J. Temminghoff, and W. H. Van Riemsdijk, *Aluminum speciation in natural waters: Measurement using Donnan membrane technique and modeling using NICA-Donnan,* Water Research **36**, 4215 (2002).

[28] C. J. Milne, D. G. Kinniburgh, W. H. Van Riemsdijk, and E. Tipping, *Generic NICA-Donnan model parameters for metal-ion binding by humic substances,* Environmental Science & Technology **37**, 958 (2003).

[29] B. Manunza, C. Gessa, S. Deiana, and R. Rausa, *A normal distribution model for the titration curves of humic acids,* Journal of Soil Science **43**, 127 (1992).

[30] T. Saito, S. Nagasaki, S. Tanaka, and L. K. Koopal, *Electrostatic interaction models for ion binding to humic substances,* Colloids and Surfaces A: Physicochemical and Engineering Aspects **265**, 104 (2005).

[31] M. F. Benedetti, W. H. Van Riemsdijk, and L. K. Koopal, *Humic substances considered as a heterogeneous Donnan gel phase,* Environmental Science & Technology **30**, 1805 (1996).

[32] A. van Zomeren and R. N. J. Comans, *Measurement of Humic and Fulvic acid concentrations and dissolution properties by a rapid batch procedure,* Environmental Science & Technology **41**, 6755 (2007).

[33] S. E. Trumbore, *Potential responses of soil organic carbon to global environmental change,* Proceedings of the National Academy of Sciences **94**, 8284 (1997).

[34] N. Tufenkji and M. Elimelech, *Deviation from the classical colloid filtration theory in the presence of repulsive DLVO interactions,* Langmuir **20**, 10818 (2004).

[35] B. Dobias and H. Stechemesser, *Coagulation and flocculation: Theory and applications* (CRC Press, 2005).

[36] M. F. Benedetti, C. J. Milne, D. G. Kinniburgh, W. H. Van Riemsdijk, and L. K. Koopal, *Metal ion binding to Humic substances: Application of the non-ideal competitive adsorption model,* Environmental Science & Technology **29**, 446 (1995).

[37] W. J. Weber, P. M. McGinley, and L. E. Katz, *Sorption phenomena in subsurface systems: Concepts, models and effects on contaminant fate and transport,* Water Research **25**, 499 (1991).

[38] J. N. Ryan and M. Elimelech, *Colloid mobilization and transport in groundwater,* Colloids and Surfaces A: Physicochemical and Engineering Aspects **107**, 1 (1996).

[39] W. Z. Tamrat, J. Rose, O. Grauby, E. Doelsch, C. Levard, P. Chaurand, and I. Basile-Doelsch, *Soil organo-mineral associations formed by co-precipitation of Fe, Si and Al in presence of organic ligands,* Geochimica et Cosmochimica Acta **260**, 15 (2019).

[40] K. A. Rittle, J. I. Drever, and P. J. S. Colberg, *Precipitation of arsenic during bacterial sulfate reduction,* Geomicrobiology Journal **13**, 1 (1995).

[41] A. J. A. Aquino, D. Tunega, G. E. Schaumann, G. Haberhauer, M. H. Gerzabek, and H. Lischka, *The functionality of cation bridges for binding polar groups in soil aggregates,* International Journal of Quantum Chemistry **111**, 1531 (2011).

6

CONCLUSIONS AND OUTLOOK

A nature-based geo-engineering technique for reducing soil permeability can be a good alternative to manage the groundwater flow field while providing an economically effective and environmentally friendly solution for dike failure prevention. This research project, SOil Sealing by Enhanced Aluminium and DOM Leaching (SoSEAL), took inspiration from Podzolization to develop a geo-engineering solution for reducing soil permeability in-situ. The essence derived from Podzolization is that the complexation of organic matter (OM) with polyvalent metals, i.e., aluminium (Al), leads to the formation of organo-metallic precipitates [1, 2] and the precipitation and accumulation of these organo-metallic precipitates results in significant reduction in soil permeability. We therefore propose to apply Al-OM complexes to reduce soil permeability in-situ. In order to effectively innovate a novel technique based on this concept, two types of process understanding have to be developed and integrated. On one hand, the quantitative process understanding of the Al-OM interaction as well as the subsequent precipitation reaction needed to be developed. On the other hand, this process understanding must be taken in to the context of engineering as the objective of the research project is to innovate a practical technique. This PhD thesis aims to advance the innovation of the nature-based technique by developing knowledge in both domains in an iterative manner. This chapter summarises the main findings of this thesis and provides a number of recommendations for future developments.

6.1. PROCESS UNDERSTANDING OF AL-OM COMPLEXATION AND FLOCCULATION

The mechanistic modelling of Al-OM complexation presented in Chapter 5 provides a quantitative understanding of the Al-OM complexation and the subsequent flocculation process. The site-specific binding of Al^{3+} ions on to the OM molecule leads to a decrease of its negative charge, which originated from the dissociation of the functional groups on the surface of the OM molecule. As a consequence, the electrical repulsion between charged particles is lowered which results in a situation that favours the occurrence of flocculation. The most deterministic environmental condition that impacts the flocculation of OM using Al^{3+} ions is the pH. The impact of pH was assessed with scenario analyses using the model. The pH has a dual role in the context of Al-OM flocculation. On one hand, low pH-values (<5) favour Al^{3+} ions as the major product of the Al hydrolysis process, which is considered as the binding agent to the functional groups on OM. Low pH-values, however, also enhance the competition of protons for functional groups on the OM molecule, which subsequently reduce the level of site-specific binding between functional groups and Al^{3+} ions. A pH-level above 6 limits the availability of ionic Al^{3+} in solution due to the precipitation of aluminium hydroxides, and thus making Al^{3+} ineffective as a flocculation agent for OM. The optimal pH range for Al^{3+} ions to coagulate OM is between 5 and 6, in which range the ionic Al^{3+} is at sufficiently high concentrations to out compete H^+ for binding with OM molecules and, due to the triple valence, ionic Al^{3+} can sufficiently lower the surface charge on OM to induce flocculation.

6.2. APPLYING THE PODZOLIZATION-INSPIRED CONCEPT IN THE CONTEXT OF ENGINEERING

The focus of this research project is to develop a geo-engineering solution for reducing soil permeability in-situ based on the knowledge of Podzolization. As such, the necessity of bringing the concept of Podzolization to the context of engineering becomes obvious. This research project relies on full-scale field experiments as a tool to obtain insights regarding the feasibility of the geo-engineering solution. In total, two full-scale field experiments were carried out, where two different approaches for delivering Al-OM flocs into the subsurface in order to install a flow barrier were tested. The success of these full-scale field experiments attributed to the 'co-makership' model we embraced for carrying out the research project. This approach makes the required resources available for implementing a successful field experiment. In addition, the modelling approach we applied makes it feasible to integrate the development of fundamental theoretical concepts with implementation in real-world applications (Chapter 2). The combination of the 'co-makership' model and the modelling approach answered three key questions: 1) why do we need to reduce soil permeability; 2) how can soil permeability be reduced and 3) what activities are required to implement the approach on site.

6.2.1. DEFINE THE OBJECTIVES OF THE FIELD EXPERIMENT

The first 'why' question was answered by analysing the site provided by dike owners using the model in order to define the required characteristics of the flow barrier. As detailed in Chapters 2, 3 and 4, the requirements for the flow barrier differed significantly in regard to the particular site and the corresponding aim. For instance the field experiment at Veersedijk (which the first pilot project was carried out, Chapter 3) aimed to explore the feasibility of using Al-OM complexes to reduce soil permeability in-situ, thus the size of the site is relatively small. Using the scenario analysis with the multi-physics modelling, the most optimal structure of the flow barrier was found to be a cylindrical geometry (inner diameter of 5 m). A cylindrical geometry makes it relatively easy to measure changes in the groundwater system caused by the presence of the low-permeability zone and therefore quantify the reduction in permeability (Chapters 2 and 3). While for the other field experiment in De Biesbosch (the second pilot project we carried out, Chapter 4), the aim was to resolve the muddy conditions and a limited bearing capacity of the top soil at the toe of the dike. The scenario analysis in this case was performed to find the explanation for the high water content in the toe of the dike and derive a solution. The proposed solution was to install an up-stream flow barrier which can lower the groundwater table at the toe of the dike. The modelling was applied to quantify the geometry of the barrier and the required reduction in permeability in order to obtain the desired hydraulic head profile in the dike (Chapters 2 and 4).

6.2.2. DESIGN THE FIELD EXPERIMENT

The 'how' and 'what' questions were tackled by universities, contractor and consultancies, using a combined science-oriented research and applied engineering approach. The cylindrical flow barrier at the site Veersedijk was to be created by injection of two solutions (Al and OM) followed by in-situ mixing and reaction, while direct injection of

Al-OM flocs was the approach for the creation of the flow barrier at the site De Biesbosch. In order to understand the feasibility of installing a flow barrier using the different approaches in-situ, a numerical 3D reactive transport model was developed in order to integrate the essence of the delivery approaches, the engineering capacity provided by the contractor and the respective site conditions. As detailed in Chapter 2, scenario analyses with the model were performed to design the well placement and injection strategy.

The other important feature of the modelling lies in its flexibility, which is essential for adapting changes that occurred on site to the initial design of the field experiment. This deserves to be emphasised because heterogeneity is part of the nature in the subsurface environment, meaning that it is not unusual to encounter local variations in soil layering. For example, during the well installation phase in the first pilot (Chapter 3), we found a 6 m thick Holocene sand layer instead of the expected 2 m thick layer. As a direct consequence, two wells with filter screens located at different depths instead of one, were installed at each of the injection points. In order to adapt this new well-setting to the design of the field experiment, new scenario analyses were quickly performed with the model to re-design the injection strategy and to predict the impact of the changes. The outcome of this step was the four step rotating injection strategy, which can both meet the hardware capacity and still achieve the objectives of the field test. The other practical significance of a flexible modelling is to understand the impact induced by changing boundary conditions on the field experiment. Dredging activities in the water reservoir at the site De Biesbosch (Chapter 4) were carried out during the same period as our field experiment. The dredging activities reduced the entry resistance for water to infiltrate into the dike which led to an increase in hydraulic head in every monitoring well, even at those located in the downstream direction of the installed flow barrier. The aim of the pilot, however, was to reduce the head at the toe of the dike. The impact of the dredging was quantified using the model. Using a scenario analysis, we were able to remove the effect of dredging in order to reveal the impact of our field implementation on the local hydraulic field. As shown by this modelling results, the flow barrier created on site would have lowered the groundwater table at its downstream side by 5 cm.

6.2.3. EVALUATE THE FIELD EXPERIMENT

The importance of monitoring was highlighted in the early phase of both field experiments. Prior to the execution of the field experiment, a number of scenario analyses were performed with the model to predict the changes in local hydraulic field as a result of the installed flow barrier, and these results were used to determine the position of the monitoring wells and the filter depths (details of the monitoring well system can be found in Chapters 3 and 4). As a result, we were able to measures the locally increased hydraulic gradient on site (i.e., at zone A in the second field experiment), which unequivocally indicates that a continuous flow barrier was created at that location (Chapter 4). However, the results from the scenario analyses also revealed that the effectiveness of the flow barrier depends on its continuity, both planar and vertical. As revealed by the simulation results performed while analysing the results from the first field experiment (Chapter 3), the on-site adaptation to the injection system (i.e., two filter screens were installed at non-overlapping segments in the confined aquifer) led to the situation where a very limited amount of precipitates is formed at the depths between the two filter screens.

This gap leads to the occurrence of preferential flow through these non-treated areas, which makes it hard to distinguish the change in hydraulic head induced by the flow barrier from the background variation in head caused by the tidal fluctuation which has a magnitude of approximately 20 cm at the site.

In order to diversify the data set that can be obtained on site and thus enhance the detectability of permeability reduction in-situ, hypothetical pumping/infiltration tests in the monitoring wells were performed using the scenario analyses to design the field hydraulic characterisation tests. These results, in the first place, provided qualitative guidance for interpreting the data that was later acquired from field pumping/infiltration tests. According to the simulation results, the presence of a flow barrier leads to distinct effects on either sides of the barrier during a pumping test. Given its low permeability, the flow barrier widens the capture zone of the pumping at the well. Therefore, a reduced discharge, which corresponds to a less profound drawdown in head, is expected at the side across the flow barrier while at the side of the pumping well, the discharge and drawdown in head is locally enhanced. Results from field pumping tests at both field experiment followed this pattern, and thus confirmed that a flow barrier was created at the two sites (Chapters 3 and 4).

In addition, the simulation results also suggest that the extent of the distinct effects is a function of the imposed flow rate at the pumping well and the permeability of the flow barrier. We therefore applied transmissivity analysis on the data from field pumping tests that were performed before and after the injection to quantify the exact permeability of the flow barrier. Key to this transmissivity analysis is to take the flow barrier, including its location, thickness and the reduction in permeability, into account. As for the first field experiment (Chapter 3), the characteristics of the flow barrier are obtained from the process-oriented modelling. Therefore, we were able to quantify that Al-OM precipitates reduced the permeability of the sand to 2% of the background permeability. The determination of the characteristics of the barrier created in the second field experiment (Chapter 4) is, however, less straightforward. Field data suggested that a flow barrier was created in zone A and its location has shifted 3 m in the downstream direction. Consequently, we cannot assess the thickness of the flow barrier from the measured data. In this case, we assumed a thickness of the flow barrier that varies from 0.1 m to 2 m in order to calculate the corresponding reduction in permeability. Results show that if the flow barrier was as thick as it was designed (1 m), the reduction in permeability is 13 times, or if the reduction in permeability is consistent as it was in the first field experiment (around 50 times), the thickness of the final barrier is around 0.26 m.

6.3. FUTURE OUTLOOK

The implementation of the SoSEAL concept in this research project has been successful. As illustrated in Figure 6.1, the whole project began with the inspiration we took from Podzolization, the initial proof of concept was to focus on the interaction between Al and OM and the corresponding reduction in permeability that can be achieved. This proof of concept was obtained from a series of laboratory experiments performed by other researchers in this research project. The next step was to test the concept in a field test. With the aids of the 'co-makership' model and the modelling (detailed in Chapter 2), this proof of concept, using mixing and reaction of two components to reduce

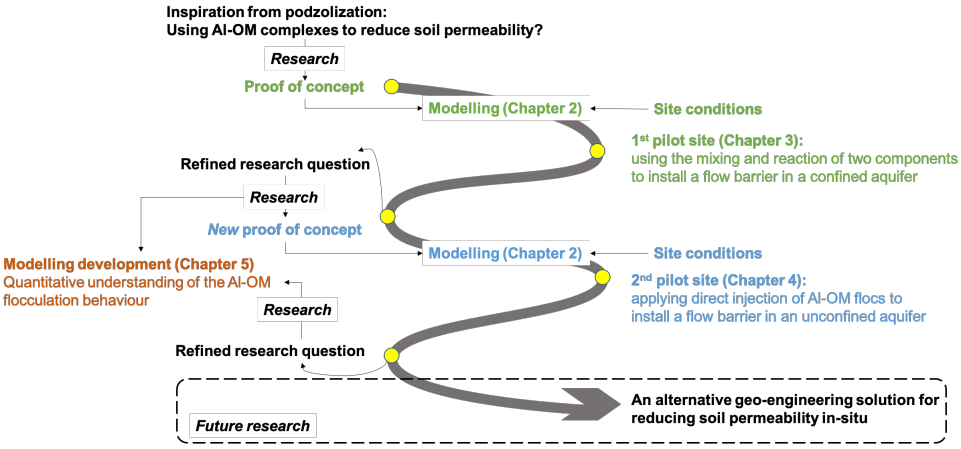

Figure 6.1: Schematic illustration of the project development

soil permeability in-situ, was examined in the context of real-world application via the first full-scale field experiment (detailed in Chapter 3). A detailed evaluation of the first field experiment led to redefined research questions: how to quantitatively describe the Al-OM flocculation process? and is there an alternative delivery approach possible in order to introduce Al-OM flocs that is more cost-effective? The first research question was answered with the development of the mechanistic model (detailed in Chapter 5). To answer the latter question, our laboratory experiments revealed the shear-dependency of the Al-OM floc size, which subsequently led to the development of an alternative approach for delivering Al-OM flocs into soils: direct injection of Al-OM flocs to reduce soil permeability in-situ. This new approach was tested in a set of column experiments. The outcomes of these column-experiments were used in the second pilot project: applying direct injection of Al-OM flocs to install a flow barrier in an unconfined aquifer (Chapter 4). As indicated in Figure 6.1, new research questions are emerging from the evaluation of this field experiment, and thus stimulate future research.

Process control of in-situ permeability reduction using Al-OM is challenging. The results from the first field experiment (Chapter 3), where a two component injection was applied, show that the precipitation of Al-OM flocs depends heavily on the mobility and reactivity of Al and OM in the subsurface. Their mobility and reactivity are a function of many processes, i.e., Al hydrolysis, interaction with soil skeleton and microbial degradation of OM, meaning that the transport distance of these two components and the mass of two components in the mixing zone are limited. The mechanistic modelling of Al-OM flocculation presented in Chapter 5 confirmed that the hydrolysis of Al, which is primary controlled by pH, has a profound impact on the flocculation of OM. The optimal pH for Al^{3+} ions to coagulate OM is found between 5 and 6.

The results of the second field experiment (Chapter 4), where direct Al-OM floc injection was applied, show that controlling the deposition of Al-OM flocs in-situ by manipulating the flow field is not as straightforward as indicated by the model. The injection practice on site did not create an ideal radial flow system. Instead it induced preferen-

tial flow paths due to micro-hydraulic fracturing. This resulted in a changing flow field that then leads to a large variation in the shear conditions on site. As a consequence, the kinetics of the breakage and regrowth of Al-OM flocs became much less predictable. Therefore, it is important to develop a better understanding of these kinetics under a wide range of shear and environmental conditions.

Further development of monitoring capability is urgently needed. In both pilot projects, field-acquired data were obtained from wells, the installation of which is costly and cannot cover the entire field site. Although the measured hydraulic signals provided direct evidence of whether the permeability on site has been reduced, they provided little to no information on the spatial distribution of the flocs in soil. The information on floc distribution is essential for 1) quantifying the achieved reduction in permeability and 2) providing insights for process control. In addition to using scenario analyses with the model to estimate the spatial distribution, we used two geophysical measurement techniques (i.e., electrical resistivity tomography and ground penetration radar) to obtain direct evidence on the spatial distribution. However, the results of these surface-based measurements have only a limited resolution at depth and no interpretation was possible. Future research is therefore needed on alternative monitoring systems or alternative application schemes.

Overall, this PhD-thesis represents a major step forward towards the application of Al-OM precipitates as a nature-based engineering tool to reduce soil permeability in-situ. The 'co-makership' consortium approach has proven to be effective and successful in ensuring fast development of the proposed technology. We can recommend it as a viable approach for other researchers who are working on innovative engineering techniques. Further research effort is required to have a better control of the processes which occur in consortia. Academic research should not underestimate the quality of technical inventions by industrial users, especially when considering the impact of such inventions on the implementation of the technology in practice.

REFERENCES

[1] H. A. Anderson, M. L. Berrow, V. C. Farmer, A. Hepburn, J. D. Russell, and A. D. Walker, *A reassessment of podzol formation processes,* Journal of Soil Science **33**, 125 (1982).

[2] U. Lundström, N. van Breemen, and D. Bain, *The podzolization process. A review,* Geoderma **94**, 91 (2000).

REFERENCES

[1] K. W. Pilarczyk, *Flood protection and management in the Netherlands,* in *Extreme Hydrological Events: New Concepts for Security* (Springer Netherlands, Dordrecht, 2007) pp. 385–407.

[2] D. Coumou and S. Rahmstorf, *A decade of weather extremes,* Nature Climate Change **2**, 491 (2012).

[3] Delta Commissioner, *Ministry of transport public works and water management, Ministry of agriculture nature and food quality, ministry of housing spatial planning and the environment, Dutch national government,* Tech. Rep. (2010).

[4] S. van Baars and I. M. van Kempen, *The causes and mechanisms of historical dike failures in the Netherlands,* E-WAter **2009**, 1 (2009).

[5] R. M. J. Schielen and L. F. M. Van Den Aarsen, *A strategy for Dutch rivers to handle climate change and new Safety Standards,* in *6th International Conference on Flood Management* (2014) pp. 1–9.

[6] J. M. van Loon-Steensma, H. A. Schelfhout, and P. Vellinga, *Green adaptation by innovative dike concepts along the Dutch Wadden Sea coast,* Environmental Science and Policy **44**, 108 (2014).

[7] A. Porbaha, S. Shibuya, and T. Kishida, *State of the art in deep mixing technology. Part III: Geomaterial characterization,* Ground Improvement **4**, 91 (2000).

[8] P. Suer, N. Hallberg, C. Carlsson, D. Bendz, and G. Holm, *Biogrouting compared to jet grouting: Environmental (LCA) and economical assessment,* Journal of Environmental Science and Health - Part A Toxic/Hazardous Substances and Environmental Engineering **44**, 346 (2009).

[9] A. Weber, X. F. Garcia, and C. Wolter, *Habitat rehabilitation in urban waterways: the ecological potential of bank protection structures for benthic invertebrates,* Urban Ecosystems **20**, 759 (2017).

[10] H. A. Anderson, M. L. Berrow, V. C. Farmer, A. Hepburn, J. D. Russell, and A. D. Walker, *A reassessment of podzol formation processes,* Journal of Soil Science **33**, 125 (1982).

[11] U. Lundström, N. van Breemen, and D. Bain, *The podzolization process. A review,* Geoderma **94**, 91 (2000).

[12] P. van Hees, U. Lundström, and R. Giesler, *Low molecular weight organic acids and their Al-complexes in soil solutionâĂŤcomposition, distribution and seasonal variation in three podzolized soils,* Geoderma **94**, 173 (2000).

[13] U. S. Lundström, N. van Breemen, D. C. Bain, P. A. van Hees, R. Giesler, J. P. Gustafsson, H. Ilvesniemi, E. Karltun, P. A. Melkerud, M. Olsson, G. Riise, O. Wahlberg, A. Bergelin, K. Bishop, R. Finlay, A. G. Jongmans, T. Magnusson, H. Mannerkoski,

A. Nordgren, L. Nyberg, M. Starr, and L. Tau Strand, *Advances in understanding the podzolization process resulting from a multidisciplinary study of three coniferous forest soils in the Nordic Countries,* Geoderma **94**, 335 (2000).

[14] K. G. Nierop, B. Jansen, and J. M. Verstraten, *Dissolved organic matter, aluminium and iron interactions: Precipitation induced by metal/carbon ratio, pH and competition,* Science of the Total Environment **300**, 201 (2002).

[15] B. Jansen, K. G. J. Nierop, and J. M. Verstraten, *Influence of pH and metal/carbon ratios on soluble organic complexation of Fe(II), Fe(III) and Al(III) in soil solutions determined by diffusive gradients in thin films,* Analytica Chimica Acta **454**, 259 (2002).

[16] V. C. Farmer and D. G. Lumsdon, *Interactions of fulvic acid with aluminium and a proto-imogolite sol: The contribution of E-horizon eluates to podzolization,* European Journal of Soil Science **52**, 177 (2001).

[17] D. Sauer, H. Sponagel, M. Sommer, L. Giani, R. Jahn, and K. Stahr, *Podzol: Soil of the year 2007. A review on its genesis, occurrence, and functions,* Journal of Plant Nutrition and Soil Science **170**, 581 (2007).

[18] R. Mikutta and K. Kaiser, *Organic matter bound to mineral surfaces: Resistance to chemical and biological oxidation,* Soil Biology and Biochemistry **43**, 1738 (2011).

[19] T. Scheel, B. Jansen, A. J. van Wijk, J. M. Verstraten, and K. Kalbitz, *Stabilization of dissolved organic matter by aluminium: a toxic effect or stabilization through precipitation?* European Journal of Soil Science **59**, 1122 (2008).

[20] E. Tipping, C. Rey-Castro, S. E. Bryan, and J. Hamilton-Taylor, *Al (III) and Fe (III) binding by humic substances in freshwaters, and implications for trace metal speciation,* Geochimica et Cosmochimica Acta **66**, 3211 (2002).

[21] L. Weng, E. P. M. J. Fest, J. Fillius, E. J. M. Temminghoff, and W. H. Van Riemsdijk, *Transport of Humic and Fulvic acids in relation to metal mobility in a copper-contaminated acid sandy soil,* Environmental Science & Technology **36**, 1699 (2002).

[22] J. Duan and J. Gregory, *Coagulation by hydrolysing metal salts,* Advances in Colloid and Interface Science **100-102**, 475 (2003).

[23] N. Rodet-Kroichvili, K. Cabaret, and F. Picard, *New Insights into Innovation: The Business Model Approach and Chesbrough's Seminal Contribution to Open Innovation,* Journal of Innovation Economics **15**, 79 (2014).

[24] J. van Popering-Verkerk and A. van Buuren, *Developing collaborative capacity in pilot projects: Lessons from three Dutch flood risk management experiments,* Journal of Cleaner Production **169**, 225 (2017).

[25] M. O. Cuthbert, L. A. McMillan, S. Handley-Sidhu, M. S. Riley, D. J. Tobler, and V. R. Phoenix, *A field and modeling study of fractured rock permeability reduction using microbially induced calcite precipitation,* Environmental Science & Technology **47**, 13637 (2013).

[26] P. F. Hudak, *Locating groundwater monitoring wells near cutoff walls,* Advances in Environmental Research **5**, 23 (2001).

[27] E. I. Anderson and E. Mesa, *The effects of vertical barrier walls on the hydraulic control of contaminated groundwater,* Advances in Water Resources **29**, 89 (2006).

[28] Y. Yihdego, *Evaluation of Flow Reduction due to Hydraulic Barrier Engineering Structure: Case of Urban Area Flood, Contamination and Pollution Risk Assessment,* Geotechnical and Geological Engineering **34**, 1643 (2016).

[29] J. T. DeJong, B. M. Mortensen, B. C. Martinez, and D. C. Nelson, *Bio-mediated soil improvement,* Ecological Engineering **36**, 197 (2010).

[30] M. G. Gomez, B. C. Martinez, J. T. DeJong, C. E. Hunt, L. A. DeVlaming, D. W. Major, and S. M. Dworatzek, *Field-scale bio-cementation tests to improve sands,* Proceedings of the Institution of Civil Engineers - Ground Improvement **168**, 206 (2015).

[31] C. J. Proto, J. T. DeJong, and D. C. Nelson, *Biomediated permeability reduction of saturated sands,* Journal of Geotechnical and Geoenvironmental Engineering **142**, 4016073 (2016).

[32] P. Jarvis, B. Jefferson, and S. A. Parsons, *Breakage, regrowth, and fractal nature of natural organic matter flocs,* Environmental Science & Technology **39**, 2307 (2005).

[33] M. Sharma and Y. Yortsos, *Transport of particulate suspensions in porous media - model formulation,* AICHE Journal **33**, 1636 (1987).

[34] J. N. Ryan and M. Elimelech, *Colloid mobilization and transport in groundwater,* Colloids and Surfaces A: Physicochemical and Engineering Aspects **107**, 1 (1996).

[35] T. Li, Z. Zhu, D. Wang, C. Yao, and H. Tang, *Characterization of floc size, strength and structure under various coagulation mechanisms,* Powder Technology **168**, 104 (2006).

[36] P. Jarvis, B. Jefferson, and S. A. Parsons, *Floc structural characteristics using conventional coagulation for a high doc, low alkalinity surface water source,* Water Research **40**, 2727 (2006).

[37] W.-Z. Yu, J. Gregory, and L. Campos, *Breakage and regrowth of Al-Humic flocs - Effect of additional coagulant dosage,* Environmental Science & Technology **44**, 6371 (2010).

[38] M. R. Wiesner, M. C. Grant, and S. R. Hutchins, *Reduced permeability in groundwater remediation systems: Role of mobilized colloids and injected chemicals,* Environmental Science & Technology **30**, 3184 (1996).

[39] V. I. Syngouna and C. V. Chrysikopoulos, *Transport of biocolloids in water saturated columns packed with sand: Effect of grain size and pore water velocity,* Journal of Contaminant Hydrology **129-130**, 11 (2012).

[40] T. Tosco and R. Sethi, *Transport of non-Newtonian suspensions of highly concentrated micro- and nanoscale iron particles in porous media: A modeling approach,* Environmental Science & Technology **44**, 9062 (2010).

[41] S. E. Trumbore, *Potential responses of soil organic carbon to global environmental change,* Proceedings of the National Academy of Sciences **94**, 8284 (1997).

[42] J. Lehmann and M. Kleber, *The contentious nature of soil organic matter,* Nature **528**, 60 (2015).

[43] J. Adusei-Gyamfi, B. Ouddane, L. Rietveld, J.-P. Cornard, and J. Criquet, *Natural organic matter-cations complexation and its impact on water treatment: A critical review,* Water Research **160**, 130 (2019).

[44] E. Tipping, *Cation binding by humic substances*, Vol. 12 (Cambridge University Press, 2002).

[45] A. van Zomeren and R. N. J. Comans, *Measurement of Humic and Fulvic acid concentrations and dissolution properties by a rapid batch procedure,* Environmental Science & Technology **41**, 6755 (2007).

[46] K. A. Rittle, J. I. Drever, and P. J. S. Colberg, *Precipitation of arsenic during bacterial sulfate reduction,* Geomicrobiology Journal **13**, 1 (1995).

[47] M. Baalousha, M. Motelica-Heino, and P. L. Coustumer, *Conformation and size of humic substances: Effects of major cation concentration and type, pH, salinity, and residence time,* Colloids and Surfaces A: Physicochemical and Engineering Aspects **272**, 48 (2006).

[48] A. Chappaz and P. J. Curtis, *Integrating empirically dissolved organic matter quality for WHAM VI using the DOM optical properties: A case study of Cu-Al-DOM interactions,* Environmental Science & Technology **47**, 2001 (2013).

[49] D. G. Kinniburgh, W. H. Van Riemsdijk, L. K. Koopal, M. Borkovec, M. F. Benedetti, and M. J. Avena, *Ion binding to natural organic matter: competition, heterogeneity, stoichiometry and thermodynamic consistency,* Colloids and Surfaces A: Physicochemical and Engineering Aspects **151**, 147 (1999).

[50] C. J. Milne, D. G. Kinniburgh, W. H. Van Riemsdijk, and E. Tipping, *Generic NICA-Donnan model parameters for metal-ion binding by humic substances,* Environmental Science & Technology **37**, 958 (2003).

[51] J. C. L. Meeussen, *ORCHESTRA: an object-oriented framework for implementing chemical equilibrium models.* Environmental science & technology **37**, 1175 (2003).

[52] E. Tipping, *Humic ion-binding model VI: an improved description of the interactions of protons and metal ions with humic substances,* Aquatic geochemistry **4**, 3 (1998).

[53] D. G. Kinniburgh, C. J. Milne, M. F. Benedetti, J. P. Pinheiro, J. Filius, L. K. Koopal, and W. H. Van Riemsdijk, *Metal ion binding by humic acid: application of the NICA-Donnan model,* Environmental Science & Technology **30**, 1687 (1996).

[54] B. Jansen, K. G. J. Nierop, and J. M. Verstraten, *Mobility of Fe(II), Fe(III) and Al in acidic forest soils mediated by dissolved organic matter: Influence of solution pH and metal/organic carbon ratios,* Geoderma **113**, 323 (2003).

[55] B. Jansen, *The mobility of aluminium, iron and organic matter in acidic sandy soils* (2003) pp. 1– 187.

[56] L. Weng, E. J. Temminghoff, and W. H. Van Riemsdijk, *Interpretation of humic acid coagulation and soluble soil organic matter using a calculated electrostatic potential,* European Journal of Soil Science **53**, 575 (2002).

[57] E. L. Sharp, P. Jarvis, S. A. Parsons, and B. Jefferson, *The impact of zeta potential on the physical properties of ferric-NOM flocs,* Environmental Science & Technology **40**, 3934 (2006).

[58] X. Wu, X. Ge, D. Wang, and H. Tang, *Distinct mechanisms of particle aggregation induced by alum and PACl: Floc structure and DLVO evaluation,* Colloids and Surfaces A: Physicochemical and Engineering Aspects **347**, 56 (2009).

[59] D. Ghernaout and B. Ghernaout, *Sweep flocculation as a second form of charge neutralisationâĂŤa review,* Desalination and Water Treatment **44**, 15 (2012).

[60] C. T. Tanneru, J. D. Rimer, and S. Chellam, *Sweep flocculation and adsorption of viruses on aluminum flocs during electrochemical treatment prior to surface water microfiltration,* Environmental Science & Technology **47**, 4612 (2013).

[61] D. G. Lee, J. S. Bonner, L. S. Garton, A. N. Ernest, and R. L. Autenrieth, *Modeling coagulation kinetics incorporating fractal theories: A fractal rectilinear approach,* Water Research **34**, 1987 (2000).

[62] T. Scheel, L. Haumaier, R. H. Ellerbrock, J. Rühlmann, and K. Kalbitz, *Properties of organic matter precipitated from acidic forest soil solutions,* Organic Geochemistry **39**, 1439 (2008).

[63] P. T. Spicer, S. E. Pratsinis, J. Raper, R. Amal, G. Bushell, and G. Meesters, *Effect of shear schedule on particle size, density, and structure during flocculation in stirred tanks,* Powder Technology **97**, 26 (1998).

[64] N. Tufenkji and M. Elimelech, *Deviation from the classical colloid filtration theory in the presence of repulsive DLVO interactions,* Langmuir **20**, 10818 (2004).

[65] D. G. Lee, J. S. Bonner, L. S. Garton, A. N. Ernest, and R. L. Autenrieth, *Modeling coagulation kinetics incorporating fractal theories: Comparison with observed data,* Water Research **36**, 1056 (2002).

[66] Y. Wang, B.-Y. Gao, X.-M. Xu, W.-Y. Xu, and G.-Y. Xu, *Characterization of floc size, strength and structure in various aluminum coagulants treatment,* Journal of Colloid and Interface Science **332**, 354 (2009).

[67] M. Yan, D. Wang, J. Ni, J. Qu, C. W. Chow, and H. Liu, *Mechanism of natural organic matter removal by polyaluminum chloride: Effect of coagulant particle size and hydrolysis kinetics,* Water Research **42**, 3361 (2008).

[68] J. Bear, *Dynamics of Fluids in Porous Media,* Soil Science **120**, 162 (1975).

[69] G. F. Pinder and M. A. Celia, *Subsurface Hydrology* (John Wiley & Sons, 2006) pp. 1–468.

[70] T. Tosco, M. Petrangeli Papini, C. Cruz Viggi, and R. Sethi, *Nanoscale zerovalent iron particles for groundwater remediation: A review,* Journal of Cleaner Production **77**, 10 (2014).

[71] T. P. Clement, B. S. Hooker, and R. S. Skeen, *Macroscopic Models for Predicting Changes in Saturated Porous Media Properties Caused by Microbial Growth,* (1996).

[72] J. Islam and N. Singhal, *A one-dimensional reactive multi-component landfill leachate transport model,* Environmental Modelling and Software **17**, 531 (2002).

[73] S. A. Bradford, J. Simunek, M. Bettahar, M. T. Van Genuchten, and S. R. Yates, *Significance of straining in colloid deposition: Evidence and implications,* Water Resources Research **42**, 1 (2006).

[74] F. Gastone, T. Tosco, and R. Sethi, *Guar gum solutions for improved delivery of iron particles in porous media (Part 1): Porous medium rheology and guar gum-induced clogging,* Journal of Contaminant Hydrology **166**, 23 (2014).

[75] C. R. Fitts, *Groundwater science* (Academic Press, 2002).

[76] C. Z. Qin and S. M. Hassanizadeh, *Pore-network modeling of solute transport and biofilm growth in porous media,* Transport in Porous Media **110**, 345 (2015).

[77] J. Zhou, S. Laumann, and T. J. Heimovaara, *Applying aluminum-organic matter precipitates to reduce soil permeability in-situ: A field and modeling study,* Science of the Total Environment **662**, 99 (2019).

[78] C. N. Mulligan, R. N. Yong, and B. F. Gibbs, *Remediation technologies for metal-contaminated soils and groundwater: An evaluation,* Engineering Geology **60**, 193 (2001), arXiv:04 .

[79] N. Benmebarek, S. Benmebarek, and R. Kastner, *Numerical studies of seepage failure of sand within a cofferdam,* Computers and Geotechnics **32**, 264 (2005).

[80] M. E. Reid, *Slope instability caused by small variations in hydraulic conductivity,* Journal of Geotechnical and Geoenvironmental Engineering **123**, 717 (1997).

[81] C. W. Ng and Q. Shi, *A numerical investigation of the stability of unsaturated soil slopes subjected to transient seepage,* Computers and Geotechnics **22**, 1 (1998).

[82] V. M. van Beek, H. T. J. de Bruijn, J. G. Knoeff, A. Bezuijen, and U. Förster, *Levee failure due to piping: A Full-Scale Experiment,* in *Scour and Erosion*, November (American Society of Civil Engineers, Reston, VA, 2010) pp. 283–292.

[83] J. M. Duncan, S. G. Wright, and T. L. Brandon, *Soil Strength and Slope Stability (2nd Edition)* (John Wiley & Sons, 2014).

[84] J. T. DeJong, K. Soga, E. Kavazanjian, S. Burns, L. A. van Paassen, A. Al Qabany, A. Aydilek, S. S. Bang, M. Burbank, L. F. Caslake, C. Y. Chen, X. Cheng, J. Chu, S. Ciurli, A. Esnault-Filet, S. Fauriel, N. Hamdan, T. Hata, Y. Inagaki, S. Jefferis, M. Kuo, L. Laloui, J. Larrahondo, D. A. C. Manning, B. Martinez, B. M. Montoya, D. C. Nelson, A. Palomino, P. Renforth, J. C. Santamarina, E. A. Seagren, B. Tanyu, M. Tsesarsky, and T. Weaver, *Biogeochemical processes and geotechnical applications: progress, opportunities and challenges,* Géotechnique **63**, 287 (2013), arXiv:9809069v1 [arXiv:gr-qc] .

[85] V. P. Pham, A. Nakano, W. R. L. van der Star, T. J. Heimovaara, and L. A. van Paassen, *Applying MICP by denitrification in soils: a process analysis,* Environmental Geotechnics , 1 (2016).

[86] A. Al Qabany and K. Soga, *Effect of chemical treatment used in MICP on engineering properties of cemented soils,* Géotechnique **63**, 331 (2013).

[87] B. C. Martinez, J. T. DeJong, T. R. Ginn, B. M. Montoya, T. H. Barkouki, C. Hunt, B. Tanyu, and D. Major, *Experimental optimization of microbial-induced carbonate precipitation for soil improvement,* Journal of Geotechnical and Geoenvironmental Engineering **139**, 587 (2013).

[88] l. A. van Paassen, R. Ghose, T. J. M. van der Linden, W. R. L. van der Star, and M. C. M. van Loosdrecht, *Quantifying biomediated ground improvement by ureolysis: large-scale biogrout experiment,* Journal of Geotechnical and Geoenvironmental Engineering **136**, 1721 (2010).

[89] A. J. Phillips, A. B. Cunningham, R. Gerlach, R. Hiebert, C. Hwang, B. P. Lomans, J. Westrich, C. Mantilla, J. Kirksey, R. Esposito, and L. Spangler, *Fracture sealing with microbially-induced calcium carbonate precipitation: A field study,* Environmental Science & Technology **50**, 4111 (2016).

[90] M. von Lützow, I. Kögel-Knabner, B. Ludwig, E. Matzner, H. Flessa, K. Ekschmitt, G. Guggenberger, B. Marschner, and K. Kalbitz, *Stabilization mechanisms of organic matter in four temperate soils: Development and application of a conceptual model,* Journal of Plant Nutrition and Soil Science **171**, 111 (2008).

[91] P. A. van Hees and U. S. Lundström, *Equilibrium models of aluminium and iron complexation with different organic acids in soil solution,* Geoderma **94**, 201 (2000).

[92] P. Baveye, P. Vandevivere, B. L. Hoyle, P. C. DeLeo, and D. S. de Lozada, *Environmental Impact and Mechanisms of the Biological Clogging of Saturated Soils and Aquifer Materials,* Critical Reviews in Environmental Science and Technology **28**, 123 (1998), arXiv:arXiv:1011.1669v3 .

[93] S. Emmanuel and B. Berkowitz, *Mixing-induced precipitation and porosity evolution in porous media,* Advances in Water Resources **28**, 337 (2005).

[94] H. G. B. Allersma, A. Rohe, and O. Dupont, *Centrifuge tests on the failure of dikes caused by uplift pressure,* International Journal of Physical Modelling in Geotechnics **3**, 747 (2002).

[95] L. W. Gelhar, C. Welty, and K. R. Rehfeldt, *A critical review of data on field-âĂŘscale dispersion in aquifers,* Water Resources Research **28**, 1955 (1992), arXiv:arXiv:1011.1669v3 .

[96] G. P. Kruseman and N. A. de Ridder, *ILRI publication*, 47 (1991) p. 377.

[97] A. J. Desbarats, *Spatial averaging of transmissivity in heterogeneous fields with flow toward a well,* Water Resources Research **28**, 757 (1992).

[98] A. Cunningham, A. Phillips, E. Troyer, E. Lauchnor, R. Hiebert, R. Gerlach, and L. Spangler, *Wellbore leakage mitigation using engineered biomineralization,* Energy Procedia **63**, 4612 (2014).

[99] J. T. DeJong, B. C. Martinez, T. R. Ginn, C. Hunt, D. Major, and B. Tanyu, *Development of a scaled repeated five-spot treatment model for examining microbial induced calcite precipitation feasibility in field applications,* Geotechnical Testing Journal **37** (2014), 10.1520/GTJ20130089.

[100] P. Bayer, M. Finkel, and T. Georg, *Combining pump-and-treat and physical barriers for contaminant plume control,* Ground Water **42**, 856 (2004).

[101] A. T. Papagianakis and D. G. Fredlund, *A steady state model for flow in saturated-unsaturated soils,* Canadian Geotechnical Journal **21**, 419 (2009).

[102] L. Shen, Q. Du, H. Wang, W. Zhong, and Y. Yang, *In situ polymerization and characterization of polyamide-6/silica nanocomposites derived from water glass,* Polymer International **53**, 1153 (2004).

[103] B. Nikbakhtan and M. Osanloo, *Effect of grout pressure and grout flow on soil physical and mechanical properties in jet grouting operations,* International Journal of Rock Mechanics and Mining Sciences **46**, 498 (2009).

[104] F. Payne, S. Potter, and J. Quinnan, *CRC Press*, Vol. 126 (CRC Press, 2008) p. 21.

[105] H. Sapion, J. Gemoets, T. Tosco, R. Muyshondt, L. Bastiaens, R. Sethi, F. Gastone, N. Klaas, M. Velimirovic, and M. Luna, *Pressure-controlled injection of guar gum stabilized microscale zerovalent iron for groundwater remediation,* Journal of Contaminant Hydrology **181**, 46 (2015).

[106] X. C. Wang, P. K. Jin, and J. Gregory, *Structure of Al-humic flocs and their removal at slightly acidic and neutral pH,* Water Science and Technology: Water Supply **2**, 99 (2002).

[107] Y. X. Zhao, B. Y. Gao, H. K. Shon, B. C. Cao, and J. H. Kim, *Coagulation characteristics of titanium (Ti) salt coagulant compared with aluminum (Al) and iron (Fe) salts,* Journal of Hazardous Materials **185**, 1536 (2011).

[108] A. Zech, C. L. Schneider, and S. Attinger, *The Extended Thiem's solution: Including the impact of heterogeneity,* Water Resources Research **48**, 1 (2012).

[109] J. A. Cunningham and M. Reinhard, *Injection-extraction treatment well pairs: An alternative to permeable reactive barriers,* (2002).

[110] EPA (U.S. Environmental Protection Agency), *A systematic approach for evaluation of capture zones at pump and treat systems*, Tech. Rep. January (U.S. Environmental Protection Agency, Washington, DC, EPA/600/R-08/003, 2008., 2008).

[111] P. Renard and G. de Marsily, *Calculating equivalent permeability: A review,* Advances in Water Resources **20**, 253 (1997).

[112] R. P. Chapuis and D. Chenaf, *Detecting a hydraulic short circuit along a monitoring well with the recovery curve of a pumping test in a confined aquifer: method and example,* Canadian Geotechnical Journal **35**, 790 (2011).

[113] A. J. Phillips, E. Lauchnor, J. J. Eldring, R. Esposito, A. C. Mitchell, R. Gerlach, A. B. Cunningham, and L. H. Spangler, *Potential CO2 leakage reduction through bbiofilm-induced calcium carbonate precipitation,* Environmental Science & Technology **47**, 142 (2013).

[114] S. Xu, B. Gao, and J. E. Saiers, *Straining of colloidal particles in saturated porous media,* Water Resources Research **42**, 1 (2006).

[115] I. L. Molnar, W. P. Johnson, J. I. Gerhard, C. S. Willson, and D. M. O'Carroll, *Predicting colloid transport through saturated porous media: A critical review,* Water Resources Research **51**, 6804 (2015).

[116] M. Ponthieu, O. Pourret, B. Marin, A. R. Schneider, X. Morvan, A. Conreux, and B. Cancès, *Evaluation of the impact of organic matter composition on metal speciation in calcareous soil solution: Comparison of Model VI and NICA-Donnan,* Journal of Geochemical Exploration **165**, 1 (2016).

[117] E. R. Unsworth, K. W. Warnken, H. Zhang, W. Davison, F. Black, J. Buffle, J. Cao, R. Cleven, J. Galceran, P. Gunkel, E. Kalis, D. Kistler, H. P. van Leeuwen,

M. Martin, S. Noël, Y. Nur, N. Odzak, J. Puy, W. van Riemsdijk, L. Sigg, E. Temminghoff, M.-L. Tercier-Waeber, S. Toepperwien, R. M. Town, L. Weng, and H. Xue, *Model predictions of metal speciation in freshwaters compared to measurements by in situ techniques,* Environmental Science & Technology **40**, 1942 (2006), arXiv:arXiv:1011.1669v3 .

[118] J. Xiong, L. Weng, L. K. Koopal, M. Wang, Z. Shi, L. Zheng, and W. Tan, *Effect of soil Fulvic and Humic acids on Pb binding to the goethite/solution interface: Ligand charge distribution modeling and speciation distribution of Pb,* Environmental Science & Technology **52**, 1348 (2018).

[119] Y. Dudal and F. Gérard, *Accounting for natural organic matter in aqueous chemical equilibrium models: A review of the theories and applications,* Earth-Science Reviews **66**, 199 (2004).

[120] MATLAB Release 2019a, *MATLAB Release 2019a* (2019).

[121] L. Weng, E. J. Temminghoff, and W. H. Van Riemsdijk, *Aluminum speciation in natural waters: Measurement using Donnan membrane technique and modeling using NICA-Donnan,* Water Research **36**, 4215 (2002).

[122] B. Manunza, C. Gessa, S. Deiana, and R. Rausa, *A normal distribution model for the titration curves of humic acids,* Journal of Soil Science **43**, 127 (1992).

[123] T. Saito, S. Nagasaki, S. Tanaka, and L. K. Koopal, *Electrostatic interaction models for ion binding to humic substances,* Colloids and Surfaces A: Physicochemical and Engineering Aspects **265**, 104 (2005).

[124] M. F. Benedetti, W. H. Van Riemsdijk, and L. K. Koopal, *Humic substances considered as a heterogeneous Donnan gel phase,* Environmental Science & Technology **30**, 1805 (1996).

[125] B. Dobias and H. Stechemesser, *Coagulation and flocculation: Theory and applications* (CRC Press, 2005).

[126] M. F. Benedetti, C. J. Milne, D. G. Kinniburgh, W. H. Van Riemsdijk, and L. K. Koopal, *Metal ion binding to Humic substances: Application of the non-ideal competitive adsorption model,* Environmental Science & Technology **29**, 446 (1995).

[127] W. J. Weber, P. M. McGinley, and L. E. Katz, *Sorption phenomena in subsurface systems: Concepts, models and effects on contaminant fate and transport,* Water Research **25**, 499 (1991).

[128] W. Z. Tamrat, J. Rose, O. Grauby, E. Doelsch, C. Levard, P. Chaurand, and I. Basile-Doelsch, *Soil organo-mineral associations formed by co-precipitation of Fe, Si and Al in presence of organic ligands,* Geochimica et Cosmochimica Acta **260**, 15 (2019).

[129] A. J. A. Aquino, D. Tunega, G. E. Schaumann, G. Haberhauer, M. H. Gerzabek, and H. Lischka, *The functionality of cation bridges for binding polar groups in soil aggregates,* International Journal of Quantum Chemistry **111**, 1531 (2011).

ACKNOWLEDGEMENTS

Looking back at the end of this long and fast journey, I am deeply grateful for the overwhelmingly abundant supports that I have received from many people. With this part of the thesis, I would like thank all of them. Writing the acknowledgement is technically easier than the rest of this thesis. However, considering the vast amount of supports and the risk of swamping you, the reader, with names, I could only articulate the tiny portion of people that had provided me with valuable inputs.

I would like to thank the entire SoSEAL consortium, which consists of Dirk, Jaap and Herald from Heijmans, Frank and Han from Tauw, Daan and Paco from Evides Waterbedrijf, Jauk from De Vries & van den Wiel, Richard from Movares, Martin from Watershap Riverenland, Jos from Deltares, Johan and Jack Hoogheemraadschap Schieland Krimpenerwaard and Rodriaan from Gemeente Rotterdam. It has been a pleasure and a privilege for me to be part of this consortium, which not only provided the finance support for the research project, but also facilitated the knowledge-sharing. As such, Timo, thank you so much for extending me this unique opportunity. The amount of freedom and inspirations that I took from you is enormous. I used to prematurely mischaracterise your guidance. However, I now understand how valuable the freedom was, where you allowed me to explore and to learn, while hold me up in moments when I was in need. This combination led to a very steep learning curve, which was both challenging and rewarding. I sincerely enjoyed it for it is exactly what I strived for. Frank, thank you for your consistent kindness and support, which had huge impact on this PhD journey. Knowledge-wise, you showed me the significance of practical thinking in research and engineering. At the personal level, your appreciation and positive feedbacks certainly motived me at the moments where I was in doubt about the relevance or meaningfulness of my work. Also I thank Dick, Jaap, Herald, Jauk, Daan and Paco for their enthusiasm and openness to people. They brought me with different perspectives of my research projects. Moreover, they often generously, even proactively, offered me with valuable feedbacks. For instance, the career advise given by Dick is so inspiring. Boris and Olaf, it has been a pleasure to work with both of you on the knowledge development part of the SoSEAL project. The commitment and passion you have demonstrated are appealing, and I enjoyed very much those insightful discussions we had together.

I must single Susanne out for she is not only a prominent member of the SoSEAL consortium but also helped me in many other areas. Susanne, thank you for everything. You were my colleague, together we worked on the SoSEAL project, celebrated the joy (i.e., field works under good weathers or being notified of the acceptance of paper) and also confronted all challenges (i.e., I will never forget the boat trip to Gijster on 1st May 2018). You were my non-official supervisor, who were patient in discussing ideas and tutoring me with scientific writing. You were critical, caring and honest. Your extensive and constructive feedbacks served as the beacon for this PhD journey. I knew by heart how much effort and time your had put in and I never took them for granted. In fact, I

often felt guilty for occupying your time too much. Because of your contribution, I was able to realise many of the potentials and had my development benchmarked. The trust we had built within the research project also has a profound impact in the personal domain. You were also my mentor and friend. Whenever I felt confused or lost, I know that I could look up on you. I particularly appreciate that you were not blindly accepting my narratives, rather than you made me recognise that I can make things better by thinking and doing differently. This invaluable awareness will impact the rest of my life.

Han, Jens, Alber, Marlijn, Marijke, Margot, Dominique, Leon, Julia, Claire, Mike, Cristina, Amin, Phil, Anne-Catherine, Federico, André, Micheal, Nor, Poly, Arash, Divya, Ali, Ivo, Juan, Florian, Hongfen, Weiyuan, Bram, Elahe and all of my colleagues, thank you for making the working environment in the Department vivid and encouraging. Thank Han, Jens and Alber for helping me with fieldwork, which is one thing that I miss most out of my PhD work. I still can recall how overwhelmed I was in the beginning, and gradually I became skilled with setting-up and coordinating the fieldworks. This had happened because of your patience and unreserved support. The help I received from Marlijn is tremendous. I thank you for being proactively supportive in arranging the administrative work for my PhD. Dominique, thank you for the passion and enthusiasm you have shown, which are very appealing and motivating. André, thank you for your supports in many areas. We had many insightful discussions, where you shared your knowledge with no reservation. Also, we had lots of fun throughout the PhD journey. I feel very grateful for having you as my colleague.

I worked with many students throughout my PhD, from whom I not only sharpened my understanding about the knowledge that I was conveying, but also took many inspirations from them. Their fresh ideas, uncomplicated motives, demonstrated enthusiasms and diverse backgrounds showed me enormous possibilities of life. Moreover, I became friends with many of them and we had great funs together. Therefore, Chiara, Jim, Niels and Max, thank you for making the experience so unique. I miss the good times we spent together.

My friends are consistently supportive. Though I did not bring up my PhD experience with them for I preferred to have the personal life insulated, the fun time we together had a significant contribution in supporting the advance of my PhD progress. Especially, I felt like I can be a completely different person when I was with you, my friend. You gave me a warm and worry-free environment, where I could put all troubles aside and enjoy the moments. Since I am a mobile person, who left my hometown at the age of 18 and went abroad 4 years after, I kept making new friends while also kept losing old friends. Fortunately, some of you remained and this means a lot to me. Mery, Sizhen, Rik, Eithan, Michele, Jiaxuan, Wenzhe, and Jasper, thank you for being with me. Mery, thank you for witnessing my entire PhD journey. I remember with pleasure those movie nights, where we could have intense discussions about any topic derived from the movie. I so look forward to your PhD journey. Sizhen, thank you for being my bro. At the beginning of my PhD we used to party a lot and had many crazy weekend trips (i.e., I can still recall the frustrating night at Warsaw, where your loud snoring made me run out for earplug at 4 am), while later in the time we spent many weekends at Cafe@home for studying or working. You are such a brave and ambitious person, I can not articulate how much I had learnt from you.

My family, especially my mom, has been backbone for every development that I have ever made, and this recognition became clear throughout my PhD. As the most educated member of my family, I was gifted for being able to articulate thoughts in a more convincing way. As a result, for a long while, my family, particularly my mom, accepted my prejudice, where I often overlooked or underestimated their talents and achievements. Though I am grateful for carrying out my PhD smoothly, it was sometimes simply hard to put life and work together. Through the taste of the hardship, I can finally appreciate my mom and family to a much better extent. My mom did not have the opportunity to purse a decent education. However, she is a true achiever. As a single mom, she raised me with unlimited love and joy while also overcame countless failures and obstacles to build her own small business. Comparing with the challenges she was confronting, all of my complaints are trivial. Mom, I am deeply proud of you, and I so wish that I could inherit your resilient, caring and optimistic mentality. Mom, thank you for everything. My cousin, Jinsong, thank you. You are my oldest friend, where we spent many parts of our childhood and adolescence together. Even though we took diverged paths, the trust we built is not eroded by time. In front of you, I am always the little brother.

This PhD experience deems to be one of the most valuable times in my life. I once read an article, where Sam, a reader of FT times, summarised his PhD experience as: 'the frontier of science requires tenacity, resilience, intelligence... Constant failure with some successes teaches invaluable skills of life like nothing else in my experience'. I resonate with his description very well. This PhD experience has profoundly impacts on my life, where many aspects are yet to reveal. This inevitably implies that this acknowledgement is subject to changes. I write the current version during the coronavirus pandemic, where many parts of it were already different than my initial ideas. I do hope that I will regularly look back at my PhD time, perhaps an update of this acknowledgement will follow. In any regard, I concluded my thesis and the PhD work with a heart full of gratitude, and I do not expect this reflection will change. Having said this, I thank you all very much.

APPENDIX A

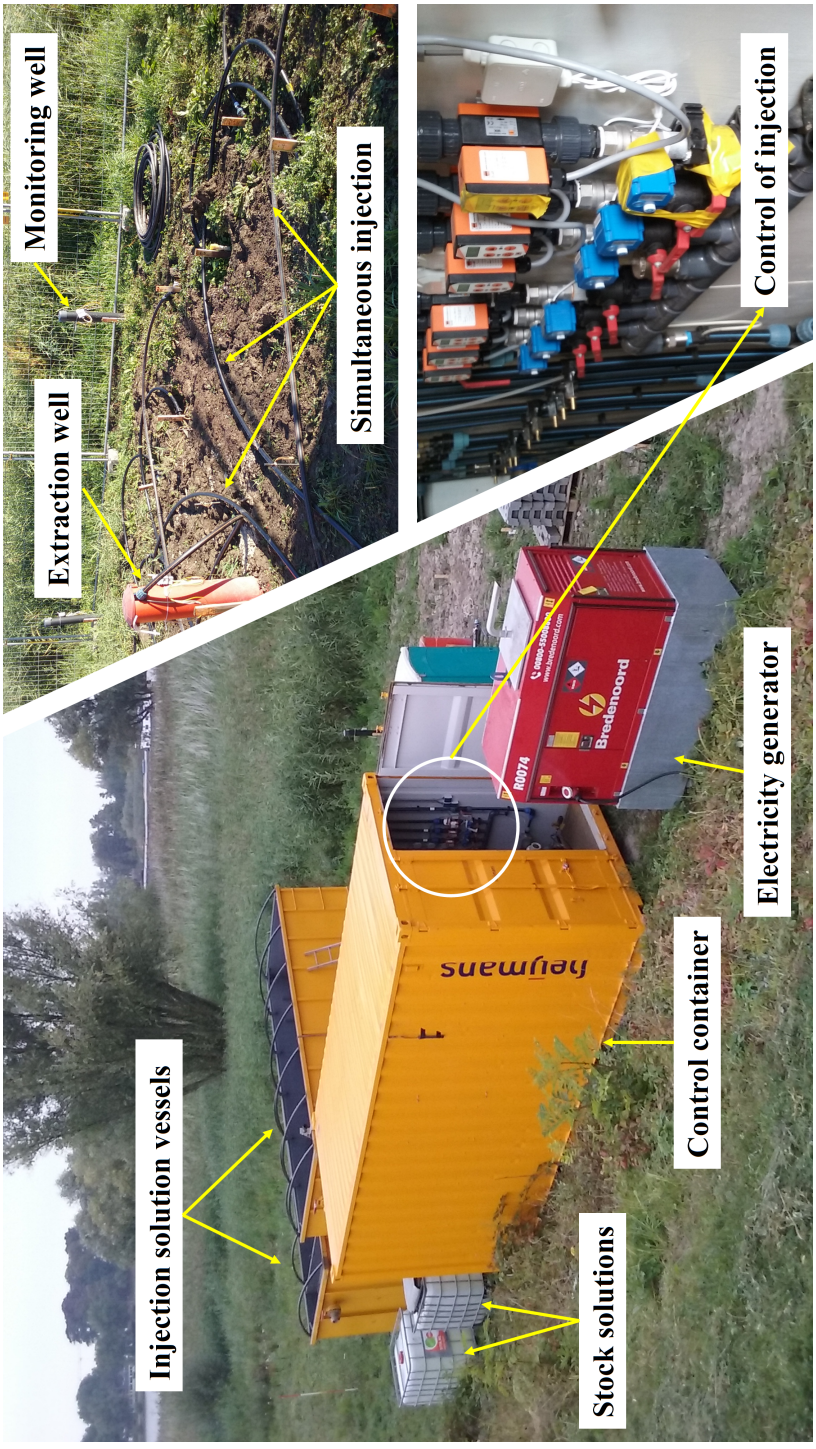

Figure A1: Illustration of the field installation.

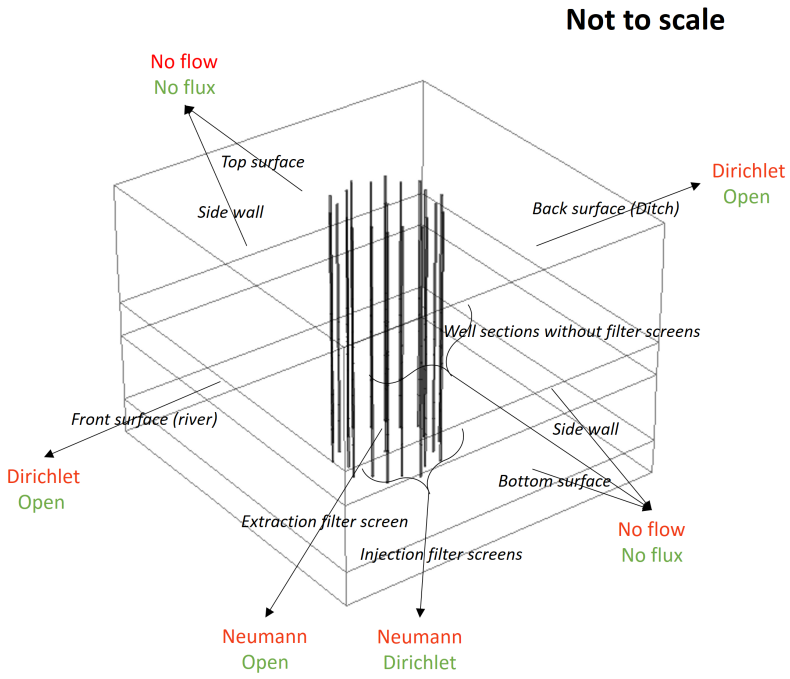

Figure A2: Description of the boundary conditions for the 3D model. Boundary conditions for water flow are denoted with a red colour, while the green colour marks the boundary conditions for solute transport.

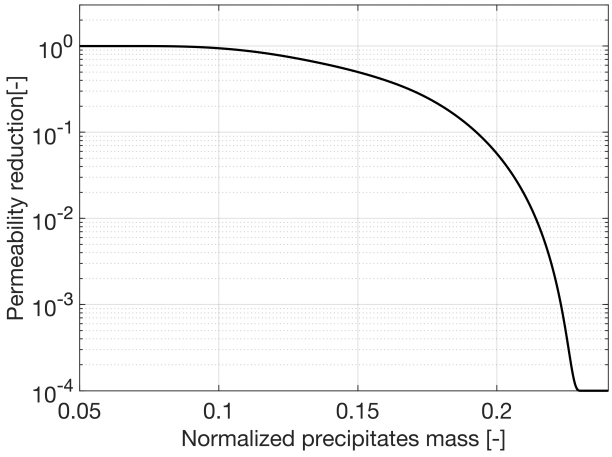

Figure A3: Ramp function used in the model to correlate Al-OM precipitates to the permeability reduction. Normalised mass of precipitates indicates the mass of Al-OM precipitates produced per unit mass of OM. We assumed a normalised precipitate mass of 0.1 to be the threshold mass that is needed to trigger the reduction in permeability. The maximum permeability reduction is set to 4 orders of magnitude.

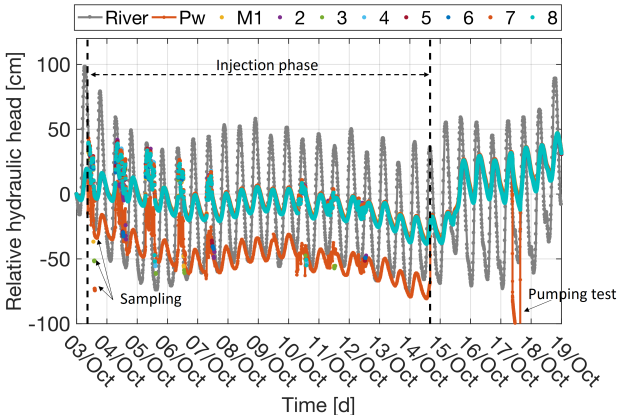

Figure A4: Relative hydraulic head measured in the monitoring wells, extraction well Pw and the river during the injection. The injection started in the midday of 3rd October, 2016 until 14th October, 2016. Sharp changes in hydraulic head in the monitoring wells are a result of groundwater sampling. A pumping test at well Pw was carried out on 17th October.

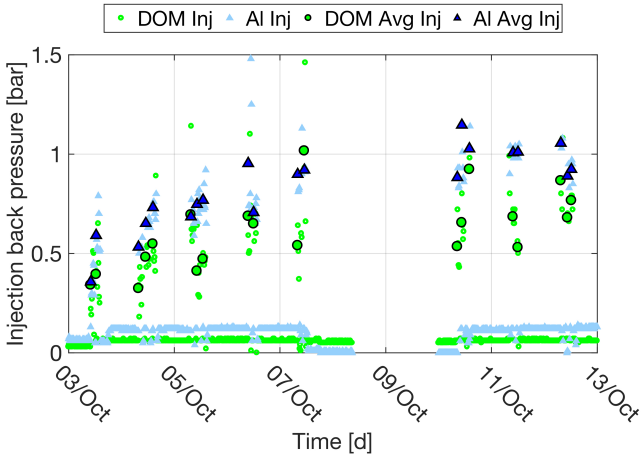

Figure A5: Recorded back pressure during the Al and OM injection . The injection back pressure is measured continuously over time. The average injection back pressure during each injection step is marked as Avg. The results show that the back pressure during the Al injection in the fine sand layer did not increase over time as in the coarse sand. This is the consequence of overflow in the deep wells installed at the same location (as illustrated in Figure A6), which resulted in pressure release. The well capping did not sustain an injection back pressure higher than 1 bar.

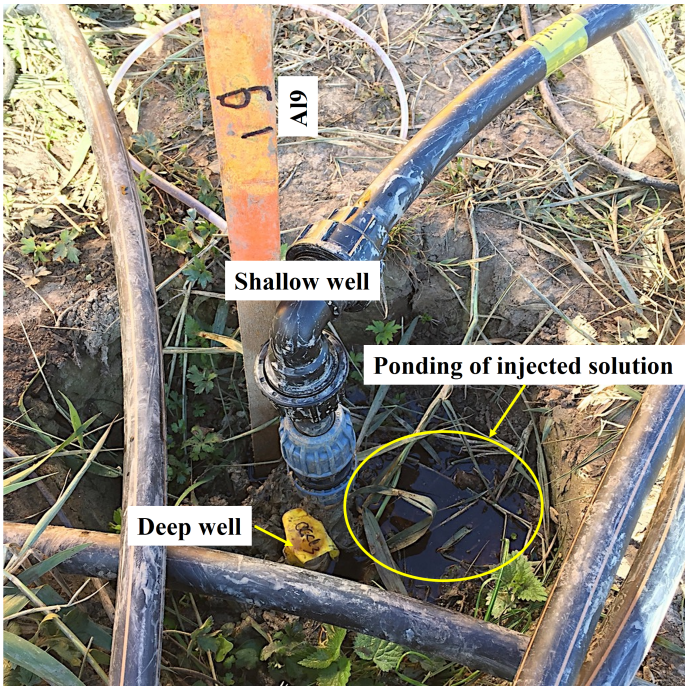

Figure A6: Overflow of injected solution at an Al injection well during the injection in the fine sand.

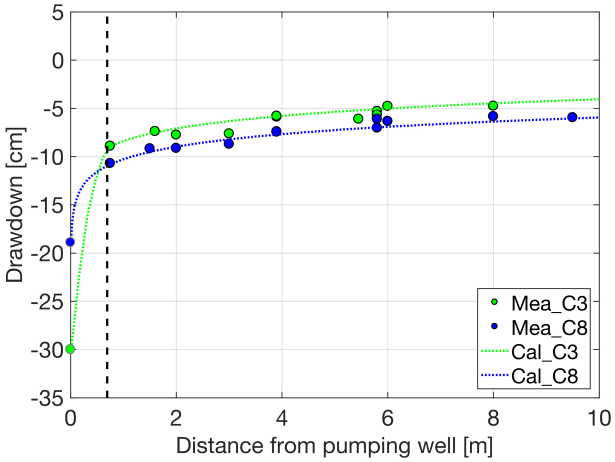

Figure A7: Measured and calculated draw down distribution from pumping tests performed after the injection at well C3 and C8 using a constant pump rate of 10 m^3/d. No reduction in transmissivity is assumed for the calculated draw down at well C8 because of the distance from the location of the barrier. A reduced transmissivity is required for the calculation of well C3 in order to obtain the best fit between calculated draw down and measured draw down. This is due to the close proximity of well C3 to the flow barrier .

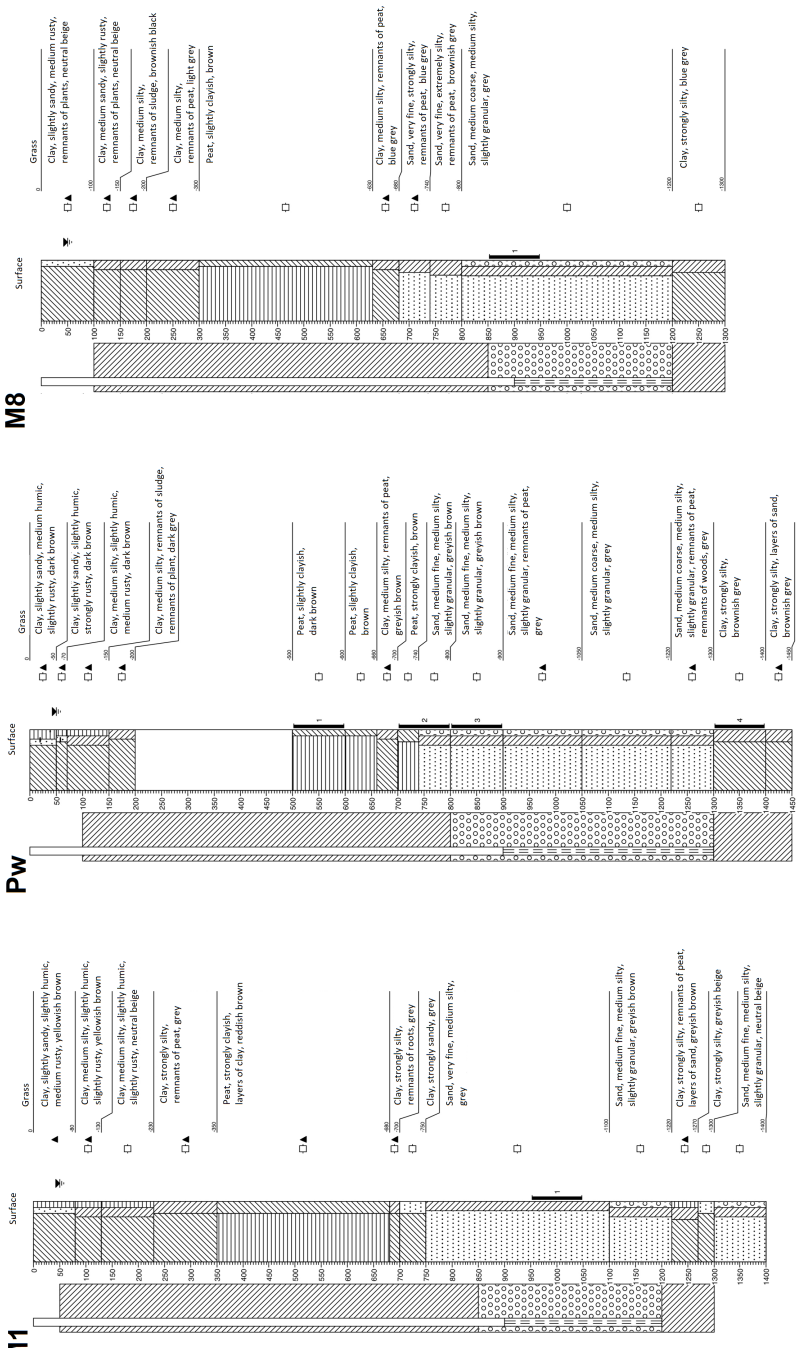

Figure A8: Soil profile at the location of well Pw, M1 and M8.

Table A1: Summary of model parameters

Parameters	Description	Value	Units	Notes
K_f	Hydraulic conductivity of the fine sand	4	m/d	Derived from lab tests with sample recovered from drilling
K_c	Hydraulic conductivity of the coarse sand	20	m/d	Derived from lab tests with sample recovered from drilling
K_{clay}	Hydraulic conductivity of clay	0.001	m/d	Representative value
ε_f	Porosity of the fine sand	0.3	-	Representative value
ε_c	Porosity of the coarse sand	0.35	-	Representative value
ε_{clay}	Porosity of clay	0.5	-	Representative value
D_D	Molecular diffusion coefficient for both Al and OM solutions	$2e^{-9}$	m^2/s	Representative value
α_L	Longitudinal dispersivity	0.5	m	One tenth of studied flow scale
α_T	Transverse dispersivity	0.1	m	One fifth of longitudinal dispersivity
$K_{\text{OM-Al}}$	Rate constant for OM-Al precipitation reaction	1	1/h	Assumed based on laboratory observation

APPENDIX B

Figure B1: The water reservoir and the location of the pilot site (marked in yellow rectangle, source: Google Maps)

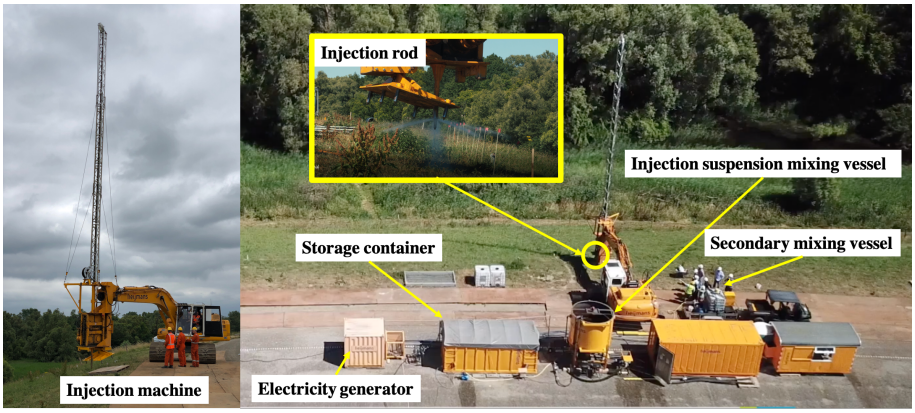

Figure B2: Illustration of the field installation

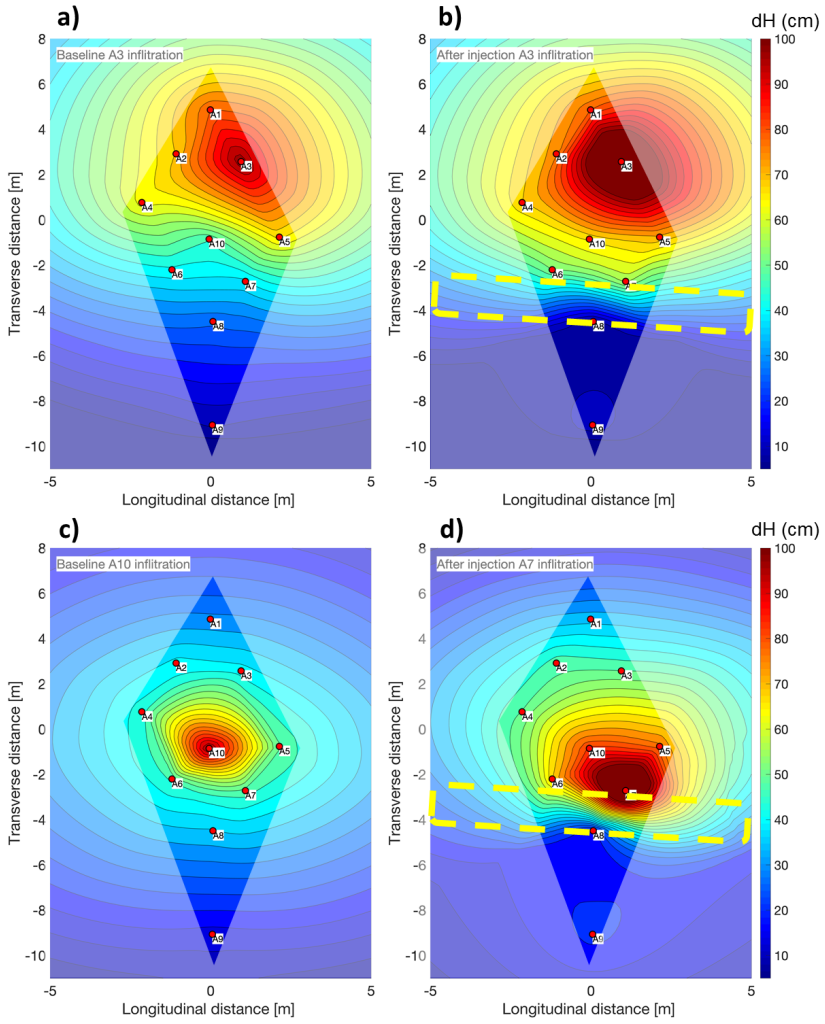

Figure B3: Measured dH during the infiltration test performed in zone A. a) and b) give test performed in well A3 before and after the injection; c) gives the infiltration test performed in well A10 before the injection and d) denotes the test performed in well A7 after the injection. The dashed rectangle suggests the location of the flow barrier.

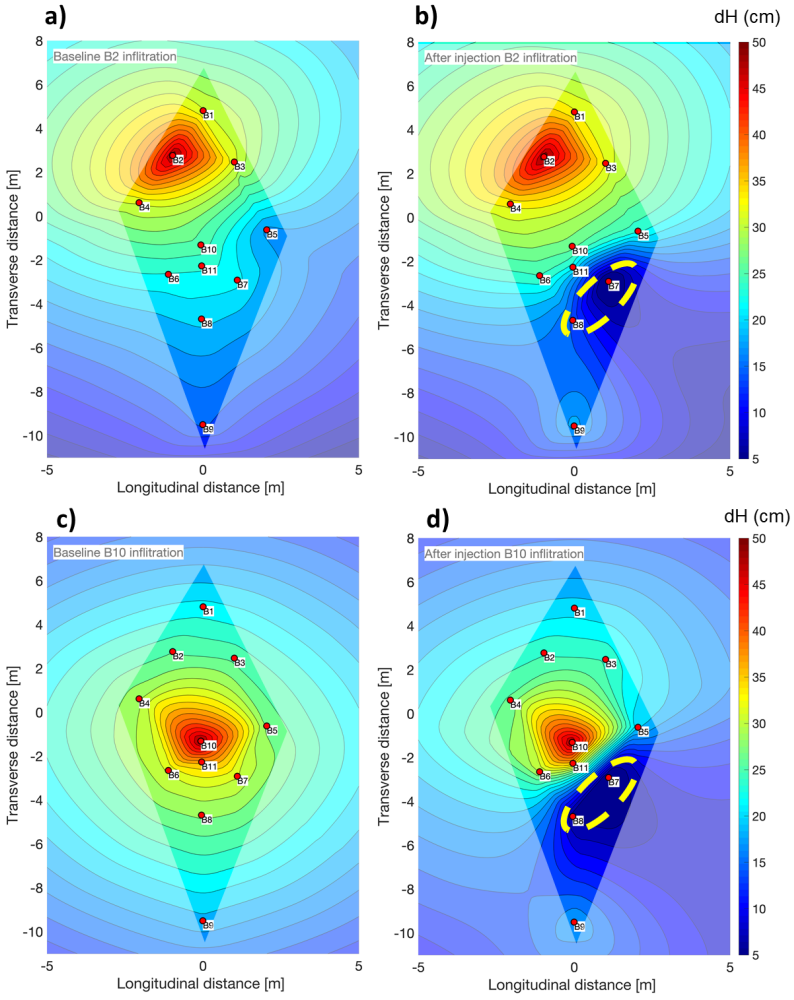

Figure B4: Measured dH during the infiltration test performed in zone B. a) and b) give test performed in well B2 before and after the injection; c) and d) give the infiltration test performed in well B10 before and after the injection. The dashed circle indicates the spot with reduced permeability.

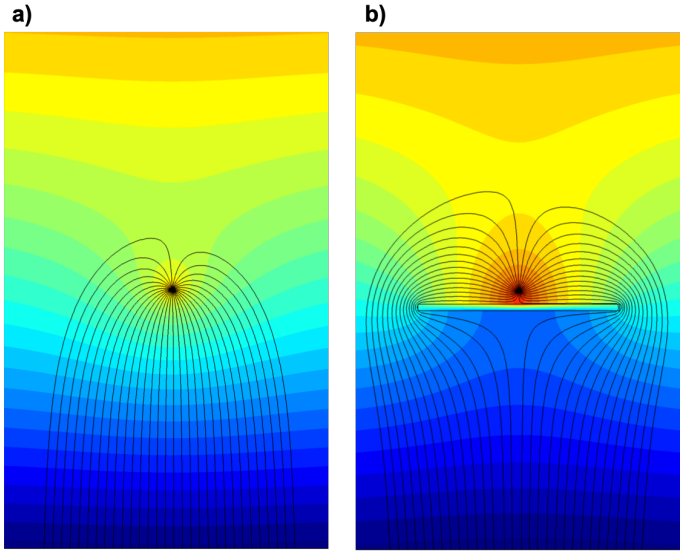

Figure B5: Illustration of the effect of a flow barrier on the infiltration test. a) is without a flow barrier and 2) includes a flow barrier. The color denotes the hydraulic head and black line denote the streamline.

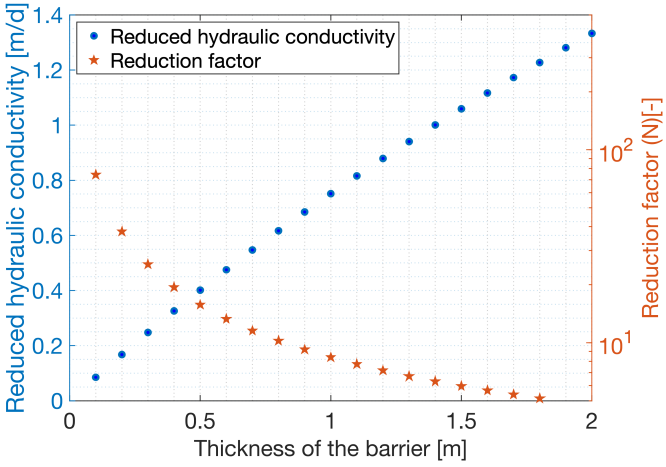

Figure B6: The value of the reduced transmissibility as a function of the assumed thickness of the flow barrier

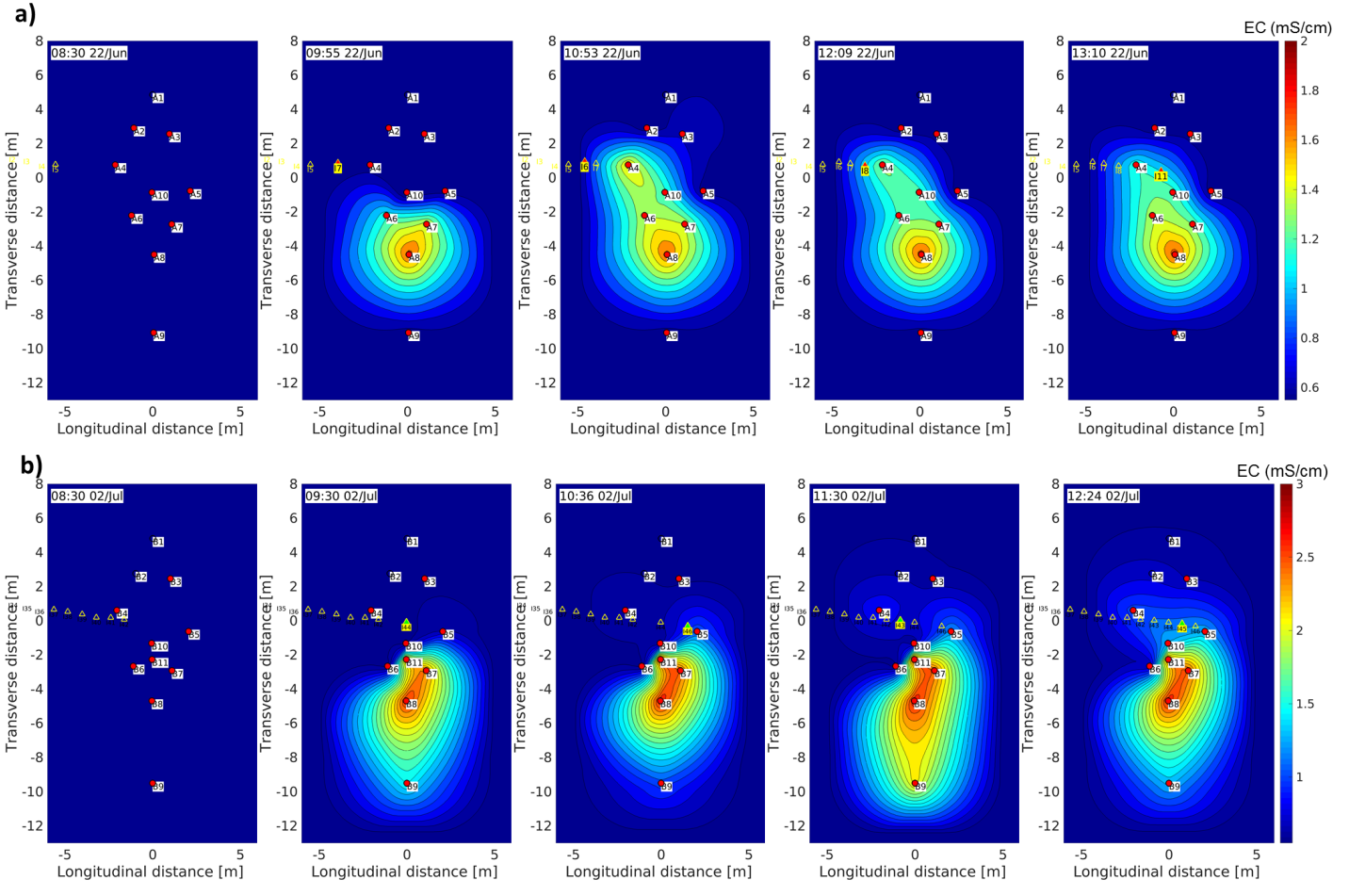

Figure B7: Measured EC at the end of each injection step performed in zone A on 22nd June 2018 (a) and in zone B on 29th June 2018 (b). The empty yellow triangles indicate the location of completed injections, while a filled triangle shows the point of the on-going injection. The monitoring wells are denoted as circle (filled means equipped with diver).

APPENDIX C

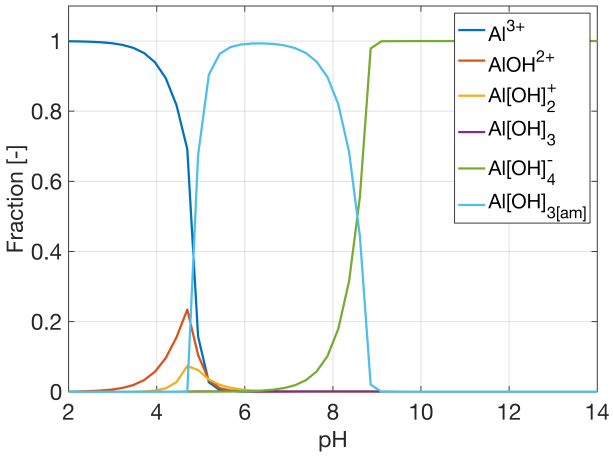

Figure C1: Mole fractions of dissolved hydrolysis products in equilibrium with amorphous hydroxides.

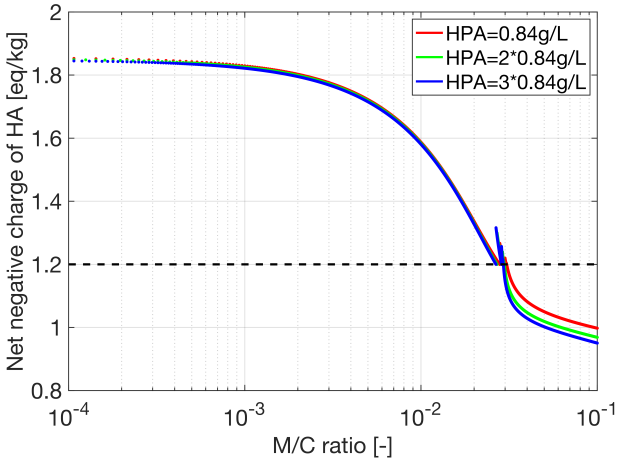

Figure C2: The simulated change in the net negative surface change during the titration of HPA using Al^{3+} at HPA concentration of 0.84 g/L, 1.68 g/L and 2.52 g/L. The dashed black line shows the critical charge level.

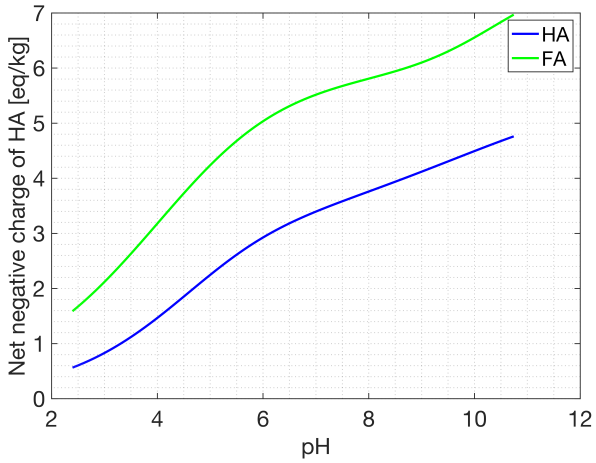

Figure C3: Change of the net negative surface change on HA and FA during the titration process.

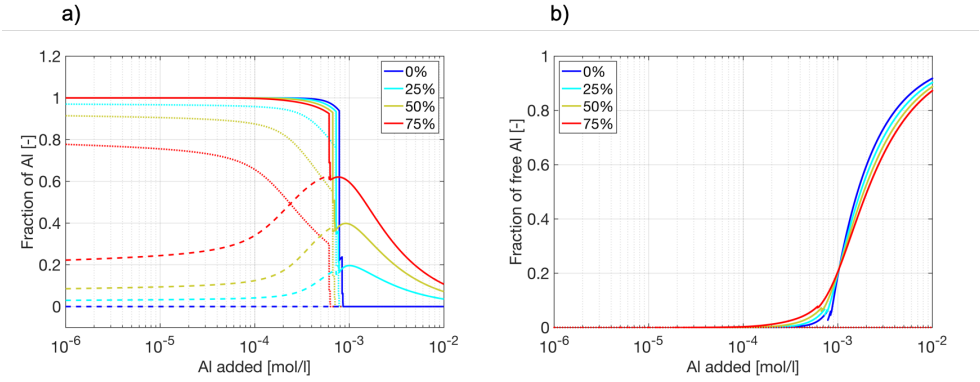

Figure C4: Fraction of Al during the titration with varying types of OM at pH = 4.5, where the fraction of FA increased from 0 to 75% with an interval of 25%. a) represents the fraction of Al that is bound to OM; and b) gives the free Al fraction.

Table C1: NICA-Donnan model parameters for generic humic and fulvic acid

	Humic acid				Fulvic acid			
*b*in Donnan model [-]	-0.49				-0.57			
	Carboxylic site		Phenolic site		Carboxylic site		Phenolic site	
Q_{max} [mol/kg]	3.15		2.55		5.88		1.86	
p[-]	0.62		0.41		0.59		0.70	
Ion specific parameters	$\log(\widetilde{K}_1)$	n_1	$\log(\widetilde{K}_2)$	n_2	$\log(\widetilde{K}_1)$	n_1	$\log(\widetilde{K}_2)$	n_2
H^+	2.93	0.81	8.0	0.63	2.34	0.66	8.60	0.76
Al^{3+}	-1.05	0.4	11.5	0.3	-4.11	0.42	12..16	0.31

CURRICULUM VITÆ

Jianchao ZHOU

04-03-1991	Born in Anhui, China.

EDUCATION

2007–2009	High School Hefei No.6 High School
2009–2013	Bachelor in Science China University of Geoscience (Beijing)
2013–2015	Master in Science Delft University of Technology
2020	PhD. in Geo-Environmental Engineering Delft University of Technology *Thesis:* Development of a nature-based geo-engineering solution to reduce soil permeability in-situ *Promotor:* Prof. dr. T.J. Heimovaara

List of Publications

Journal papers

4. **J. Zhou**, S. Laumann, T.J. Heimovaara, *A mechanistic understanding of the flocculation of organic matter induced by aluminium ions*, ready to submit.

3. **J. Zhou**, S. Laumann, T.J. Heimovaara, *Applying aluminium-organic flocs via direct-push injection to reduce soil permeability in-situ: a field study*, ready to submit.

2. **J. Zhou**, S. Laumann, T.J. Heimovaara, *Applying aluminium-organic matter precipitates to reduce soil permeability in-situ: A field and modelling study*, Science of the Total Environment **662**, 99-109 (2019).

1. **J. Zhou**, C. J, J. L, *Experimental study on progressive failure process of brittle rock with prefabricated cracks under uniaxial compression (in Chinese)*, Journal of Exploration Engineerning (in Chinese) **9**, 66-70 (2012).

Conference Proceedings (oral presentation)

5. **J. Zhou**, S. Laumann, T.J. Heimovaara, *Creation of a flow barrier in-situ by shear-controlled direct aluminium- organic matter floc injection*, Proceedings of the 27th Meeting of European Working Group on Internal Erosion, (2019), Vancouver (Canada).

4. **J. Zhou**, S. Laumann, T.J. Heimovaara, *In situ precipitation of aluminium and organic matter as a geo-engineering tool to reduce soil permeability ? a field test*, Proceedings European Geosciences Union (EGU) general assembly meeting, (2018), Vienna (Austria).

3. **J. Zhou**, S. Laumann, T.J. Heimovaara, *In-situ soil permeability reduction through Al and OM precipitation as a geo-engineering tool for dike stabilisation*, Proceedings of the 25th Meeting of European Working Group on Internal Erosion, (2017), Delft (The Netherlands).

2. S. Laumann, **J. Zhou**, F. Volkering, D. van den Heuvel, J. Stroo, R. Rijkers, T.J. Heimovaara, *Soil Sealing by Enhanced Aluminium and organic matter Leaching (SoSEAL): a novel geo-engineering technique for in situ soil permeability reduction*, Proceedings of the 14th International Conference on Sustainable Use and Management of Soil, Sediment and Water Resources "AquaConSoil", (2017), Lyon (France).

1. **J. Zhou**, A.G. van Turnhout, T.J. Heimovaara, M. Afanasyev, *A generic transport- reactive model for simulating microbially influence mineral precipitation in porous medium*, Proceedings of the 6th International Workshop ?Hydro-Physico-Mechanics of Landfill?, (2015), Delft (The Netherlands).

Conference Proceedings

4. S. Laumann, **J. Zhou**, T.J. Heimovaara, *Laboratory investigations on the interaction between aluminium and organic matter and its impact on soil permeability*, Proceedings European Geosciences Union (EGU) general assembly meeting, (2018), Vienna (Austria).

3. M. Afanasyev, **J. Zhou**, A.G. van Turnhout, L.A. van Paassen, T.J. Heimovaara, *A generic transport-reactive model for simulating microbially influenced mineral precipitation in porous medium*, Proceedings of the 9th International Conference on Porous Media, (2017), Rotterdam (The Netherlands).

2. S. Laumann, **J. Zhou**, T. J. Heimovaara, *Aluminium-organic matter precipitation as a geo-engineering tool for in situ permeability reduction in a porous media*, Proceedings 26th Goldschmidt Conference, (2016), Yokohama (Japan).

1. S. Laumann, **J. Zhou**, B. Jansen, K. Kalbitz, T.J. Heimovaara; *The SoSeal project - Bio-based geo-engineering for in situ permeability reduction in subsurface systems*, Proceedings Bio-GeoCivil Summit, (2015), Delft (The Netherlands).